NOTE TO USERS

This reproduction is the best copy available.

UMI®

uOttawa

L'Université canadienne
Canada's university

FACULTÉ DES ÉTUDES SUPÉRIEURES ET POSTOCTORALES

uOttawa

L'Université canadienne
Canada's university

FACULTY OF GRADUATE AND POSDOCTORAL STUDIES

Kevin Gilbank

AUTEUR DE LA THÈSE / AUTHOR OF THESIS

M.A.Sc. (Mechanical Engineering)

GRADE / DEGREE

Department of Mechanical Engineering

FACULTÉ, ÉCOLE, DÉPARTEMENT / FACULTY, SCHOOL, DEPARTMENT

Design and Control of a 3-DOF Spherical Tendon Based Manipulator

TITRE DE LA THÈSE / TITLE OF THESIS

D. Necsulescu

DIRECTEUR (DIRECTRICE) DE LA THÈSE / THESIS SUPERVISOR

CO-DIRECTEUR (CO-DIRECTRICE) DE LA THÈSE / THESIS CO-SUPERVISOR

EXAMINATEURS (EXAMINATRICES) DE LA THÈSE / THESIS EXAMINERS

E. Nitsche

E. Petriu

Gary W. Slater

LE DOYEN DE LA FACULTÉ DES ÉTUDES SUPÉRIEURES ET POSTDOCTORALES /
DEAN OF THE FACULTY OF GRADUATE AND POSTDOCORAL STUDIES

DESIGN AND CONTROL OF A 3-DOF SPHERICAL TENDON BASED MANIPULATOR

Kevin Gilbank

A thesis submitted to the Faculty of Graduate and Postdoctoral Studies in partial fulfillment of the requirements for the degree of

MASTER OF APPLIED SCIENCE

In Mechanical Engineering

Ottawa-Carleton Institute for Mechanical and Aerospace Engineering
University of Ottawa
Ottawa, Canada

© Kevin Gilbank

Library and Archives Canada

Published Heritage Branch

395 Wellington Street
Ottawa ON K1A 0N4
Canada

Bibliothèque et Archives Canada

Direction du Patrimoine de l'édition

395, rue Wellington
Ottawa ON K1A 0N4
Canada

Your file Votre référence
ISBN: 978-0-494-11279-3
Our file Notre référence
ISBN: 978-0-494-11279-3

NOTICE:
The author has granted a non-exclusive license allowing Library and Archives Canada to reproduce, publish, archive, preserve, conserve, communicate to the public by telecommunication or on the Internet, loan, distribute and sell theses worldwide, for commercial or non-commercial purposes, in microform, paper, electronic and/or any other formats.

The author retains copyright ownership and moral rights in this thesis. Neither the thesis nor substantial extracts from it may be printed or otherwise reproduced without the author's permission.

AVIS:
L'auteur a accordé une licence non exclusive permettant à la Bibliothèque et Archives Canada de reproduire, publier, archiver, sauvegarder, conserver, transmettre au public par télécommunication ou par l'Internet, prêter, distribuer et vendre des thèses partout dans le monde, à des fins commerciales ou autres, sur support microforme, papier, électronique et/ou autres formats.

L'auteur conserve la propriété du droit d'auteur et des droits moraux qui protège cette thèse. Ni la thèse ni des extraits substantiels de celle-ci ne doivent être imprimés ou autrement reproduits sans son autorisation.

In compliance with the Canadian Privacy Act some supporting forms may have been removed from this thesis.

While these forms may be included in the document page count, their removal does not represent any loss of content from the thesis.

Conformément à la loi canadienne sur la protection de la vie privée, quelques formulaires secondaires ont été enlevés de cette thèse.

Bien que ces formulaires aient inclus dans la pagination, il n'y aura aucun contenu manquant.

Canada

ABSTRACT

Within robotics, areas such as locomotion, unmanned aerial vehicles (UAV's), machine vision, and dexterity of robots intensive research has been performed. In considering the dexterity of robots, work has been done for various types of robots. Also the robotic ability to manipulate or closely mimic the agility of humans has been extensively investigated. Humans are able to do a wide variety of tasks based on the complex series of joints at the wrists. The area of research into robotic wrists has however never attempted to emulate the human wrist. The wrist with its tendons, ligaments, and metacarpals allow three degrees of freedom (DOF's), and this would be extremely advantageous in many scenarios where robots are used.

The goal of this thesis was to emulate the human wrist, by conceiving and designing a 3 DOF manipulator which could be easily attached to any robot arm or similar device.

The end result of this thesis was to design an easy to implement 3 DOF spherical tendon based manipulator, complete with control system for which the approximate systems response would be known.

At the conclusion of the work this was indeed the end result, and all lessons learned are enclosed herein.

ACKNOWLEDGEMENTS

First of, I must thank my supervisor on this project, Professor Dan S. Necsulescu, for always making himself available to answer all my questions, advise me when I was on the right track and to let me discover for myself when I wasn't. Without his knowledge and expertise I don't think I could have finished this project with such a good result.

I would also like to thank Professor Emil Petriu, for taking interest in my project adding a few of his own ideas and to trust me enough to donate some of his equipment. The donation of equipment and his advice were key to the success of the overall project.

Last but not least I must thank my parents, for their relentless support, without that I wouldn't be able to have done what I did.

Table of Contents

List of Tables and Figures

Chapter 1

Chapter 2

Chapter 3

Tables

Nomenclature:

Symbol	Meaning
θ	Angular Position
ω	Angular Velocity
V_i	Voltage Input
τ	Torque
i	Current
μ	Coefficient of friction
υ	Back electromagnetive force
P	Electrical power
L	DC motor inductance
J	Inertial load
M_p	Mechanical Power
E or e	Error
K_1	Mechanical gain
K_2	Electrical gain
Y	Measured state
W	Triangular Toeplitz matrix
R	Motor armature resistance
F	Force
φ_r	Feedforward velocity value
F_s	Sampling frequency
F_c	Cutoff frequency

CHAPTER 1
LITERATURE REVIEW

1.1 Introduction

This project's objective, as defined at the outset was to design a 3-DOF tendon-driven manipulator. The literature review therefore aims at specific key areas required to make this project successful. Through analyzing the best available structured wrist – that of the human wrist, and taking into account the strengths and weaknesses it is thought that this will result in a stronger design. One of those strengths is the use of tendon manipulators, of which there are a variety of types, each with their own application and specialty niche. After the wrist is designed, it must be controlled using an efficient controller, for which the PID controller and a new observer feedback system were considered. Finally through studying and critiquing other tendon-driven machines that researchers have developed, and exploiting the key benefits of each, the expected outcome will be an improved 3 DOF tendon manipulated wrist.

1.2 The Human Wrist:

As seen in figure 1.2.1, the wrist is made up of eight carpal bones, the radius and the ulna. The carpal bones, as seen in figure 1.2.2 can be divided into two sub categories, the proximal and distal rows. The proximal row (closer to the centre of the body) is made up of the scaphoid, lunate, triquetrium and pisiform. The capitate, trapezium, trapezoid and hamate form the distal row (further from point of attachment).

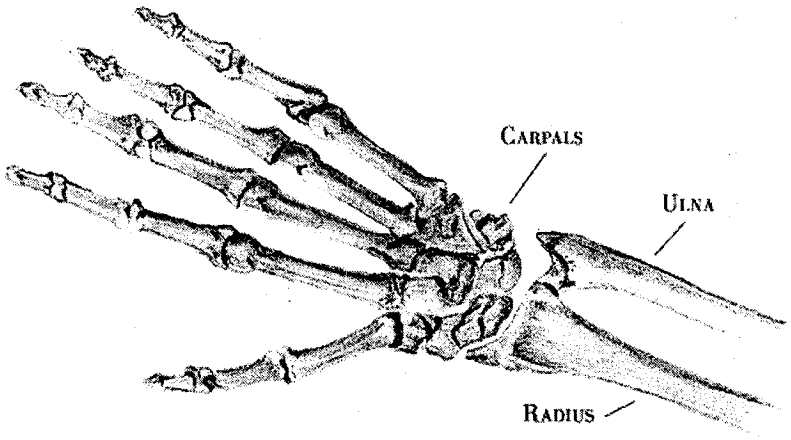

Figure 1.2.1 Anatomy of the human wrist

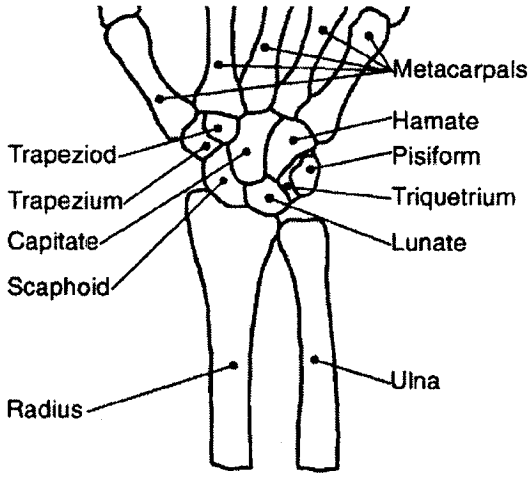

Figure 1.2.2 Anatomy diagram of the carpal bones

Connecting all these bones is an interweaving network of ligaments. Ligaments work their way through the wrist joining the carpals to each other, and also connecting the carpal bones to the radius and ulna. The vast network of ligaments can be seen in figure 1.2.3 [2].

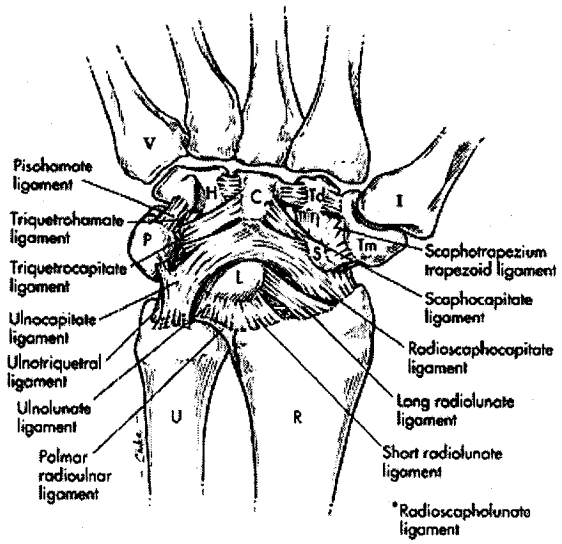

Figure 1.2.3 Wrist diagram showing ligaments

The movement of the wrist is as complex as the wrist itself. The proximal and distal rows articulate to enable movement. The movements of the wrist can be divided into three major components, as shown in figure 1.2.4 [2].

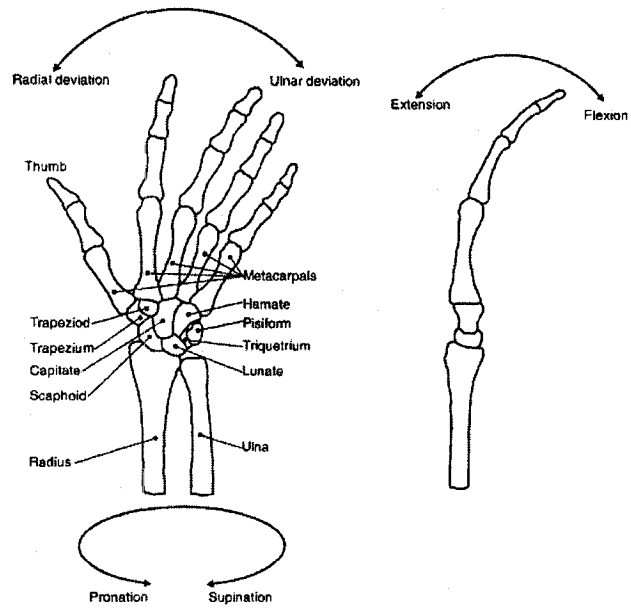

Figure 1.2.4 Movement of the human wrist

1. Deviation is subdivided into radial deviation and ulnar deviation. Deviation is the side-to-side movement of the wrist. This movement is approximately 22° for radial deviation and 36° for ulnar deviation. The name of the movement implies that it is centered around the radial and ulna bones and as such the centre of movement is the capitate (tip of the radial and ulna bones) [3].

2. Extension/Flexion is the fore/aft movement of the wrist, and healthy wrist joints normally exhibit around 76° for flexion and 75° for extension. This direction of movement is as well centered around the capitate of the radial/ulna bone region [3].

3. Pronation/Supination is the twisting motion (about the forearm) of the wrist. Motion is again centered around the capitate of the radial/ulna bone region.

Some research has indicated that this full range of motion is not required to perform normal everyday tasks. Recent studies have indicated that even a small amount of movement can allow an increase of the reach of the fingers by approximately 5-6cm [3]

However, most tasks such as drinking from a glass use the wrist movement, humans would have difficulties with a serious reduction or lack of mobility in the wrist.

1.3 Tendon Manipulators

Control of tendon driven manipulators, sometimes referred to as antagonistically driven manipulators (in reference to the push-pull drive method) have been the subject of numerous papers.

The majority of research with tendon driven manipulators has been in the area of versatile fingers. There are three basic actuation methods to any single joint tendon driven manipulator [1]:

1. Infinite length continuous cable
2. Actuator pulling with relaxing spring
3. Dual actuator drive

The first drive method, which involves a single actuator continuously driving a joint, is shown below in figure 1.3.1.

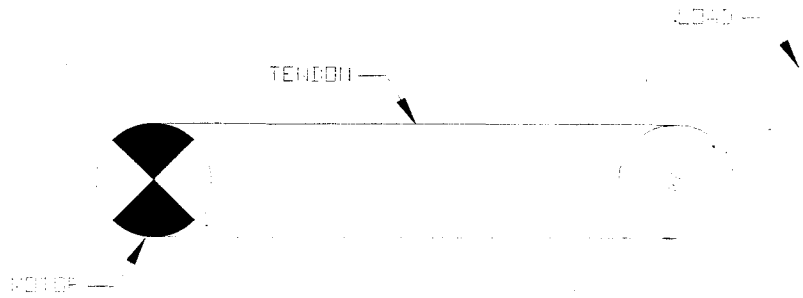

Figure 1.3.1 Model of an infinite length cable with single joint actuator

This type of design has been used successfully to develop three fingered hands, in the past [1]. Using this method of simple actuation requires that the tendon cable be heavily pre-tensioned in order to prevent slipping or slacking of the tendons when the joint moves at higher velocities, or when unexpected disturbances are introduced to the joint. The pre-tensioning however creates a large amount of friction and backlash which then gives a serious degradation of performance.

The second approach also utilizes a single actuator, but instead of looping the cable infinitely as in figure 1.3.1, a pre-tensioning spring is used. The spring acts as a pull only actuator, done by preloading the spring, through pre-tightening of the tendon and actuator. As the load is released from the actuator the spring unloads keeping tension on the tendon. This method of actuation is presented in figure 1.3.2.

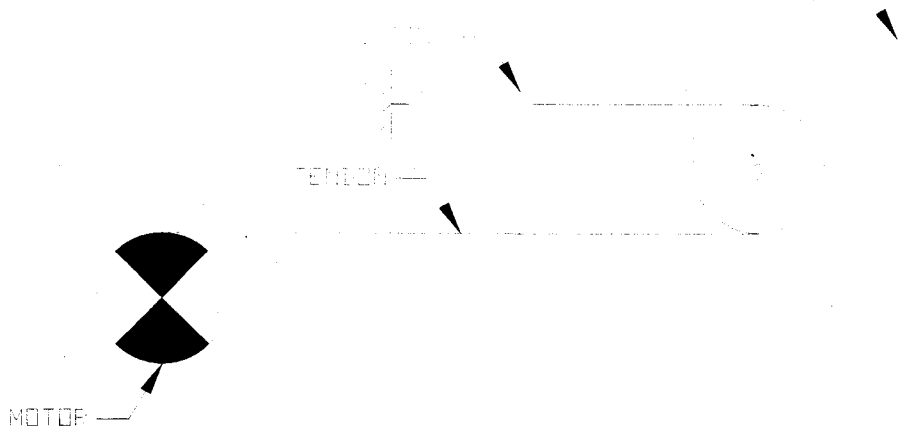

Figure 1.3.2 Model of pulling spring and actuator for single joint

For short response times the spring used has to be of extremely high stiffness, which then results in a larger load transferred to the actuator, subsequently resulting in a required stronger actuator to load the spring completely. The other disadvantage is that if any sort of tendon/cable slip is experienced, then the joint will experience a large amount of error.

The final system, using one cable and two actuators (a true push-pull system), is similar in nature to the one proposed in this thesis. This system shown in figure 1.3.3 uses two actuators which closely resemble the human bodies' actuators (ligaments and joints).

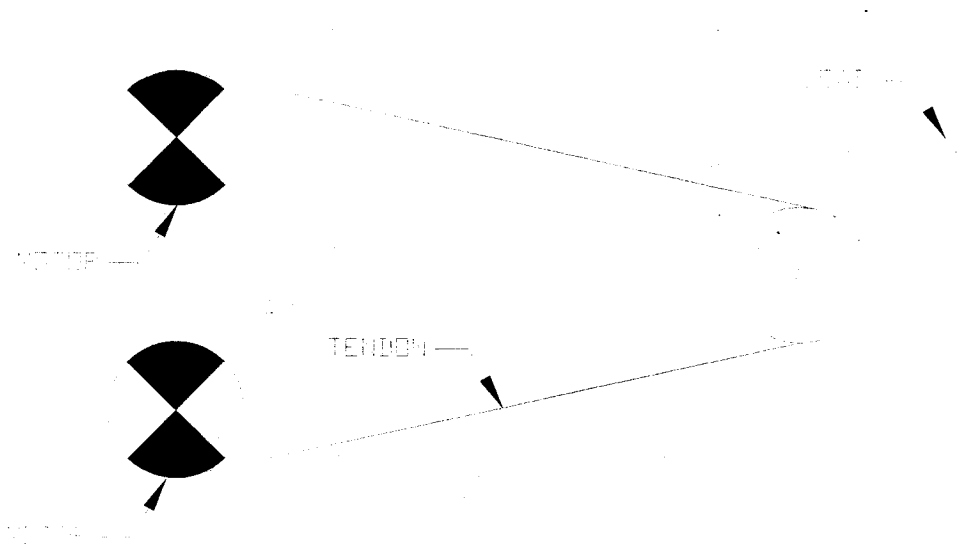

Figure 1.3.3 dual actuators driving single joint

The advantages of this type of actuation over the previous two methods include [1]:

1. Minimum amount of drag on the opposing actuator
2. Minimum tension required of the tendon (cocontraction)
3. Simple implementation
4. good positional control

The disadvantage to this method is obviously that a second actuator is required, which results in a more complex control system and in some cases, in an increased weight; the size of the actuator can also be a significant disadvantage.

Typically, these tendon-driven manipulators are compared to a double acting single actuator system such as a load driven by a stepper or DC motor through a backlash free gear train. While the tendon driven manipulators will most likely never exceed

the performance of these systems with the correct control system they can come to have comparable performance.

1.4 Control Systems:

For each tendon driven robotic system currently under research there is a different type of controller. One of the more common approaches is the traditional PID controller. PID control is easy to implement and can be developed using time-domain methods. [9]

The PID controller includes a PD controller, using its damping to resolve overshoot, rise time and settling time, these improvements however come at the expense of higher bandwidth and resonant frequency. Steady state error is not typically affected unless it varies with time. When required to modify this controller by including I control. PI control reduces overshoot, decreases bandwidth, improves gain margin and phase margin, but it increases the overall rise time [21].

Table 4.4.1 below, illustrates the advantages and disadvantages of the three steps in the PID of controllers and what each means to the overall system response. [9]

Controller	Damping	Max. Overshoot	Rise Time	Settling Time	Bandwidth	Gain & Phase Margin	Steady State Error (Ess)
PD	Improve	Small Change	Reduced	Reduced	Improve	Improve	Not Affected
PI	Improve	Increase	Increased	Increased	Decreased	Improve	Eliminate
PID	Small Change	Decrease	Reduced	Decreases	Improve	Improve	Small Change

Table 1.4.1 System response of PD/PI/PID controller

Another form of controller that has been used in tendon controlled robots is that of fuzzy logic. [10] Fuzzy logic values are not the precisely true or false values of conventional logic. Fuzzy Logic was developed in the early 60's [11], yet it did not experience wide spread application in the area of control systems until the later 70's, due to the lack of computer processing capabilities. By definition fuzzy logic is

"a structured, model-free estimator that approximates a function through linguistic input/output associations" [11]

Basically fuzzy logic allows a certain "vagueness" for answers and the solutions are not of just true or false values, but can be of a range of possible values. Hritsu et al, [10] used fuzzy logic to control a five fingered tendon driven robot with 18 degrees of freedom. Their fuzzy controller is based on a force command input from the user, and the logic control algorithm contains feedback from the velocities from two joints and the motor velocity. These three feedbacks are partitioned into five sections which range from negative big to positive big. This simple fuzzy controller was reported to give the multifingered hand much better performance than the traditional PID control. [10]

The results of the experiments, where the users input command was to move a single finger 45 degrees, the performance of the PID controller versus fuzzy logic, are shown below in figure 1.4.1 [10].

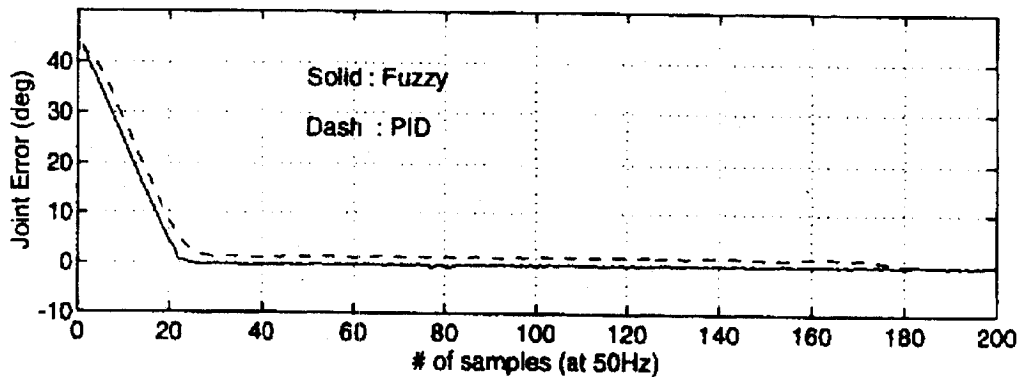

Figure 1.4.1 Fuzzy logic vs. PID (Hristu et. al [10])

As can be seen from this figure, the PID controller requires about 0.5 seconds to settle to within a one degree error and the fuzzy controller takes approximately 0.4 seconds to come within the same one degree of error but then eventually settles near zero error.

While both of these systems gave very good responses, there is one other option that has previously been untested for use in tendon based control systems, it is that of the observer based control system.

1.5 UTAH/MIT Dexterous Hand

Most of the work done with tendon driven manipulators has been in the area of dexterous hands. The robotic end effector is a very natural choice for a place to start in this research as it presents many problems and offers a very sufficient base for testing.

The Utah/MIT Dexterous Hand (DH) was designed by S.C. Jacobsen et al, and is now available commercially mostly for the research community, primarily for use as

a general research tool for the study of machine based manipulation [8]. The DH can be seen below in figure 1.5.1. [8]

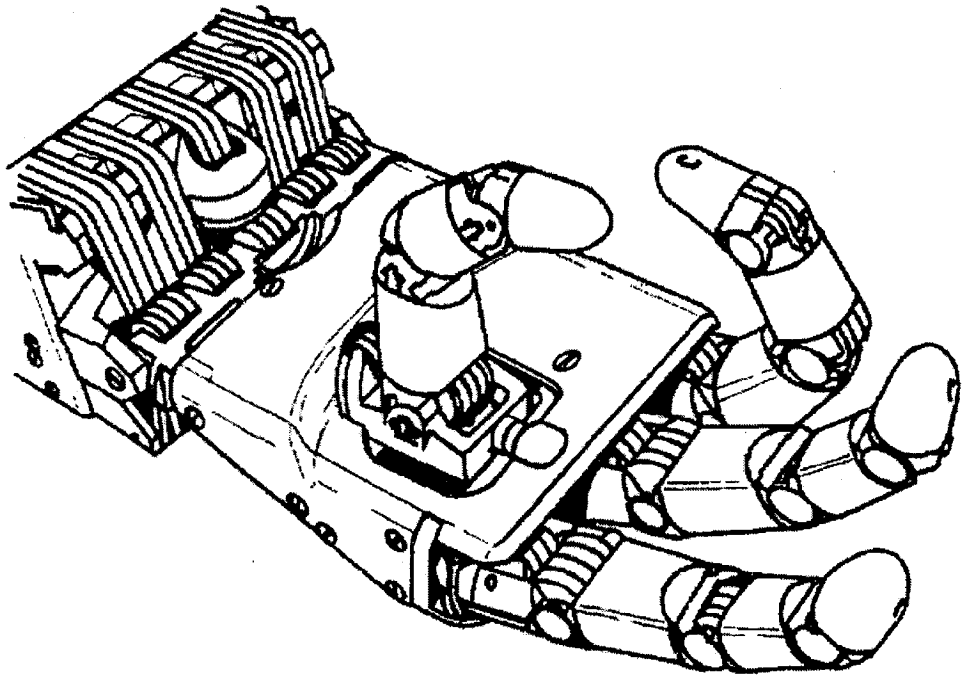

Figure 1.5.1 Utah/MIT dexterous hand

The source of motion for this hand are the actuators that drive the tendons, where the actuators are pressure controlled valves with low stiction cylinders, as shown in figure 1.5.2 and figure 1.5.3.

The cylinders (B in figure 1.5.3) and valves (A in figure 1.5.3) for each tendon are included with an adjustable pneumatic damper (C in figure 1.5.3), and a spring tensioning unit (B in figure 1.5.3) which are paired with the opposing end of the tendon to make up one module. This setup allows for the release of any residual

tension when the system is unused, as long-term residual tension can lead to misalignment of tendons, which can affect tendon life.

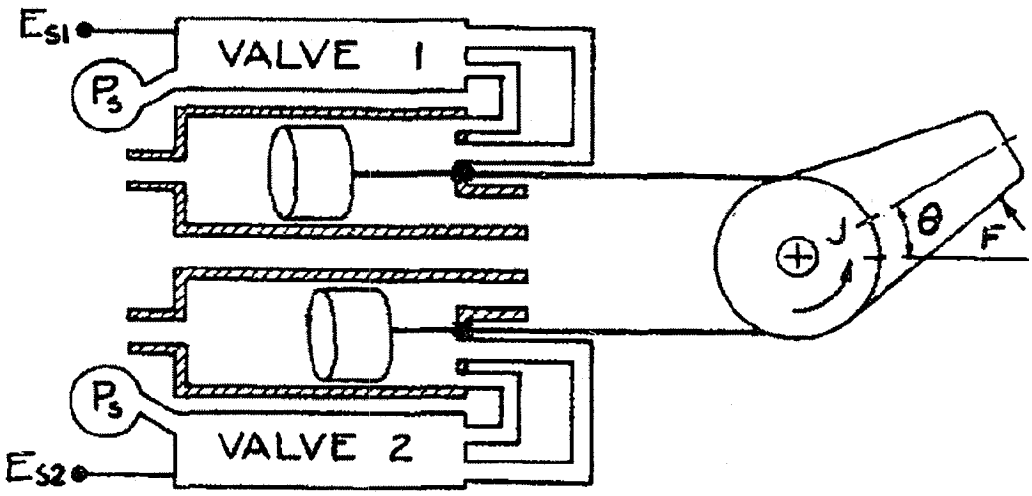

Figure 1.5.2 Actuation system of Utah/MIT dexterous hand

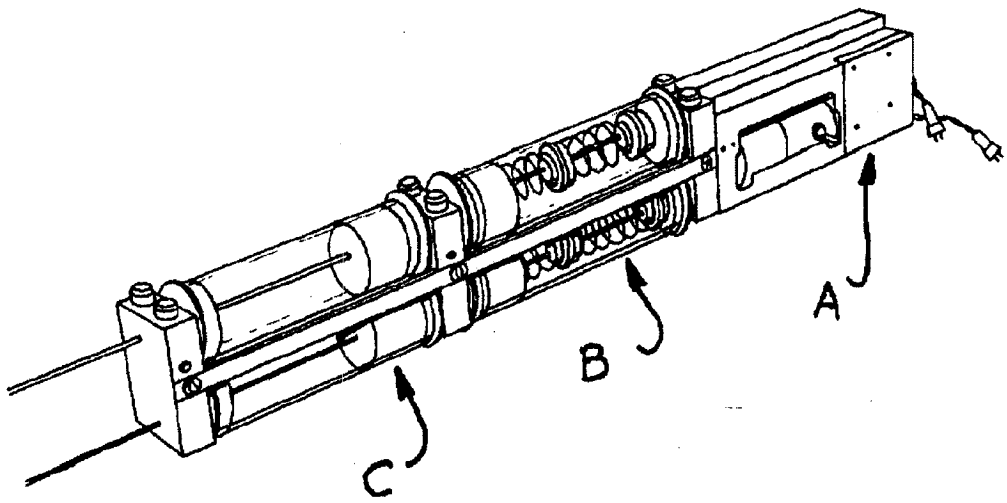

Figure 1.5.3 Complete Actuation system including dampers of the Utah/MIT Dexterous Hand

These modules of the DH have to be relocated outside of the hand, due to their larger volume, as most of the available space in the hand is taken up with structures, joints and sensors. Having moved the actuator modules to the wrist location, allows the added advantage of making the modules larger allowing for more performance (strength, torque) and less restrictions in size, shape, weight, cost and volume. Due to the fact that the actuation modules are in such a remote area, the tendon routing is very critical.

Once the tendon leaves the module it is routed through what the Utah/MIT group refer to as "quasianthromorhic geometry" - meaning that it resembles the human hand as closely as permissible. The DH contains only 3 fingers and an opposable thumb, the reason for this being that they saw no immediate advantage for the 4^{th} finger (little finger).

The routing of the tendons through the hand is shown in figure 1.5.4.

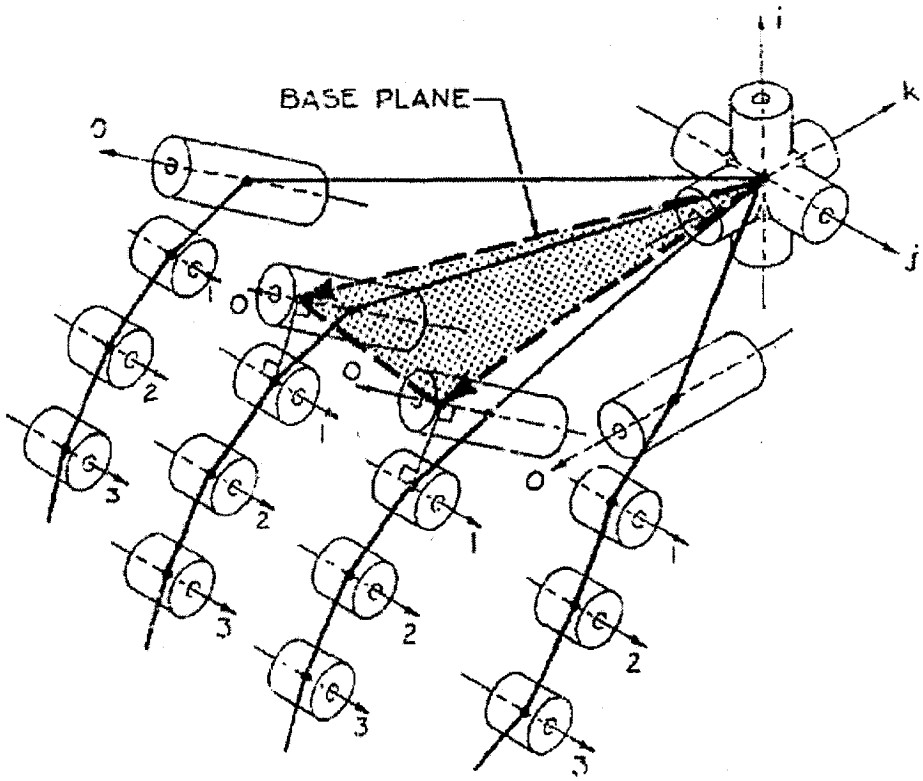

Figure 1.5.4 Routing of the UTAH/MIT dexterous hand

As can be seen from Figure 1.5.4, the routing is very complex, especially considering that only the path of the most outlier cables have been shown. The first two joints of each finger (joints 0 and 1 in Figure 1.5.4) were changed to use flat belt tendons, because these joints make sharp axial twists, and therefore require good strength and fatigue life.

The remaining joints (joint 2 and 3 in Figure 1.5.4) use a composite structure for the tendon material. The tendon material is routed through the hand around pulleys and axial twists. The 288 pulleys vary in diameter from .95 of an inch to as small as .38 inches in diameter. All pulleys contain domed contact surfaces which enable the pulleys to self align. The composite tendon material is made up of Dacron Fibers that

are woven around multiple longitudinal elements of Kevlar. [8] Through the use of having Dacron as the outer sheath material serves both purposes of aligning and protecting the interal Kevlar fibres, which is the load bearing material.

According to Jacobsen et al [8], one of the most important factors to system reliability is the fixation of the tendon ends, and for this reason they have implemented three types of termination methods for the tendons.

As can be seen in figure 1.5.5, the three types are a permanent clipping method (A in figure 1.5.5), a doubled back clip (C in figure 1.5.6) and simply a knot (not shown).

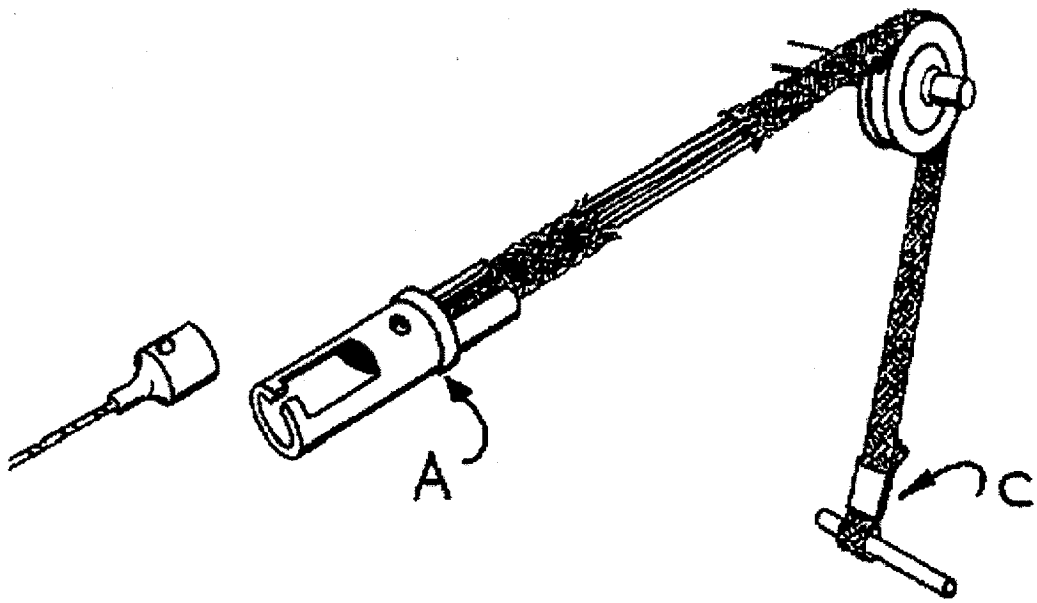

Figure 1.5.5 Tendon and tendon terminating method of the UTAH/MIT Dexterous Hand

The doubled back clip, which relies on friction to keep the tendon restrained, allows for adjustment of the tendon, if stretching has occurred, as it is reversible.

The permanent clipping method, which is made up of an injection molded component, allows for quick disconnecting capabilities.

The remaining sensors, that are required to drive the hand, include joint angle sensors and tendon tension sensors.

At each joint is a Hall effect sensor which measures the angular deflection. The Hall effect sensor is located in the proximal link (A in figure 1.5.6) while the distal link contains a disc with two magnets that are placed in a dipolar configuration (B in figure 1.5.6), as can be seen in figure 1.5.6. The disc's magnetic field, as it passes under the Hall effect sensor, produces an output current that corresponds to the angular deflection (varying between 0 and 95 degrees). The reported benefits of the Hall effect sensor include a linearity within 5%, a continuous output signal, high bandwidth operation, low friction, no mechanical contact, long life and tolerance to external environments. [8]

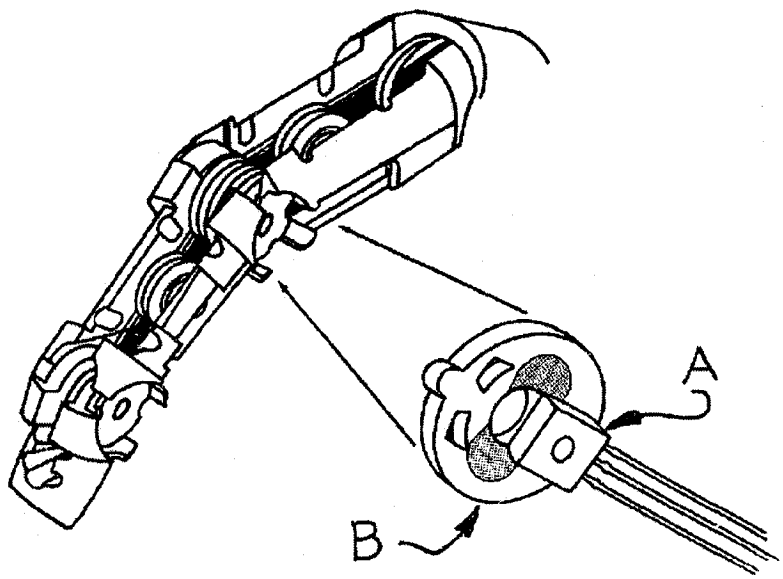

Figure 1.5.6 Hall Effect Sensor contained in each joint of the UTAH/Mit Hand

The 32 tendon tension sensors, are contained in the wrist and consist of a pulley which diverts the path of the tendon. The tendon tension sensor shown in figure 1.5.7, and is basically a semiconductor strain gauge that is installed on a cantilevered beam, and provides a linear output of strain which can vary between 0 and 30 pounds.

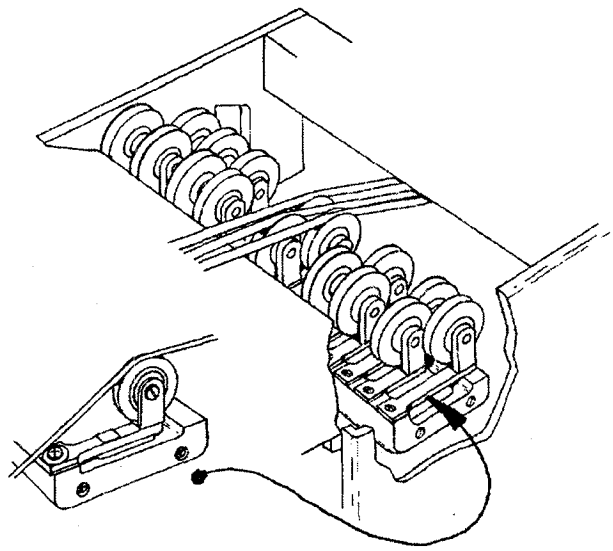

Figure 1.5.7 Tendon tension sensor contained in the wrist of the UTAH/Mit dexterous hand

CHAPTER 2

OBSERVER DEVELOPMENT

2.1 Introduction

The first step in this problem was to design a linear observer control system and then to move into the more complex tendon-driven problems. What was required then would be a simulation with simple feedback – a DC motor equipped with tachometer and potentiometer sensors. For this purpose, a commercially available laboratory experiment setup was used, allowing for quick and easy set-up and modifications. The experiment used – MathWorks MATLAB™ for writing of the control software, and Feedback Instruments experimentation hardware. The fact that commercially available equipment was used, which was readily available, proved to be an asset, as the actual task is to design the tendon-driven manipulator and not to rework control system experiments.

An observer control system is ideally used where some of the state variable feedbacks that would normally be measured are not accessible for measurement. Observer control systems use feedback estimates of state variables that are not measurable from state variables from another system. Through using these state-variable estimates, rather than measured values, it is possible to achieve very suitable performance, in some cases even exceeding that of direct measurement systems. This is only the case when the measured errors are larger, due to the inaccuracy of the measuring instrument (sensor) being larger than the errors in estimating these state variables. [12]

Observer based control was introduced as a theory by D. Luenberger in 1963 [12] who showed that, for a linear system, an observer can be developed that will have an estimation error that will go to zero as quickly as designed [12].

2.2 Experiment Set-up

The initial step in building the tendon driven mechanical wrist was to develop and verify the control system. The Luenberger linear observer based controller was assumed to be ideally suited for this application, but this had to be proven. To validate and fine-tune the linear observer was the preliminary task undertaken and a feedback control system in its most basic form would be the launching platform for this task. The most elementary control system decided upon would be a basic DC motor driving an inertial load with feedback from a tachometer and potentiometer. This feedback system while simple has numerous applications in the real world, from a heavy inertial load such as an antenna positioning system to a small load like a precision gauge in the dashboard of an automotive vehicle.

The apparatus to build this basic feedback system was using Feedback Instruments Ltd.'s Modular Servo MS150 System [13], shown below in figure 2.2.1 [13]

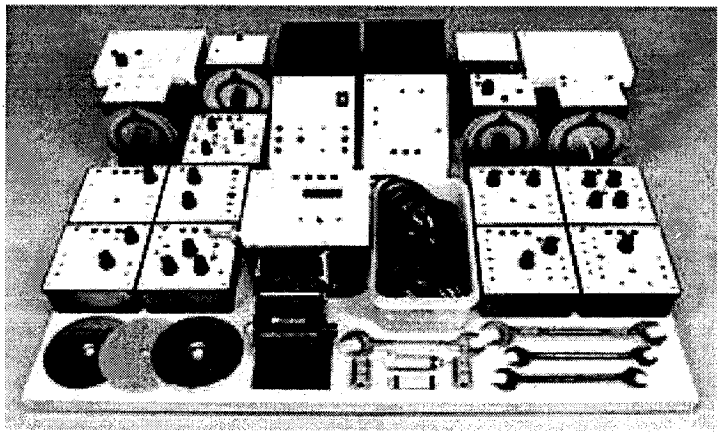

Figure 2.2.1 Feedback Instruments MS150 Modular System

This system is a very valuable tool as it allows quick and easy setup (the units are all magnetically placed on a steel table) and the wiring is simplified by using simple push-in connectors. The versatility of the system is due to the sub-units available for various configurations:

- OP-Amp Unit (OU150A)
- Pre-Amp Unit (PA15OC)
- Servo Amplifier (SA1500)
- DC Motor-Tacho Unit (MT150F)
- Input Potentiometer Unit (IN150H)
- Output Potentiometer Unit (OP150K)
- Power Supply (PS150E)
- Attenuator Unit (AU150B)
- Motor Loading Unit (LU150L)

With the components configured, next was to develop the control system. The system consisted in a data Acquisition board (DAQ) from National Instruments, model PCI-6024E, and initially with software from National Instruments called LabVIEW Virtual Instrument (VI) to communicate between the two. LabVIEW VI allows quick control of software development for the DAQ, but does not allow true real-time control. It was realized that a better option for real-time control of the DAQ, was available, MATLAB xPC Target toolbox from MathWorks™. The main reason why xPC target is useful to the Mechatronics Designer, is flexibility. Besides this flexibility, the xPC target system is based on the popular Simulink software which is easily applied to numerous control systems problems. MATLAB xPC Target is a true real-time solution for Hardware-in-loop (HIL) setups and uses two Personal computers interfaced to the DAQ board that allows real-time testing of applications (figure 2.2.2). Using one computer, the host, running MATLAB, Simulink, Real-Time Workshop, xPC Target, and a C compiler, the system is modeled, and then the code is downloaded to the second PC. Known as the target PC, a slave computer in this process; it needs a real-time operating system and is started using a special boot disk, that loads the real-time Kernel onto the Target PC. The real time application is downloaded from the host to the target computer, where it can be run in real-time with HIL equipment; all this allows for no interruptions to the target PC and avoids

real-time operation disruptions due to interrupts that are associated with Windows based software.

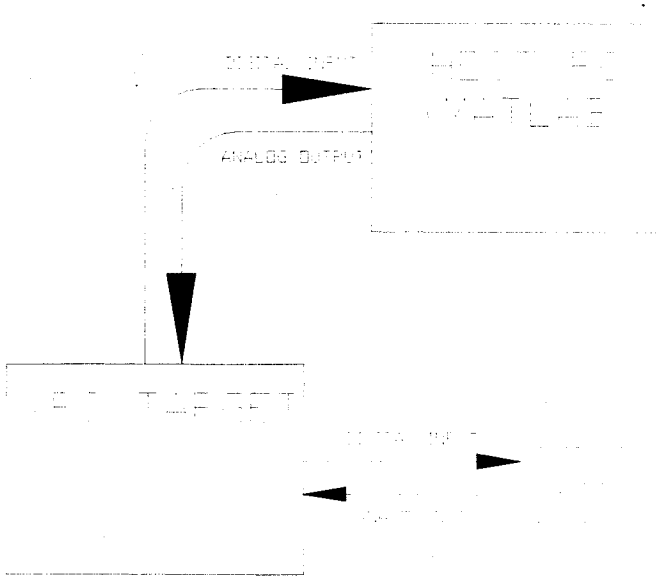

Figure 2.2.2 MATLAB xPC interface

The following MATLAB toolboxes (version 6.5.1 Release 13) were installed to allow the design of xPC applications and to execute the real-time code (table 2.2.1).

MATLAB	Version 6.5.1
Simulink	Version 5.1
Control System Toolbox	Version 5.2.1
DSP Blockset	Version 5.1
Data Acquisition Toolbox	Version 2.2
Dials & Gauges Blockset	Version 1.1.3
Real-Time Windows Target	Version 2.2
Real-Time Workshop	Version 5.1
Signal Processing Toolbox	Version 6.1
xPC Target	Version 2.0.1
xPC Target Embedded Option	Version 2.0.1

Table 2.2.1 Required MATLAB Toolboxes for xPC Target

The next required program is the C/C++ Compiler. This is required because, before the program is downloaded to the Target xPC machine, it is converted into a basic C program which enables the real-time process to be run. The C/C++ compiler chosen for this development was Microsoft Visual Basic (version 6.0).

The next step was to model the circuit and the control system which was to be developed using MATLAB. The first step was to obtain the differential equations based on the model and the block diagrams which would permit the development of linear observer block diagram.

2.3 System Model:

The DC motor driving the inertial load can be seen in figure 2.3.1.

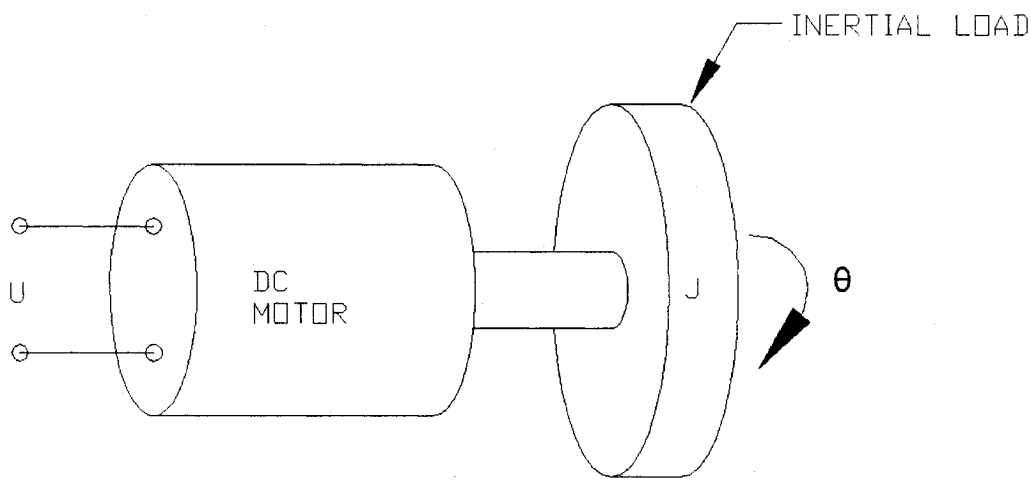

Figure 2.3.1 DC motor driving an inertial load

The torque (τ) developed at the output shaft of the motor is directly proportional to the current (i):

$$\tau = K_1 i \tag{1}$$

The back EMF (υ) is directly proportional to the speed of rotation or angular velocity (ω) :

$$v = K_2 \omega \tag{2}$$

The electrical power (P) is:

$$P = vi = \frac{K_2 \omega \tau}{K_1} \tag{3}$$

Mechanical Output Power (M_p) is the product of the torque and anguiar velocity:

$$M_P = \omega \tau \tag{4}$$

If no conversion loss occurs, then mechanical power and Electrical Power are then equal and:

$$K_1 = K_2 \tag{5}$$

The rotor electric circuit gives, for which mechanical inductance is negligible and thus L = 0:

$$V_i - v = iR \tag{6}$$

For a purely inertial load (J):

$$\tau = J \frac{\partial w}{\partial t} \tag{7}$$

Eliminating τ and i from Eq.'s 1, 4 and 5 gives:

$$J\frac{\partial w}{\partial t} = K_1 i$$
$$= \frac{K_1}{R}(V_i - v) \tag{8}$$

Eq. 8, Eq. 2 and Eq. 9 give:

$$J\frac{\partial w}{\partial t} = \frac{K_1}{R}(V_i - v) \quad \& \quad \mathrm{v} = \mathrm{K}_2\omega$$
$$J\frac{\partial w}{\partial t} = \frac{K_1}{R}(V_i - \mathrm{K}_2\omega)$$
$$J\frac{\partial w}{\partial t} = \frac{K_1}{R}V_i - \frac{K_1}{R}\mathrm{K}_2\omega$$
$$\frac{\partial w}{\partial t} = \frac{K_1}{JR}V_i - \frac{K_1K_2}{JR}\omega \tag{9}$$

Eq. 9 is a first order equation with angular velocity (ω) as the measured variable and voltage (V_i) as the input. With regard to the position (θ), this equation becomes in matrix form:

$$\frac{\partial}{\partial t}\begin{bmatrix}\theta \\ \omega\end{bmatrix} = \begin{bmatrix}0 & 1 \\ 0 & -\frac{K_1K_2}{JR}\end{bmatrix}\begin{bmatrix}\theta \\ \omega\end{bmatrix} + \begin{bmatrix}0 \\ \frac{K_1}{JR}\end{bmatrix}e \tag{10}$$

Substituting:

$$\alpha = \frac{K_1 K_2}{JR} \qquad (11)$$

$$\beta = \frac{K_1}{JR}$$

The following state-space equations result:

$$\dot{\vartheta} = \omega \qquad (12)$$

$$\dot{\omega} = -\alpha\omega + \beta u \qquad (13)$$

This is the dynamic system represented in the usual state-space representation of control systems:

$$\dot{x} = Ax + Bu \qquad (14)$$

Along with the control law:

$$U = -Gx \qquad (15)$$

It is assumed that it is not possible to measure the state X directly but only y

$$y = Cx \qquad (16)$$

It is also assumed that the matrix dimensions of observation value y are less than the matrix dimensions of x. It is then obvious that if y(t) and matrix C are known, one could invert matrix C and solve for x(t). This is not the case however because C is a singular matrix it is only possible to obtain an *estimate* $\hat{x}(t)$ of x(t) . The estimate of the output of the dynamic system can then be written as:

$$\dot{\hat{x}} = \hat{A}\hat{x} + \hat{B}\hat{u} + Ky$$

Through carefully selecting matrices $\hat{A}, \hat{B}$ and K in relation to the measurement Y and input U, the error between X the actual value and the estimate $\hat{X}$ can be found as:

$$e = X - \hat{X}$$

By substituting the above equations into the error formula e the differential equation becomes:

$$\begin{aligned}\dot{e} &= \dot{X} - \dot{\hat{X}} \\ &= Ax + Bu - \hat{A}(x - e) - \hat{B}u - Kcx \\ &= \hat{A}e + (A - KC - \hat{A})x + (B - \hat{B})u\end{aligned}$$

The goal is to make the error go to zero asymptotically, for any x and u. As a result the coefficients of x and u must be zero. $\hat{A}$ must then be the dynamics matrix of the stable system:

$$\hat{A} = A - KC$$
$$\hat{B} = B$$

and this puts conditions on the selectable matrix K. The matrix B is determined from the control matrix and the estimate of $(\hat{A})$ is chosen depending on the values of that matrix.

Thus the defining equation of an observer is:

$$\begin{aligned}\dot{\hat{x}} &= (A - KC)\hat{x} + Bu + ky \\ &= A\hat{x} + Bu + k(y - C\hat{x})\end{aligned}$$

The only difference in this final equation and the earlier equation of the normal state space representation:

$$\dot{x} = Ax + Bu$$

is the addition of $k(y - C\hat{x})$, referred to as the *residual*, the difference between the actual measurement of y and the estimated measurement of y.

If the error $e = X - \hat{X}$ is forced towards zero then the residual will tend towards zero as well.

Figure 2.3.2 shows the typical outline of a Luenberger linear observer.

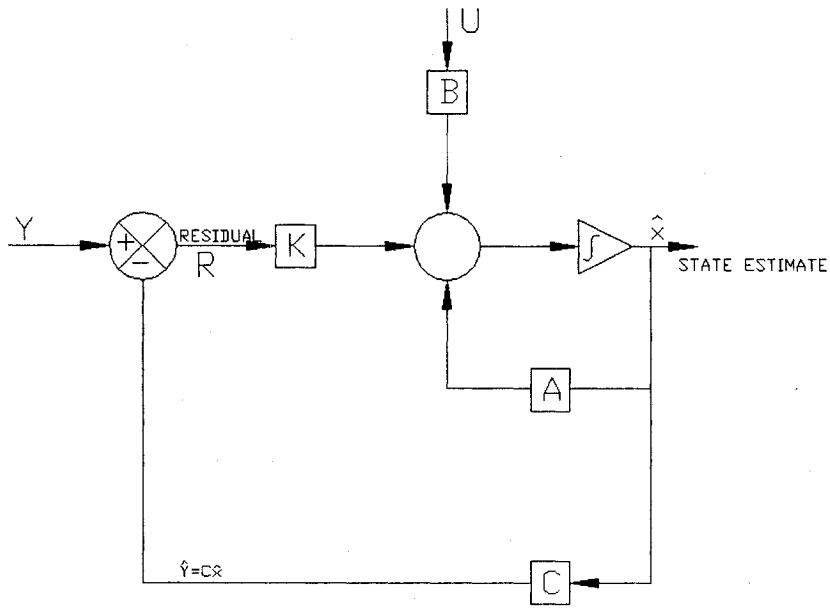

Figure 2.3.2 Block diagram of Luenberger linear observer

The only question remaining now is to obtain the gain matrix K:

$$k = \begin{bmatrix} k_1 \\ k_2 \end{bmatrix}$$

The Bass-Gura formula [12]:

$$k = \left[(NW)'\right]^{-1}(\hat{a} - a) \tag{17}$$

For which the variable N, the observability test matrix in this is defined as:

$$N = \left[C', A'C', ...(A')^{k-1}C')\right]$$

Where:

$$\hat{a} = \begin{bmatrix} \hat{a}_1 \\ \vdots \\ \hat{a}_k \end{bmatrix} \quad \text{and} \quad a = \begin{bmatrix} a_1 \\ \vdots \\ a_k \end{bmatrix}$$

and $\hat{a}_1$ ... $\hat{a}_k$ are defined through the desired charateristic equation :

$$\left|sI - A\right| = s^k + \hat{a}_1 s^{k-1} + ...\hat{a}_k = 0$$

a_1 ... a_k are defined through the original charateristic equation :

$$\left|sI - A\right| = s^k + a_1 s^{k-1} + ...a_k = 0$$

and W:

$$W = \begin{bmatrix} 1 & a_1 & \dots & a_{k-1} \\ 0 & 1 & \dots & a_{k-2} \\ \dots & \dots & \dots & \dots \\ 0 & 0 & \dots & 1 \end{bmatrix}$$

where W is referred to as a triangular Toeplitz matrix [12]

For the desired angular position (θ_r), the error can be defined as:

$$e = \theta - \theta_D \tag{18}$$

The state vectors are defined as:

$$\hat{x} = \begin{bmatrix} \hat{e} \\ \hat{w} \end{bmatrix}$$

The only quantity that can be measured in the system is the error (e), and not the estimate of angular velocity therefore the systems input (y) is:

$$y = e = \begin{bmatrix} 1 & 0 \end{bmatrix} \begin{bmatrix} e \\ w \end{bmatrix} \tag{19}$$

The observation matrix C is:

$$C = \begin{bmatrix} 1 & 0 \end{bmatrix}$$

The following matrixes can now be defined:

$$A = \begin{bmatrix} -a_1 & -a_2 & \cdots & -a_{k-1} & -a_k \\ 1 & 0 & \cdots & 0 & 0 \\ 0 & 1 & \cdots & 0 & 0 \\ \cdots & \cdots & \cdots & \cdots & \cdots \\ 0 & 0 & \cdots & 1 & 0 \end{bmatrix}$$

$$\mathrm{A} = \begin{bmatrix} 0 & 1 \\ 0 & -\alpha \end{bmatrix}$$

$$B = b = \begin{bmatrix} b_1 \\ \vdots \\ b_k \end{bmatrix} \qquad b = \begin{bmatrix} 0 \\ \beta \end{bmatrix}$$

Using Eq. 19, which defines the system input, and using them in the equation for the structure of the observer, Eq. 16, gives the two differential equations to define this observer:

$$\dot{\hat{e}} = \hat{w} + k_1(e - \hat{e}) \tag{20}$$

$$\dot{\hat{w}} = -\alpha\omega + \beta u + k_2(e - \hat{e}) \tag{21}$$

Figure 2.3.3 shows the block diagram of the observer:

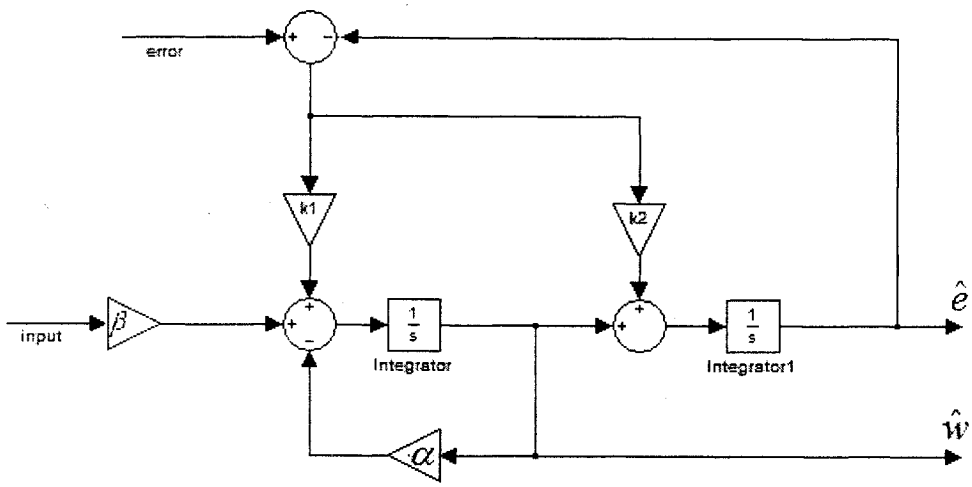

Figure 2.3.3 Observer structure

The gain matrix K:

$$K = k = \begin{bmatrix} k_1 \\ k_2 \end{bmatrix}$$

is obtained using the Bass-GURA formula $k = [(NW)']^{-1}(\hat{a} - a)$ to find the gain matrix values. The observability test matrix N and the triangular Toeplitz matrix W must now be solved for:

$$N = [C' \;\; A'C'] = \begin{bmatrix} 1 & 0 \\ 0 & 1 \end{bmatrix}$$

where C and A are defined above.

$$W = \begin{bmatrix} 1 & \alpha \\ 0 & 1 \end{bmatrix}$$

Substituting into N and W into Equation 20, the Bass-Gura formula gives:

$$(NW') = \begin{bmatrix} 1 & 0 \\ \alpha & 1 \end{bmatrix}$$

$$[(NW')]^{-1} = \begin{bmatrix} 1 & 0 \\ -\alpha & 1 \end{bmatrix}$$

The estimate of $\hat{a}$ and a matrix must be defined to solve Eq. 17.

The characteristic polynomial of the 2nd order open-loop system is defined as:

$$|\mathrm{sI - A}| = \begin{vmatrix} s & -1 \\ 0 & s+\alpha \end{vmatrix} = \mathrm{s}^2 + \alpha s \tag{22}$$

The 'a' matrix can now be derived from this characteristic equation:

$$a = \begin{bmatrix} \alpha \\ 0 \end{bmatrix} \tag{23}$$

which gives for Eq. 17:

$$k = \begin{bmatrix} k_1 \\ k_2 \end{bmatrix} = \begin{bmatrix} 1 & 0 \\ -\alpha & 1 \end{bmatrix} \left(\begin{bmatrix} \hat{a}_1 \\ \hat{a}_2 \end{bmatrix} - \begin{bmatrix} \alpha \\ 0 \end{bmatrix} \right)$$

$$k = \begin{bmatrix} k_1 \\ k_2 \end{bmatrix} = \begin{bmatrix} 1 & 0 \\ -\alpha & 1 \end{bmatrix} \begin{bmatrix} \hat{a}_1 - \alpha \\ \hat{a}_2 \end{bmatrix}$$

$$or$$

$$k_1 = \hat{a}_1 - \alpha \tag{24}$$

$$k_2 = \hat{a}_2 - \alpha(\hat{a}_1 - \alpha)$$

In Eq. 22, the characteristic polynomial of the open loop system was defined as:

$$D(s) = s^2 + \alpha s$$

The desired characteristic polynomial of the closed loop system also must be defined:

$$s^2 + \hat{a}_1 s + \hat{a}_2 = 0 \tag{25}$$

where if a_1 and a_2 are the coefficients of the desired characteristic equation, then:

$$a_1 = \alpha \qquad a_2 = 0$$
$$s^2 + \alpha s + 0 = 0$$
$$s(s + \alpha) = 0$$

If we let P_1 and P_2 represent the poles in this equation, then:

$$P_1 = 0 \text{ and } P_2 = -\alpha$$

If these values are plotted on the real and imaginary axis, an estimate of the value required for critical damping ($\hat{P}_1$ and $\hat{P}_2$) can be found. An estimate for a critically damped system could then be anywhere from -α to zero. Let the estimate be equal to:

$$\hat{P}_1 = \hat{P}_2 = -\frac{\alpha}{3}$$

Substituting these into the desired characteristic polynomial of the closed loop system:

$$\left(s + \frac{\alpha}{3}\right)\left(s + \frac{\alpha}{3}\right) \Rightarrow s^2 + \frac{2}{3}\alpha s + \frac{\alpha^2}{9} = 0$$
$$\therefore \hat{a}_1 = \frac{2}{3}\alpha \tag{26}$$
$$\therefore \hat{a}_2 = \frac{\alpha^2}{9}$$

Suitable values for α and then values K_1 and K_2 from eq. 24 and 25 can be found. These values are specific to the Hardware in the Loop equipment, the values for the Feedback Instruments Ltd.'s Modular Servo MS150 System are given below in table 2.2.2 (Appendix V):

Parameter	Value
Moment of inertia of unloaded Motor/Tach (Jm)	- $30x10^{-6}kgm^2$
Moment of inertia of Disc (Jd)	- $412x10^{-6}kgm^2$
Back emf Constant of Motor (K2)	- $60x10^{-3}rad^{-1}$
Effective back emf Constant of Motor	- $100x10^{-3}rad^{-1}$
Motor Armature Resistance (R)	- 3.2ohms
Torque Constant of Motor (K_1)	- $17x10^{-3}Nm/A$

Table 2.2.2 Values required for Feedback Instruments equipment

Therefore K_1 (Torque Gain) $=17x10^{-3}Nm/A$

K_2 (EMF Gain) $= 60x10^{-3}rad^{-1}$

J_T (Total Moment of Inertia)* $= 442x10^{-6}kgm^2$

* Total Moment of inertia includes unloaded motor and tachometer ($J_t = J_m + J_d$)

Substituting these values into the equations as follows:

$$\alpha = \frac{-K_1 K_2}{JR}$$

$$\alpha = \frac{-(17x10^{-3})(60x10^{-3})}{(442x10^{-6})(3.2)} \quad (27)$$

$$\alpha = -1.2$$

$$\beta = \frac{K_1}{JR}$$

$$\beta = \frac{17x10^{-3}}{(442x10^{-6})(3.2)} \quad (28)$$

$$\beta = 12.01$$

Eq 27 and Eq 28 can then be substituted into Eq 26:

$$\hat{a}_1 = \frac{2}{3}\alpha \qquad \hat{a}_2 = \frac{\alpha^2}{9}$$

$$\hat{a}_1 = \frac{2}{3}(-1.2) \qquad (29) \qquad \hat{a}_2 = \frac{(-1.2)^2}{9} \qquad (30)$$

$$\hat{a}_1 = -0.8 \qquad \hat{a}_2 = 0.16$$

Eq 29 and Eq 30 can then be substituted into Eq 23/24:

$$K = \begin{bmatrix} k_1 \\ k_2 \end{bmatrix} = \begin{bmatrix} 1 & 0 \\ -\alpha & 1 \end{bmatrix} \begin{bmatrix} \hat{a}_1 - \alpha \\ \hat{a}_2 \end{bmatrix} = \begin{matrix} \hat{a}_1 - \alpha \\ \hat{a}_2 - \alpha(\hat{a}_1 - \alpha) \end{matrix}$$

This gives the values of the Gain Matrix K.

$$k_1 = (\hat{a}_1 - \alpha) = \left(\frac{2}{3}(-1.2) - (-1.2)\right) = 0.4$$

$$k_2 = (\hat{a}_2 - \alpha(\hat{a}_1 - \alpha)) \Rightarrow \left(\frac{\alpha^2}{9} - \alpha\left(\frac{2}{3}\alpha - \alpha\right)\right)$$

$$k_2 = \left(\frac{\alpha^2}{9} - \left(\frac{1}{3}\alpha^2\right)\right) \Rightarrow \left(-\frac{3}{9}\alpha^2\right) \Rightarrow -.48$$

Combining the two estimated state vectors to obtain a single input to the plant gives:

$$U = -G\hat{x}$$

$$or$$

$$U = -g_1\hat{e} - g_2\hat{\omega}$$

Where g_1 and g_2 are the position and velocity gains respectively [12], and these gains are determined as follows:

First with defining a second matrix (b) from the open loop characteristic polynomial, Eq. 21:

$$b = \begin{bmatrix} \beta \\ 0 \end{bmatrix}$$

which can now be substituted into controllability test matrix Q and matrix W

$$Q = [a, ab]$$

$$Q = \begin{bmatrix} 0 & \beta \\ \beta & -\alpha\beta \end{bmatrix}$$

and

$$W = \begin{bmatrix} 1 & \alpha \\ 0 & 1 \end{bmatrix}$$

These two matrices Q and W are now ready to be calculated using the Bass-GURA formula:

$$g = [(QW)']^{-1}(\hat{a} - a)$$

$$QW = \begin{bmatrix} 0 & \beta \\ \beta & 0 \end{bmatrix}$$

$$QW' = \begin{bmatrix} 0 & \beta \\ \beta & 0 \end{bmatrix}$$

$$[QW']^{-1} = \begin{bmatrix} 0 & 1/\beta \\ 1/\beta & 0 \end{bmatrix}$$

$$g = \begin{bmatrix} 0 & 1/\beta \\ 1/\beta & 0 \end{bmatrix}(\hat{a} - a) \qquad (31)$$

Substituting Matrix A now gives:

$$g = \begin{bmatrix} 0 & 1/\beta \\ 1/\beta & 0 \end{bmatrix} \begin{bmatrix} \hat{a}_1 - \alpha \\ \hat{a}_2 \end{bmatrix}$$

or

$$g = \begin{bmatrix} \hat{a}_2 / \beta \\ (\hat{a}_1 - \alpha)/\beta \end{bmatrix} \tag{32}$$

Using the values from Eq. 27 – Eq. 30 gives

$$g_1 = \hat{a}_2 / \beta$$
$$g_1 = 0.16/12.01$$
$$= .01332$$
$$g_2 = (\hat{a}_1 - \alpha)/\beta = (-.8 - (-1.2))/12.01 = 4.804$$

This now defines all variables for the Luenberger linear observer and it takes the form as shown below in figure 2.3.4.

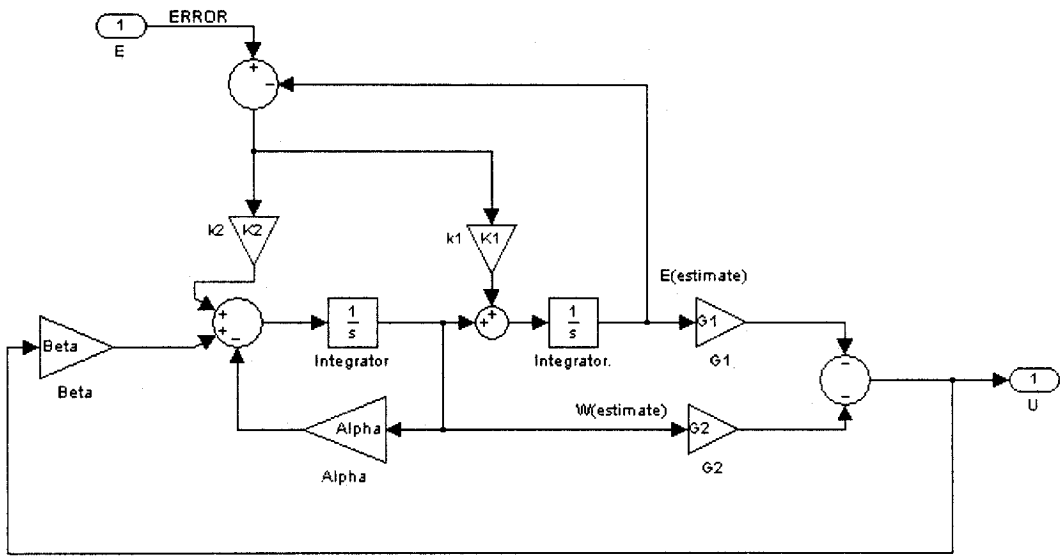

Figure 2.3.4 Complete Luenberger Linear Observer

2.4 Software Implementation:

The linear observer is ready to implement with the software and eventually with the hardware in the loop setup. For every xPC target program, run with MATLAB, basically two files are required a Simulink Model Front Panel, and an xPC target Simulink model.

Simulink Model Front Panel – This block diagram is so named because it interfaces with the user and it is used to change variables while the program is running. Once the xPC target Simulink file is downloaded to the target computer, this file is the only means to "communicate" with the program.

xPC Target Simulink Model – In this file are the blocks that run the target computer, the Simulink blocks, including any files used to communicate the target PC with the DAQ.

The xPC target Simulink model and the linear observer, and can be seen in figure 2.4.1.

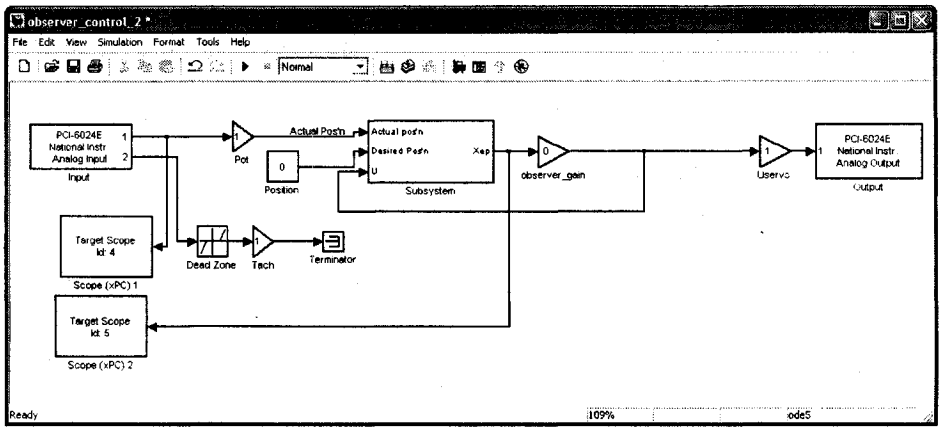

Figure 2.4.1 xPC Target Simulink model with observer

The interface to the NI PCI-6024E DAQ can be seen in this Simulink file, in the form of the analog input and output, as well as the observer subsystem.

The observer subsystem can be seen in figure 2.4.2.

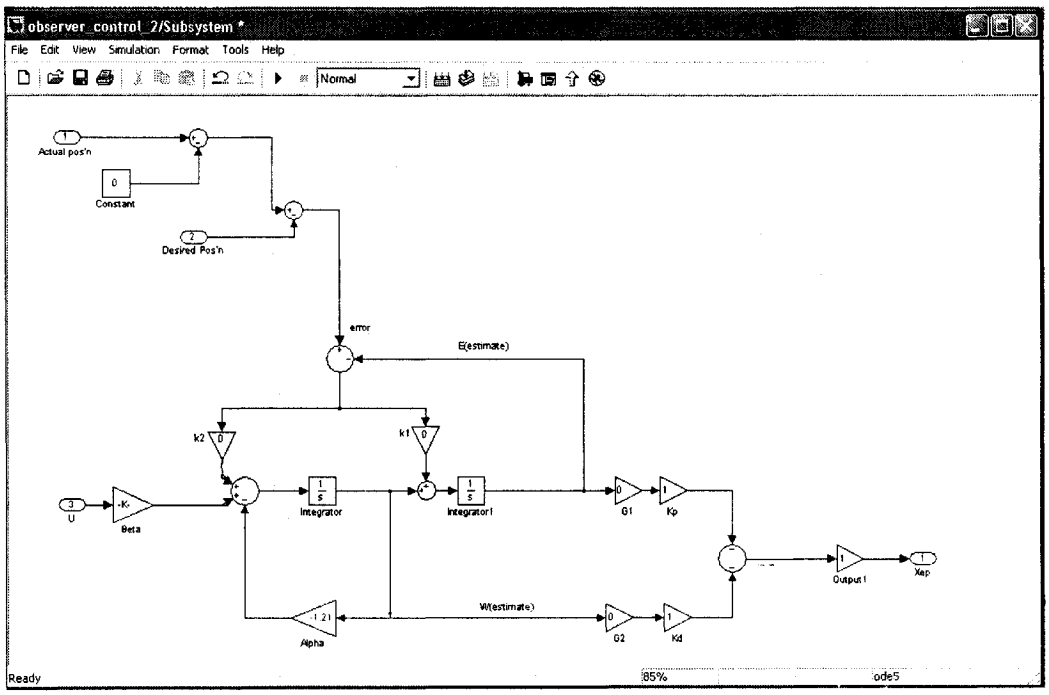

Figure 2.4.2 Observer subsystem

The next stage was to make the Target PC and DAQ communicate with the Feedback Instruments equipment, and this required that the tachometer, the operational

amplifier and the output potentiometer be connected with the DAQ as shown below in figure 2.4.3.

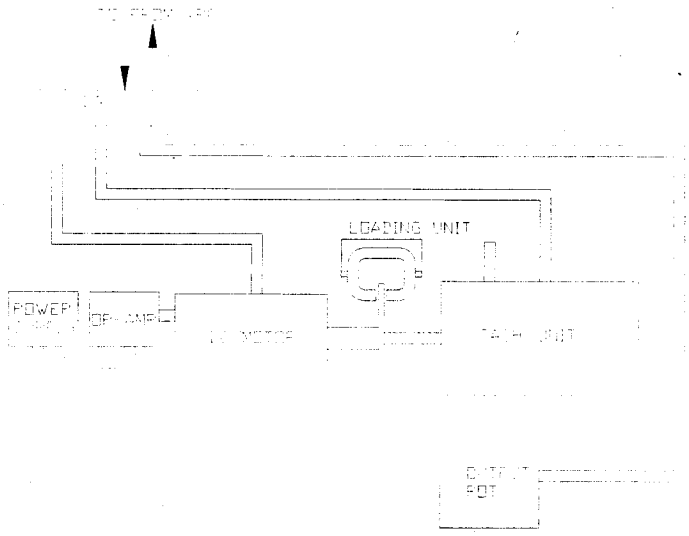

Figure 2.4. 3 Wiring and layout of Feedback Instruments equipment

At this stage, the xPC Target Simulink Model file communicates with all the hardware of the Feedback Instruments setup. The Simulink front end panel file is now required to be able to communicate with the user. The file for this application was required to follow the criteria:

1. User Interface – The user must be able to change the desired input, in this case angular position.
2. User Output – For calculating and displaying both the experiments results and the positional error of the setup. In this form, the problems are easily identified and resolved.
3. Gains and Parameters –The gains and parameters can be changed through the Simulink front end panel file at this stage; this prevents time-inefficient reconfiguring and recompiling of the xPC Target Simulink Model File.

Having defined the requirements, next step is to start building the file; that basically contained all the parameters that are required for the equipment to communicate with each other and to the user.

The flow of information is as follows:

User → System

1. User Input –the user inputs the desired Angular Position (θ_D)
2. Conversion – converting degrees to voltage required for the output potentiometer.
3. Observer Input –values are sent to the xPC Target Simulink file

System → User

1. Angular Position – the angular Position of the DC motor is returned in terms of voltage.
2. Conversion – the position is again converted, this time from voltage to degrees, so the user can reread the values and compare.
3. Display to the user – The positional values are then displayed to the user.

Information from System ←→ Information from User

A large amount of data is continuously "cross talked" back and forth between the two file requirements this data includes values for the gains (G and K Matrix values). The values are sent and their resultant mathematical products are watched and plotted, to verify that the observer is working correctly.

The Simulink front panel was constructed, with all these criteria, and can be seen below in figure 2.4.4.

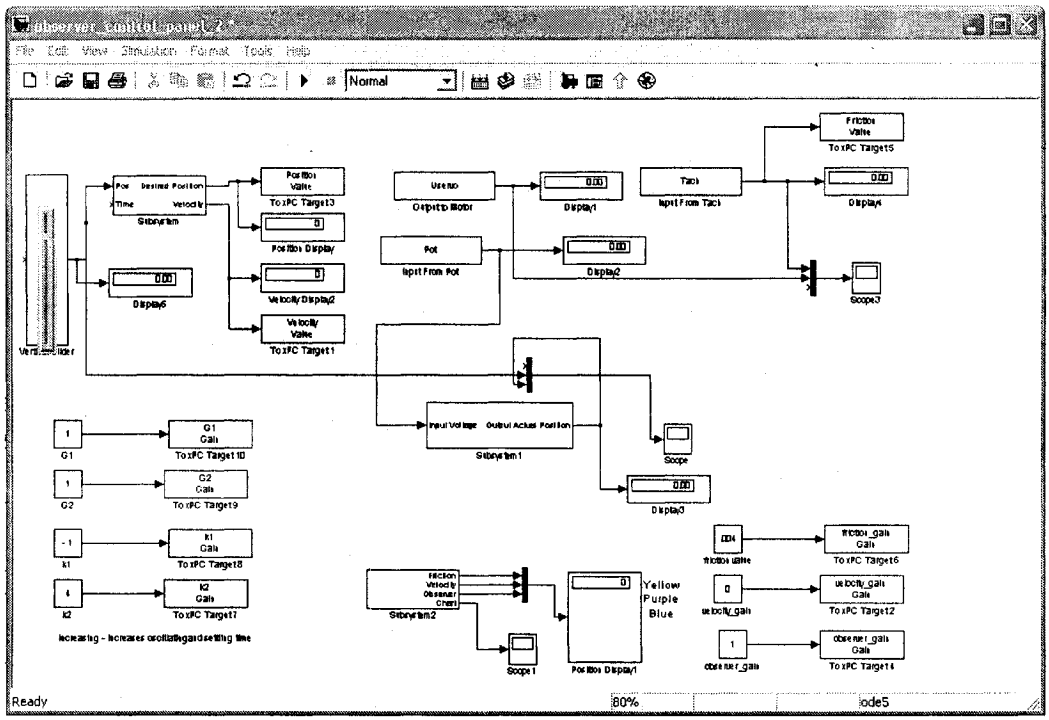

Figure 2.4.4 Simulink front panel for controlling equipment

2.5 Observer Development Results

After the equipment communicates correctly the next step is to gather data and interpret the observers results. The system was completely calibrated and then reset to zero degrees, a step input of 45 degrees was applied to the system, and the results can be seen in figure 2.5.1.

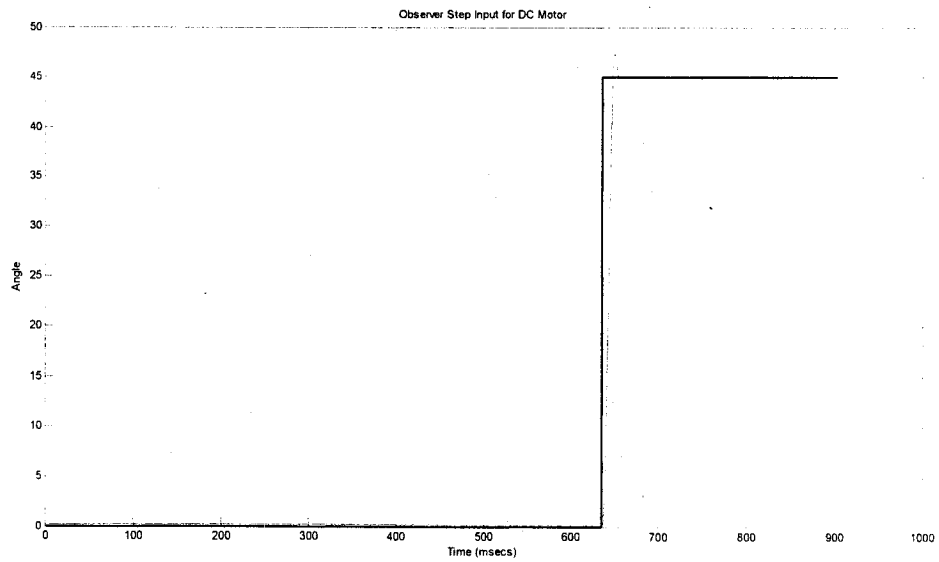

Figure 2.5.1 Observer response to 45° step input

It can be seen that the observer works well, but it has a significant amount of overshooting, most probably as a result of friction. A solution to a similar problem using the observer based control system was used very successfully by the Cologne Laboratory of Mechatronics (CLM) from the University of Applied Sciences Cologne, Germany, to investigate the effects of friction on a high speed, highly accurate electromechanical Positioning System (EMPS) [18]. The EMPS, which can be seen in Figure 2.5.2, uses a current controlled DC motor to drive a backlash free ballscrew drive linear positioning unit. The unit converts the rotary movement of the DC motor to displace the carriage linearly. Through measuring the position of the carriage at high precision (1.25 μm) and then controlling the input voltage to the DC motor, the CLM group claims that the setup they have developed very closely mimics drive systems used in industrial applications such as machine tools or robotics. [18]

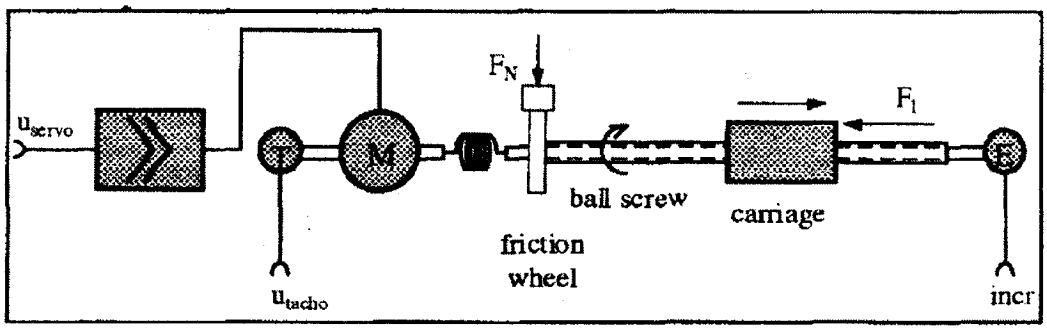

Figure 2.5.2 Electromechanical Positioning System (EMPS) used by CLM

The CLM group uses an observer with a feedforward value of the velocity of the DC motor to provide compensation for the static torque in the system. The system differentiates between the effect different directions of motion has on friction by the direction of the motor, and then gives a positive or a negative friction torque value. Their controller is shown in figure 2.5.3 [18], where the feedforward of the velocity value (φ_r) are displayed.

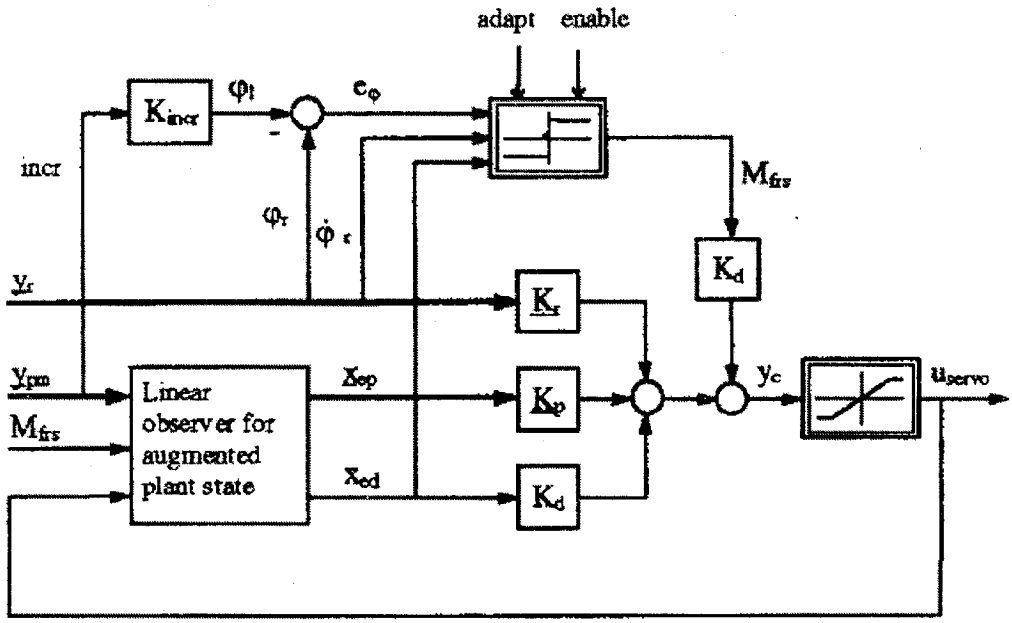

Figure 2.5.3 CLM Controller with Feedforward Friction compensation

The conclusion of CLM investigation is:

"Compensation of friction by feedforward of a suitable estimate for this non-measurable disturbance is a feasible method to reduce the position errors in the control of drives with friction. A linear estimate was evaluated with a linear observer for the plant which was augmented by an appropriate disturbance model. The friction compensation scheme is well suitable for numerous applications. It turned out to be very robust and is easy to realize."[18].

This method was then applied in this thesis for the observer design. The velocity was calculated in the Simulink Front End Panel file in terms of Voltage/Sec, such that by using these unusual units, no rounding error was created. This is very crucial as the value for the coefficient of friction in this particular setup was estimated to be very small (.0004). The velocity value was then feedforward to the output of the observer, where the two values were coupled, as is shown below in figure 2.5.4.

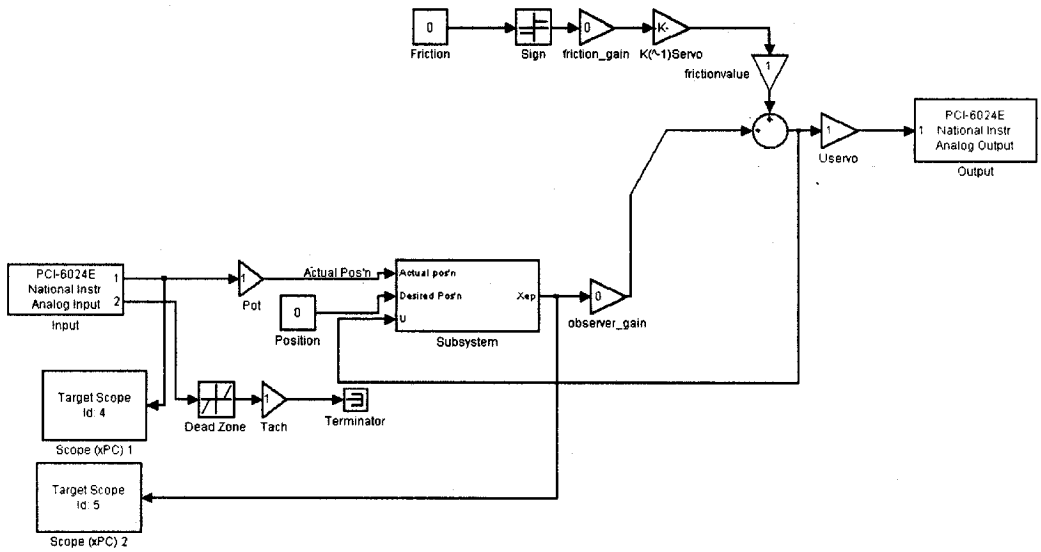

Figure 2.5.4 Linear observer with feedforward friction value

The significant improvement of the response to the step input is shown below in figure 2.5.5.

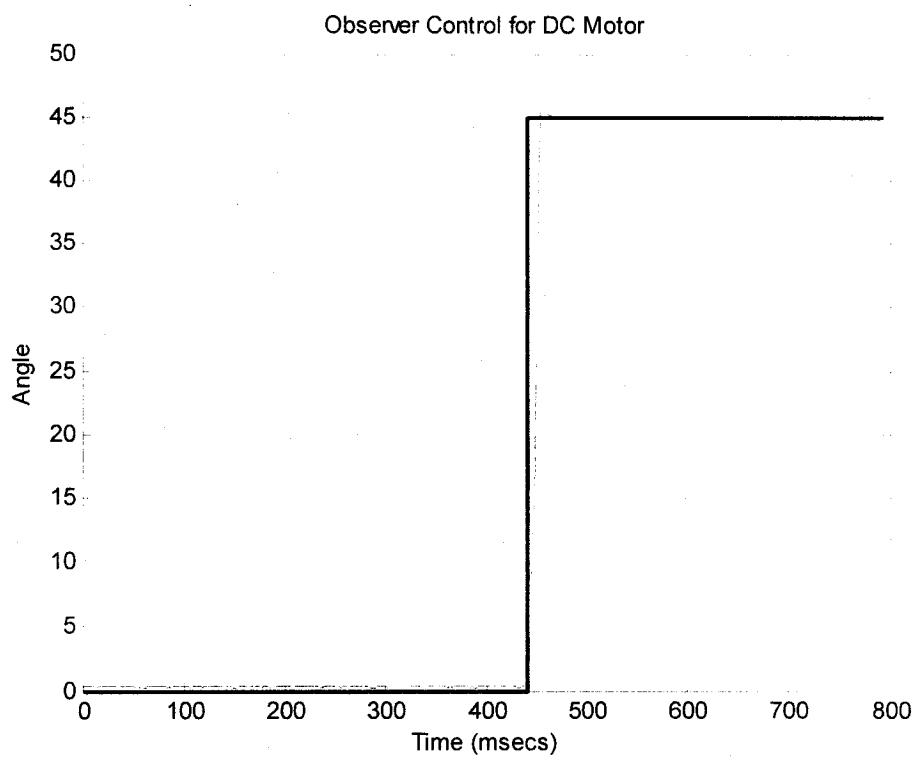

Figure 2.5.5 Linear Observer with feedforward friction - response to step input

CHAPTER 3
TENDON-MANIPULATOR DEVICE

3.1 Introduction:

After finalizing the simulations and the observer, documented in Chapter 2, the next step was to build a tendon-manipulator device. In this phase a one Degree-of-Freedom (DOF) system was developed, which would then lend help to designing a three DOF system.

3.2 Device Requirements:

The first phase in building this apparatus was to consider what functions it would have to perform:

1. Position Control – required to measure and provide feedback on angular position
2. Low Friction –to avoid detrimental affects of high friction which would degrade performance.
3. Versatility – to allow for research and development and retrofitting of the equipment, if required.
4. Size – for a concept-proving design, size is not an imposing problem, however should be substantial enough to allow adjustments to be easily made and to be possible use "off-the-shelf" products.

After some research, a suitable device was found in the form of a system manufactured by ECP (Educational Control Products) under the name of Model 505:

Inverted Pendulum. The device is described in detail in Appendix VI, and can be seen below in figure 3.2.1.

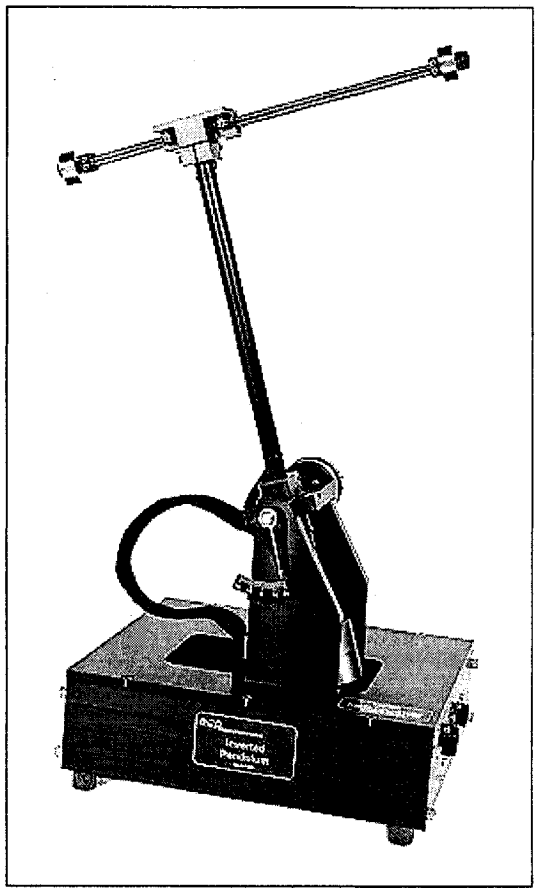

Figure 3.2.1 ECP Model 505: Inverted Pendulum

This device proved to be suitable for this study. The device contains a large number of components that could be modified and utilized as required.

The inverted pendulum according to ECP is

"not the conventional rod-on-cart inverted pendulum, but rather steers a horizontal rod in the presence of gravity to balance and control the vertical rod" [17]

The inverted pendulum can be seen in figure 3.2.2. [12]

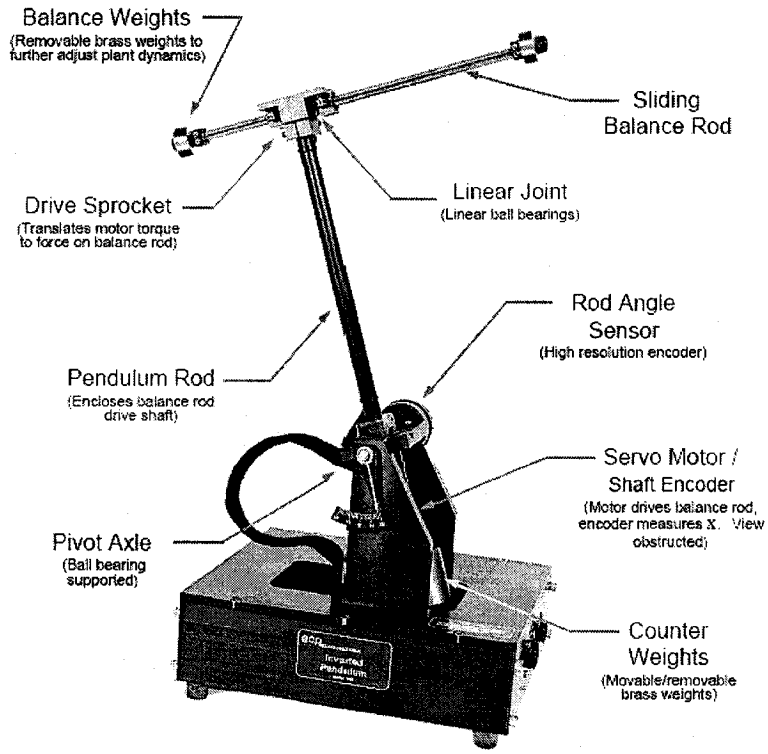

Figure 3.2.2 Breakdown of ECP Model 505: Inverted Pendulum

With some slight modifications this device will satisfy all criteria outlined above to be met. All shafts and moving components are either ball or roller bearing equipped, the vertical rod already had an optical encoder to measure angular velocity, and the pendulum even had the ability to add or remove counterweights.

3.3 Device Retrofitting:

Retrofitting of the device consisted of creating a Computer Aided Design (CAD) model, using a 3D CAD/CAE package, SolidWorks 2003, The device was measured using common engineering metrology tools (calipers, verniers, etc) and reproduced into the SolidWorks CAD package. The Inverted Pendulum can be seen in Figure 3.3.1, stripped down to its essential components and before any modifications took place, optical encoder as well as the vertical rod are omitted for clarity.

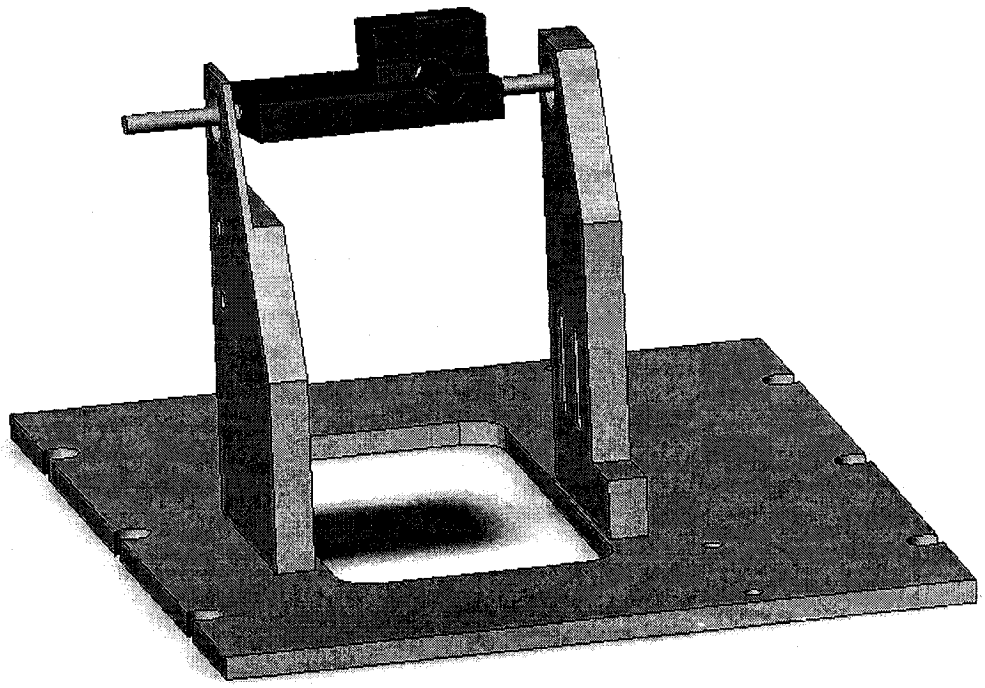

Figure 3.3.1 SolidWorks model of ECP Model 505: Inverted Pendulum

The first step in developing the tendon-manipulated device was to acquire the actuators to drive the tendons and the pulleys which would handle the actual tendon. The motors chosen to deliver the power to the tendon were dual Pittman DC Electric Servomotors, Harleysville, PA, USA No: GM14602D261, (see Appendix III for

further information). These motors were chosen because they were readily available, offered a large gear reduction (75:1) and, if further work was required, each motor was already equipped with an optical encoder on its output shaft.

The placement and layout of the two motors can be seen below in figure 3.3.2.

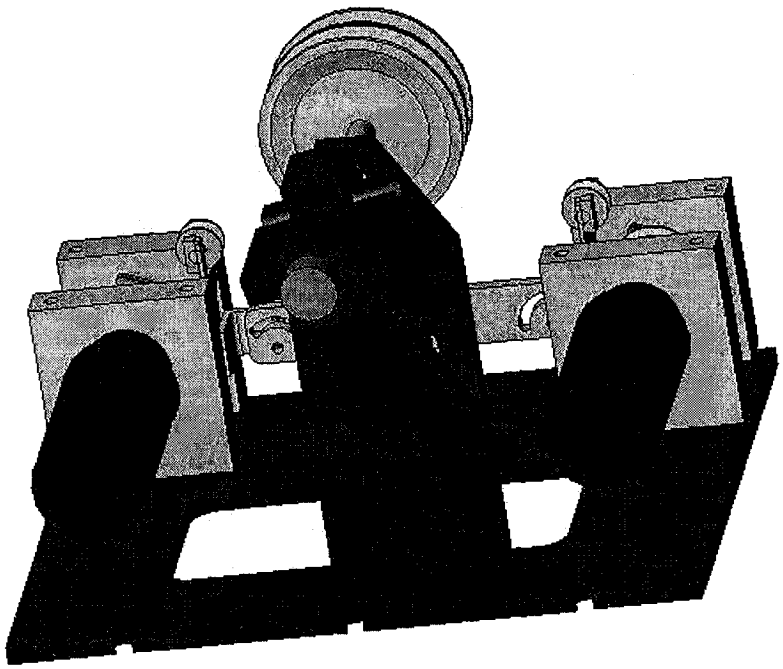

Figure 3.3.2 Placement of the Pittman DC motors

On the pivot shaft of the main rotor (vertical shaft omitted from view) two standard ½" V belt Pulleys with ¼" inside diameters were purchased and installed onto a common shaft but the two motors for this application were required to have custom made pulleys. All component drawings can be seen in Appendix I. With the tendon

routed and the pulleys installed, the next step was to develop a system that would ensure that the tendon was kept in acceptable tension at all times.

For this purpose a pulley on a cantilever beam where the tendon would ride up and over, was built to provide feedback, as to when the tendon was in tension and when it was not. The concept can be seen below in figure 3.3.3.

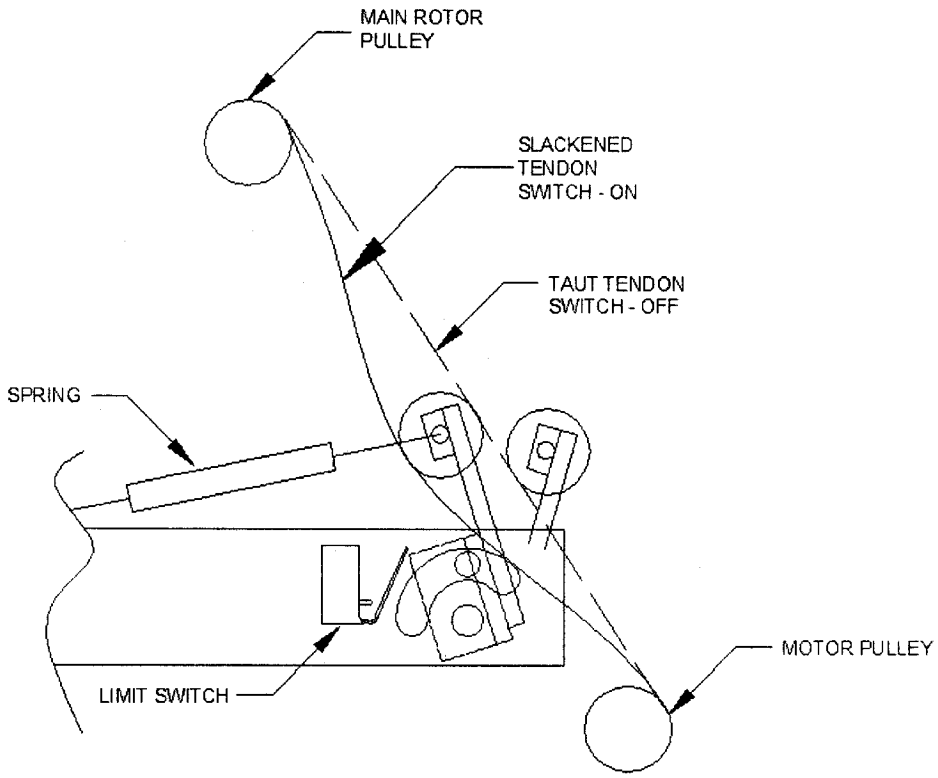

Figure 3.3.3 Conceptual drawing of tendon tension system

Packaging the tendon tensioning system proved to be quite difficult and the only solution was custom made parts with micro switches. It was found that two limit micro switches would be suitable for use, these limit switches basically either sense whether the tendon is tight enough, they are not able to measure the tendon tension

which would prove to be a problem later. The fully packaged and finished assembly is shown below in figure 3.3.4 and figure 3.3.5.

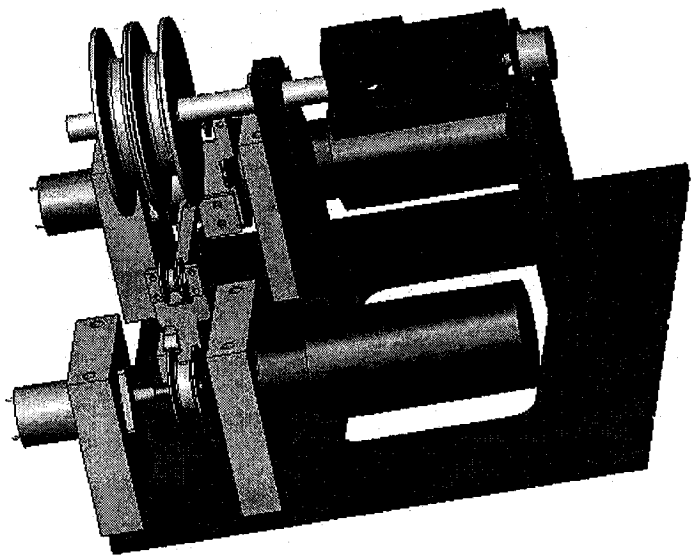

Figure 3.3.4 Completed modified inverted pendulum with tendon tension system

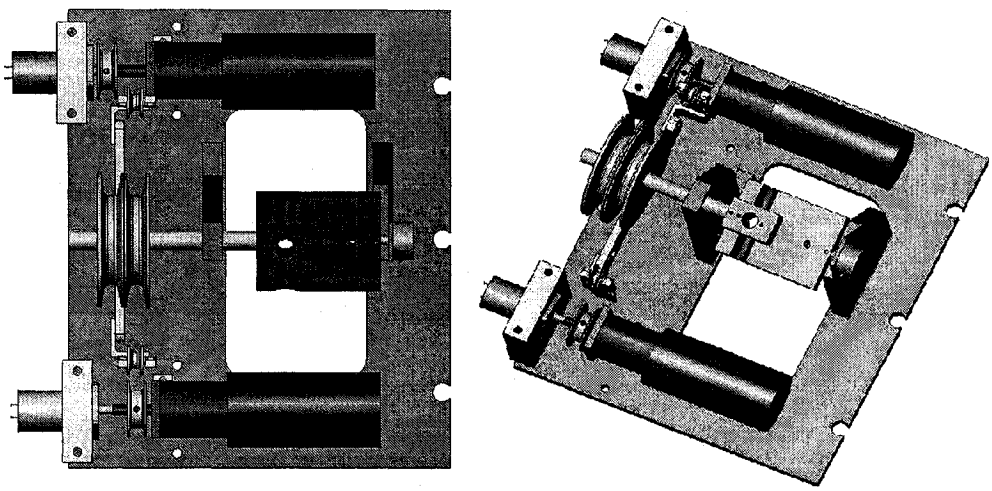

Figure 3.3.5 Completed modified inverted pendulum views

It was first observed during initial testing of the tendon-driven experiment was that any amount of slack in the tendons would create a downward spiraling unstable system, the solution was to control each motor independently and to monitor the angular position of the actual wrist joint. It is a well known fact that no two identical motors will have the same performance, this is due to many factors, friction, useable life of the motor, slight differences in op-amp gains, etc. To check the differences in the performance of the motors, two tests were run.

The first test was checking the current drawn by the individual motors at varying voltage inputs, shown in figure 3.3.6.

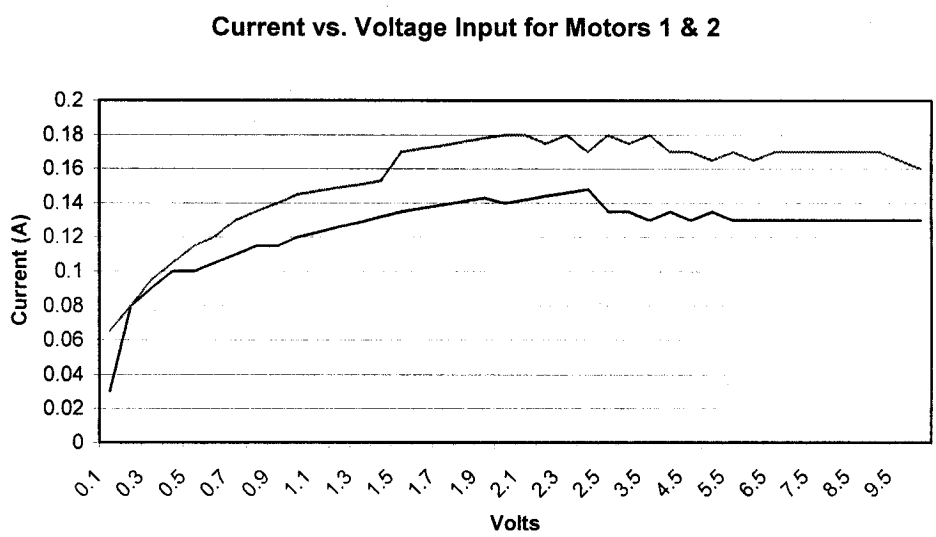

Figure 3.3.6 Plot of Current vs. Voltage for Motors 1&2

The average current difference in the two motors over the 0 – 10 V input is 0.0296 A and the maximum difference is 0.05 A. Therefore, this could result in a torque

difference of .1375*10^{-3}N-m/A. The second test to measure the differences in motor performance was to plot RPM vs. volts, this can be seen in figure 3.3.7

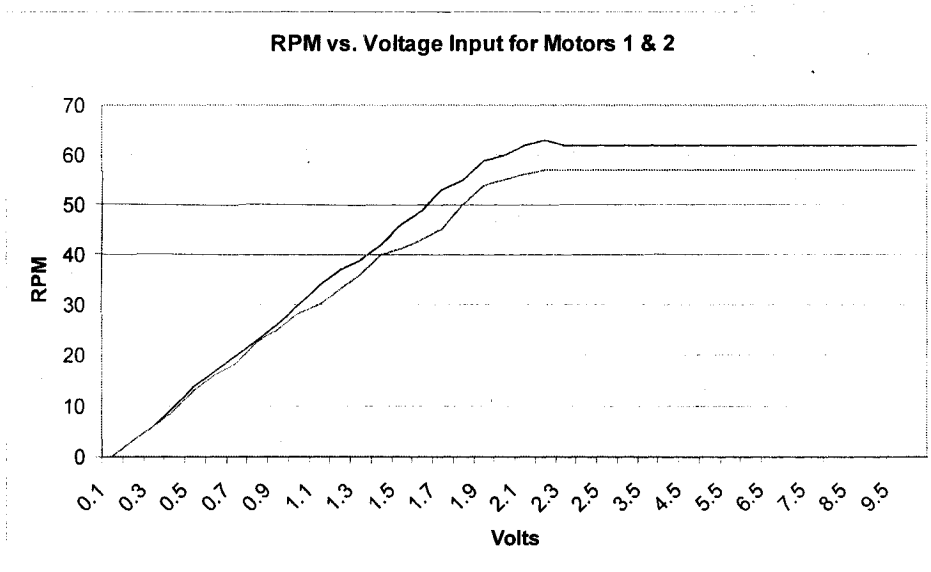

Figure 3.3.7 Plot of angular velocity [rpm] vs. voltage for motors 1 & 2

The average difference over the range of volts is 3.8 rpm and the maximum difference is 8 rpm. This shows how important it is for the two DC motors to be closely monitored and controlled. The motors were overseen by installing two DC tacho-generators (Servo-Tek Type SB 740B-1, Appendix VII). These tachometers would serve for monitoring and feedback control to ensure that both monitors were turning in equal time. Although this is not ideal, as it would have been in the case of using optical encoders, the limitations of the experimental system (xPC and National Instruments DAQ) limited the experiment to only monitoring speed.

The dual tachometers were placed at the output side of the DC motors (same side as the pulley) instead of the opposite end. In that manner the tachometers were subjected

to the same velocity as the pulley, as opposed to the opposite end, which is not run through the geartrain. The position measurement of the main rotation shaft is monitored by an analog potentiometer, mounted on the end of the shaft opposite the pulleys. The movement of the shaft, which is limited to 90 degrees of rotation by the nature of the retrofitted machine, means that the potentiometer is more than accurate enough for this application.

3.4 Control System Development:

The control system was implemented on xPC Target. The first step was to build the xPC target Simulink Model, as with earlier xPC target files. The block diagram is relatively simple as all the work is done by the Simulink Front End panel file. The tendon driven manipulator xPC target Simulink Model can be seen below in figure 3.4.1 below.

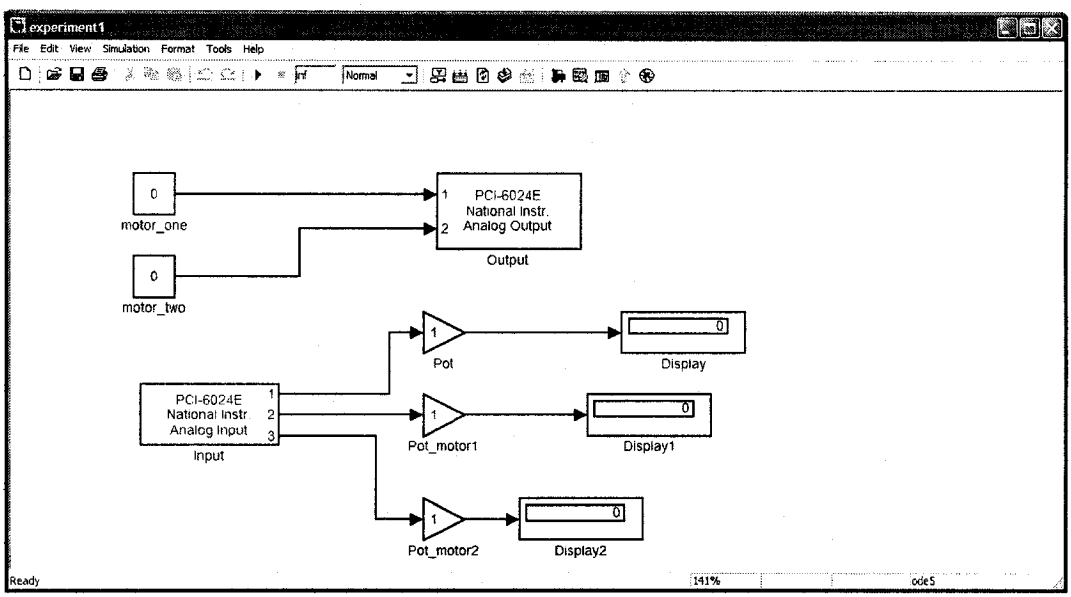

Figure 3.4.1 xPC Target Simulink model file

The main purpose of this file is to control the DAQ and to communicate with the Simulink Front End Panel file. The file has two main flows: the first from the Simulink Front End Panel to the DAQ and, the second, for information from the DAQ to the Simulink Front End Panel.

All calculations are therefore done in the Simulink Front End Panel file. The Simulink front end panel file is shown below in figure 3.4.2.

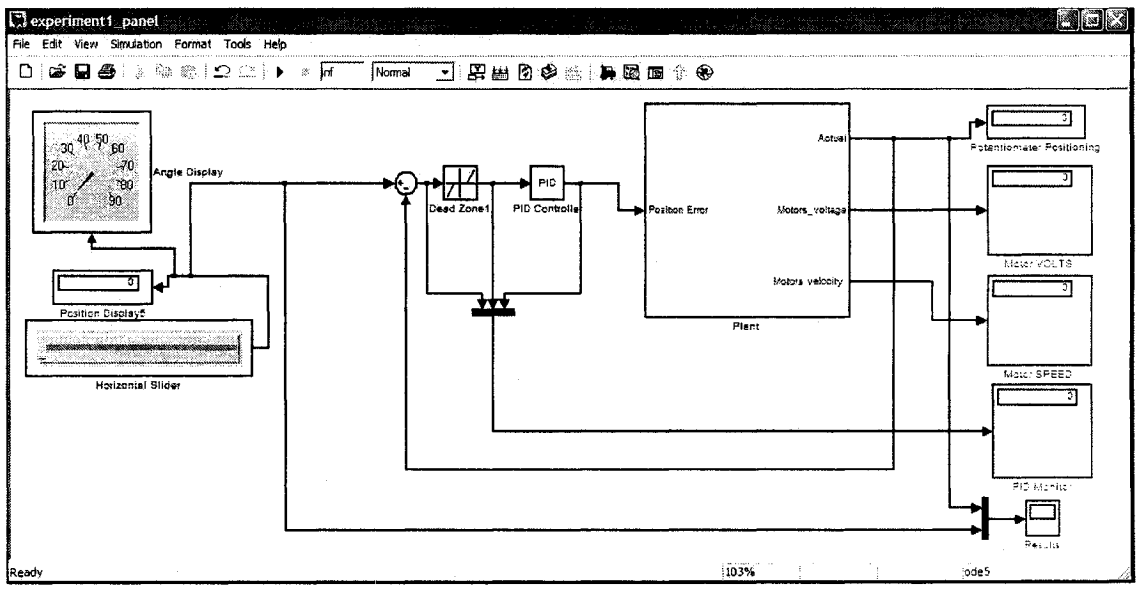

Figure 3.4.2 Simulink Front End Panel File

The Simulink Front End Panel File can be broken down into three basic components

1. User Input – The user inputs the amount of angle that is desired (for this system between 0 - 90°) by a horizontal slider bar, displayed on an angular gauge.

2. PID, Plant & Feedback loop – The Control system feedback in this case PID, Plant and Feedback loop are the main blocks, with numerous subsystems contained within.

3. Display Output via Front End Panel – For the results to be monitored and viewed.

The three components can be seen below in figure 3.4.3.

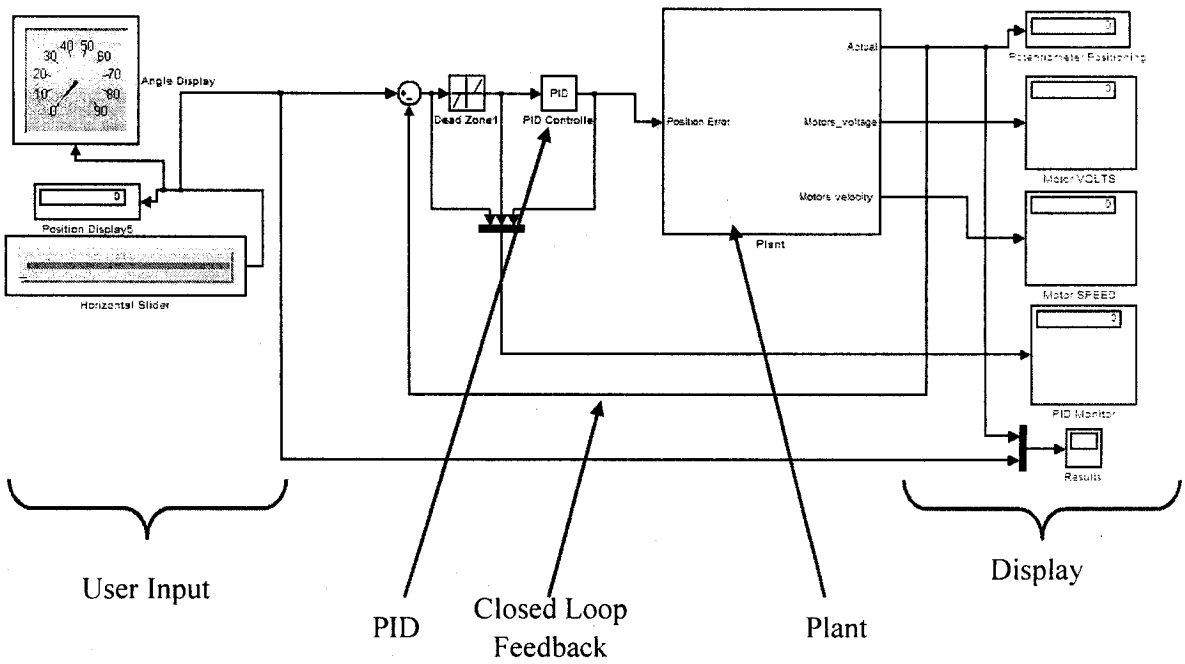

Figure 3.4.3 Breakdown of functions within Simulink front end panel

In the Simulink diagram, in front of the PID controller block, is a dead zone block, as can be seen in figure 3.4.3, that is set to exclude passing of very small errors into the PID controller (±0.25°). This is done so that these very small differences in error,

which can often be due to fluctuations of the potentiometer's signal, are ignored and do not cause excessive "deterring". Once the desired angle is entered and compared to the feedback from the actual angle, the error is the passed through the PID controller and is the command sent to the plant. This subsystem can be seen in figure 3.4.4 below.

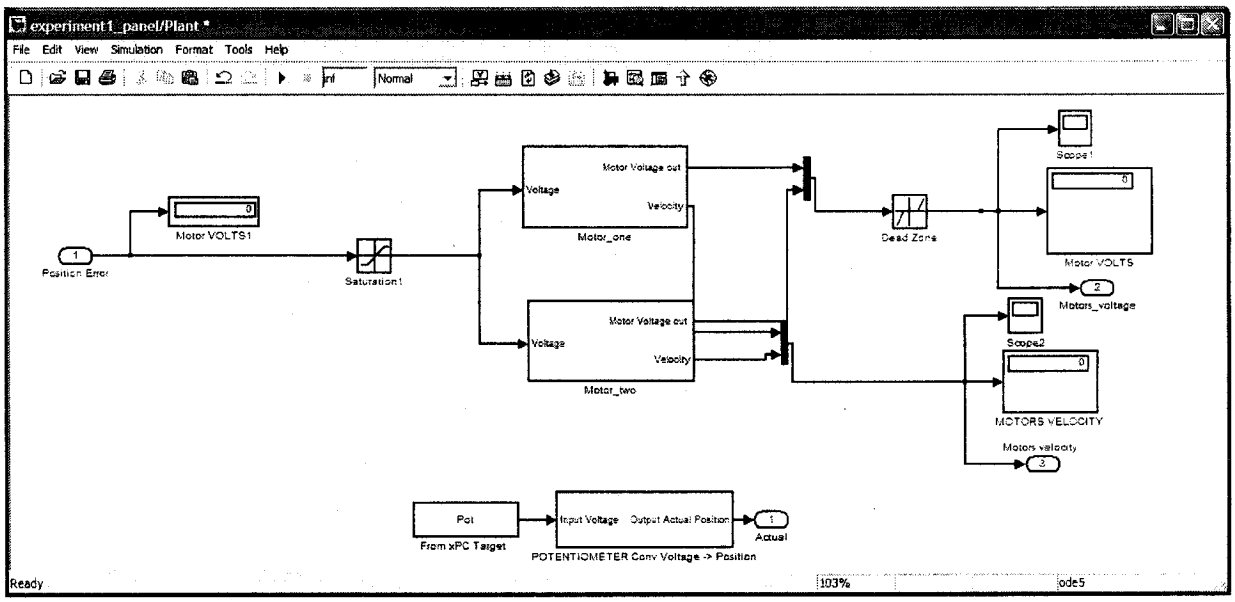

Figure 3.4.4 Plant subsystem

The main objective of the plant subsystem is to take the PID value for the position error and calculate the voltage commands to be sent to the two DC motors. Before any voltage is applied to the DC motors it is passed through a saturation block as seen in figure 3.4.4, such that no voltages greater than ±10 volts will pass, thereby protecting the DAQ board from voltages higher than its allotted amount. Also, enclosed in this plant subsystem, shown in figure 3.4.4, is the potentiometer

block converting voltage to position. The input in volts, sent from the xPC Target Simulink file is converted to angular position for the user to read.

After voltage saturation, the signal is sent to each of the two DC motors.

Analyzing only one of these subsystem blocks, (as they are identical in structure), another subsystem and subsequently another PD controller are contained within.

Figure 3.4.5 details what is contained within these DC motor subsystems.

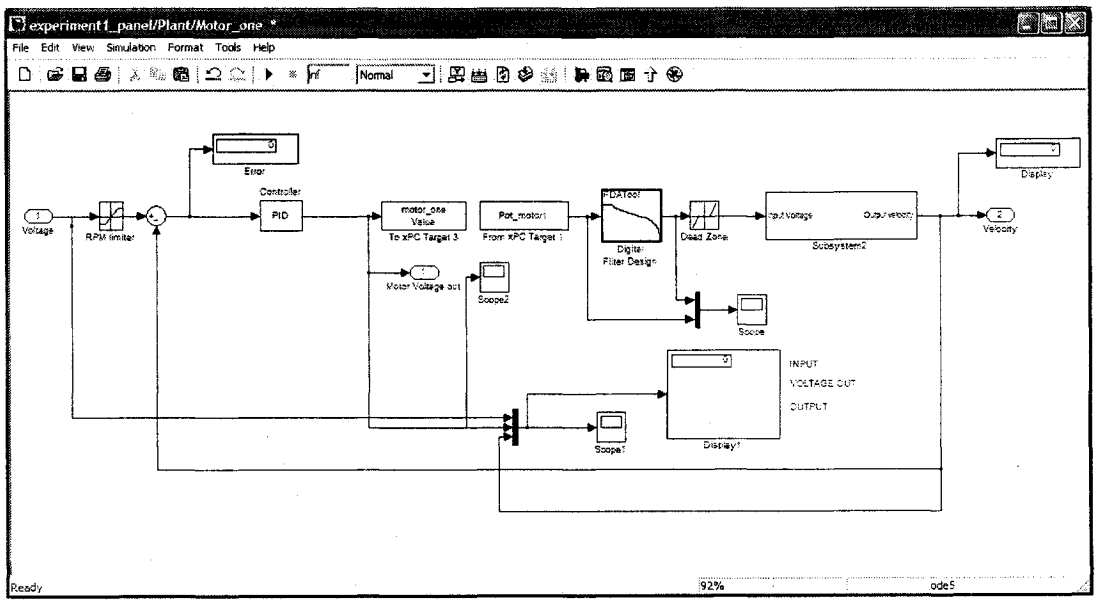

Figure 3.4.5 DC motor subsystem

The DC motor subsystem is the center of all the motor functions; the flow of the functions through this block is shown in figure 3.4.6.

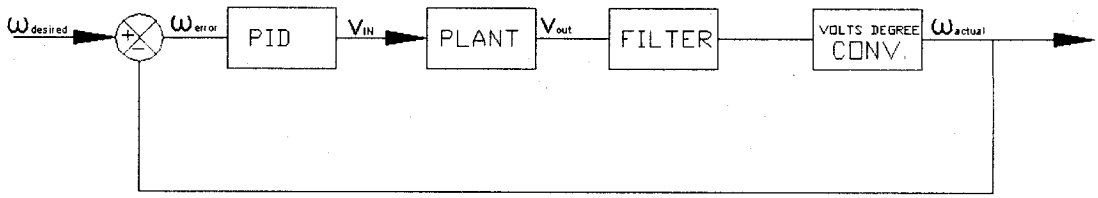

Figure 3.4.6 DC motor subsystem block diagram

In figure 34.6 it is shown that the velocity error (ω_{error}) is fed into the PID control system and thus calculates the voltage command that is to be sent to the plant, through the analog input ports of xPC.

3.5 DC Motor Transfer Function Derivation:

To determine the values for the PD control system that would control the velocity of the DC motor, the transfer function would have to be derived. The motor torque (T) is directly related to the armature current (i) by the torque constant factor (K_t):

$$T = K_t i$$

whereby the back electromagnetic force (emf) (E_m) is directly related to the rotational velocity (ω) by the electrical constant (K_e)

$$E_m = K_e \omega$$

Modeling the diagram of a DC motor will aid in the derivation of the electrical portion of the transfer function. The diagram can be seen in figure 3.5.1. [15]

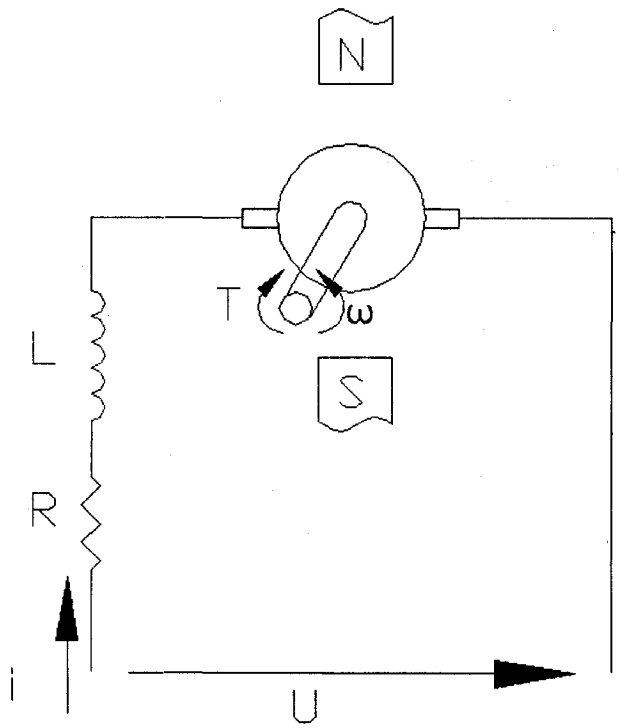

Figure 3.5.1 Diagram of a DC motor

From the above figure and using Newton's second law combined with Kirchhoff's law, the following equation can be acquired to show the voltage (U) drop:

$$U = Ri + l\frac{di}{dt} + E_m$$

where the armature-winding resistance (R) is a function of current (i) and armature winding inductance (L) added to the back emf (E_m), which was obtained earlier. Figure 3.5.2, shows a free-body diagram (FBD), which is required to obtain the final equation for a DC motor. [15]

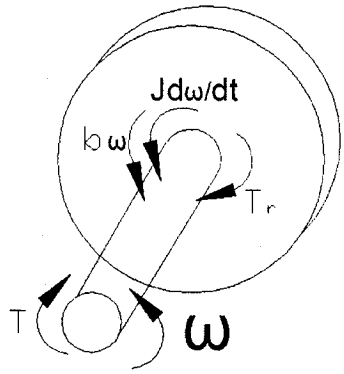

Figure 3.5.2 FBD of mechanical portion of DC motor

The mechanical portion must be analyzed, to obtain the final equation of the system:

$$J\frac{d\omega}{dt} = T_r - b\omega - T$$

Two differential equations, two algebraic equations and six unknowns (T, ω, T_r, E_m, i, and U), can be further reduced by taking the laplace transforms. Before this is done using the algebraic equations, two variables can be eliminated, the internal variables of the rotor torque (T_r) and the back emf (E_m):

$$U(s) = Ri(s) + Li(s) + E_m(s)$$
$$E_m(s) = K_e\omega(s)$$
$$T_r(s) = K_t i(s)$$
$$Js\omega(s) = T_r(s) - b\omega(s) - T(s)$$

Next step in attaining the transfer function of the DC motor, is to start combining and reducing the equations, by combining the last two equations:

$$Js\omega(s) = K_t i(s) - b\omega(s) - T(s)$$

$$i(s) = \left[Js\omega(s) + b\omega(s) - T(s)\right] \cdot \frac{1}{K_t}$$

Taking this newly obtained equation, combining it with the back emf equation and substituting it into the equation for voltage gives:

$$U(s) = \left[R + L\right] i(s) + E_m(\mathrm{s})$$

$$i(s) = \frac{1}{K_t}\left[Js^2\theta(s) + b(s)\theta(s)\right]$$

$$E_m(s) = K_e(s) \cdot \omega(s)$$

$$U(s) = \left[R + L\right] \cdot \frac{1}{K_t}\left[Js^2\theta(s) + b(s)\theta(s)\right] + K_e(s) \cdot \omega(s)$$

This new equation now can be used to give the following transfer function:

$$U(s) = R \cdot \left[\frac{R}{L}(s+1)\right] \cdot \frac{b}{K_t}\mathrm{s} \cdot \theta(s)\left[\frac{J}{b}s + 1\right] + K_e(s) \cdot \omega(s)$$

$$= \frac{Rb}{K_t}\mathrm{s} \cdot \theta(s)\left[\left(\frac{L}{R}(s+1)\right)\left(\frac{J}{b}(s+1)\right)\right] + K_e(s) \cdot \omega(s)$$

Substituting $\tau_a = \frac{L}{R}$ and $\tau_m = \frac{J}{b}$ into the equation to simplify further yields the final transfer function of a DC motor.

$$\frac{S\cdot\omega(s)}{U(s)}=\frac{\frac{K_t}{Rb}}{\tau_m\tau_a S^2+(\tau_a+\tau_m)S+\left[\frac{K_eK_t}{Rb}+1\right]}$$

The values for the parameters, taken from the PITTMAN DC catalogue (appendix III) are shown in table 3.5.1:

Parameter	Nomenclature	Value
Torque Constant	K_t	$27.5*10^{-3}$N-m/A
Electrical Constant	K_e	$27.3*10^{-3}$Vs/Rad
Moment of Inertia	J	$1.62*10^{-5}$kg/m^2
Armature-Winding Resistance	R	0.45Ω
Armature-Winding Inductance (negligible)	L	$5.5*10^{-3}$
Viscous Friction Coefficient of Motor (negligible)	b	.0001
Viscous Friction of Load (negligible)	B_l	.0001

Table 3.5.1 PITTMAN DC motor parameters

These values can now be entered into the transfer function which gives:

$$\frac{U(s)}{\theta(s)}=\frac{\frac{27.5*10^{-3}}{(.45)(.000)}}{\left[\left(\frac{1*10^{-3}}{.45}\right)\left(\frac{1.62*10^{-5}}{.0001}\right)S^2\right]+\left[\left(\frac{1*10^{-3}}{.45}\right)+\left(\frac{1.62*10^{-5}}{.0001}\right)\right]S+\left[\frac{(27.3*10^{-3})(27.5*10^{-3})}{(.45)(.000)}+1\right]}$$

$$\frac{U(s)}{\theta(s)}=\frac{61111}{3.5*10^{-5}S^2+1622*10^{-2}S+17.68}$$

PID controller transfer function is: [21]

$$G_c(s)=K_p\left(1+\frac{1}{T_is}+T_ds\right)$$

The characteristic equation for the closed-loop system is given by:

$$3.5*10^{-5}s^2+16.22*10^{-2}s+17.68+K_p=0$$

Using the Routh-Hurwitz stability criterion, the Routh array becomes:

$$\begin{array}{lll} s^2 & 3.5*10^{-5} & 17.68 \\ s^1 & 16.22*10^{-2} & K_p \\ s^0 & \dfrac{2.867-3.5*10^{-5}K_p}{16.22*10^{-2}} & \end{array}$$

Now setting the equation to zero and solving for K_p will give the critical gain.

$$\frac{2.867-3.5*10^{-5}K_p}{16.22*10^{-2}}=0$$
$$K_p=17.67*10^{-3}-2.15*10^{-8}$$
$$K_p\approx .02$$

The critical gain, was chosen as $K_{CR}= 0.02$, and the characteristic equation now becomes:

$$3.5*10^{-5}s^2+16.22*10^{-2}s+17.7+0.02=0$$

To find the frequency of oscillation, substituting $s = j\omega$ into the characteristic equation gives:

$$3.5*10^{-5}(j\omega)^2+16.22*10^{-2}(j\omega)+17.7=0$$
$$-3.5*10^{-5}\omega^2+16.22*10^{-2}j\omega+17.7=0$$

Giving the values of:

$$\omega=-3480 \text{ or } 8114.28$$

From these two values, the frequency of the sustained oscillation can then be determined,

$$P_{cr} = \frac{2\pi}{\omega}$$

$$P_{cr} = \frac{2\pi}{-1606} = -.0018$$

$$P_{cr} = \frac{2\pi}{233919.6} = 7.74 * 10^{-4}$$

The smaller value ($2.68*10^{-5}$) as it is very closely approaching zero, is ignored. Table 3.5.2 from the Ziegler-Nichols Tuning Rule based is required to solve for the gains: [21]

Type Of Controller	K_p	T_i	T_d
P	$0.5K_{cr}$	∞	0
PI	$0.45\ K_{cr}$	$1/1.2P_{cr}$	0
PID	$0.6\ K_{cr}$	$0.5P_{cr}$	$0.125P_{cr}$

Table 3.5.2 Ziegler Nichols tuning rule parameters

Using the value of K_{cr} and P_{cr}, the values that are finally determined are shown as below, respectively.

$$K_p = 0.6K_{cr} = 0.12$$

$$T_i = 0.5P_{cr} = -0.0009$$

$$Td = 0.125P_{cr} = -2.25 * 10^{-4}$$

Having derived the transfer function for the DC motor, and subsequently the PID controller, the next step was to check the system response in MATLAB/Simulink. Figure 3.5.3 shows the Simulink file with all blocks contained within, including the gain from the amp and the gear ratio of the motor (75:1).

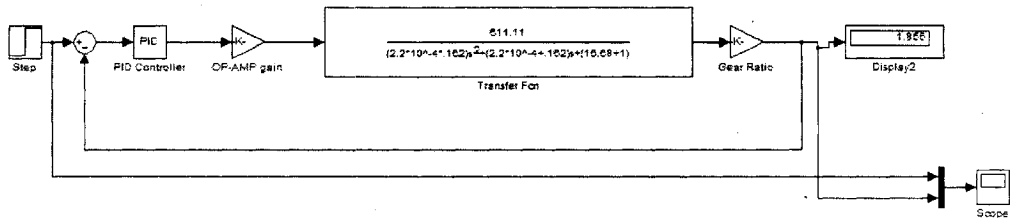

Figure 3.5.3 DC motor transfer function

The system response from the PID controller, as shown in figure 3.5.4, required some small adjustments to the controller during the actual experiment. The values found, could be used as a starting point for the PID values in the experimentation.

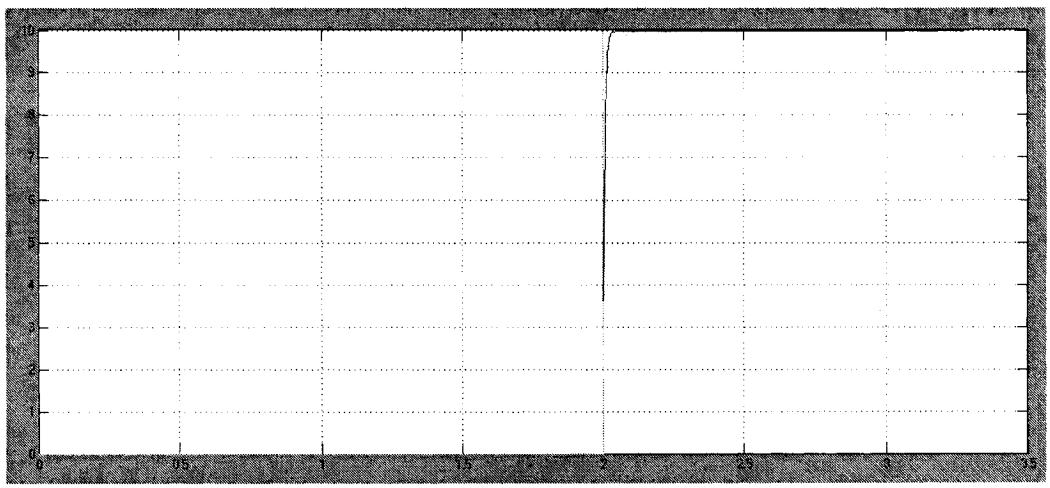

Figure 3.5.4 System response to initial PID controller

3.6 Butterworth Digital Filter

The plant, as seen previously in figure 3.4.5, also contains the feedback from the DC generator; this signal however is very noisy, due to the nature of DC tacho-generators, hence it must be filtered. The filter chosen was a lowpass filter, sometimes referred to as high-cut filters or treble cut filters. As the DC generator can produce high-

frequency noise, the low pass filters can filter out unwanted higher frequencies and pass the lower useful frequencies.

One of the more common types of lowpass filters are Butterworth filters, originally designed by the British engineer S. Butterworth in 1930, it is designed to have a frequency response which is as flat as mathematically possible in the passband [19]. The most basic Butterworth filter is the standard first-order lowpass filter whose frequency response can be described as that of figure 3.6.1.

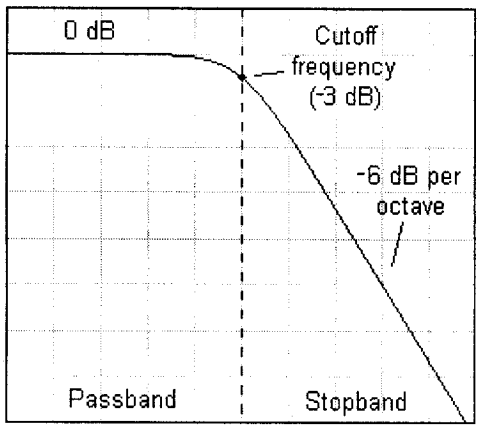

Figure 3.6.1 Frequency response of a 1st order lowpass Butterworth filter

The passband of the filter, is designed to ideally have no ripples. The stopband or the cutband of the filter must therefore perform the attenuating function. The first order filter as shown in figure 3.6.1 on a logarithmic Bode plot, slopes off at -6 dB per octave for a first order, -12 dB per octave for a second order filter. The magnitude of the frequency response of an n order filter can be defined as [25]:

$$|G(j\omega)| = \frac{1}{\sqrt{1+\omega^{2n}}}$$

Where: G – gain of filter
ω – frequency of the signal in radians
n – order of the filter

The first step in creating the Butterworth filter is to look at the noisy raw signal coming out of the tachometer, shown in Figure 3.6.2.

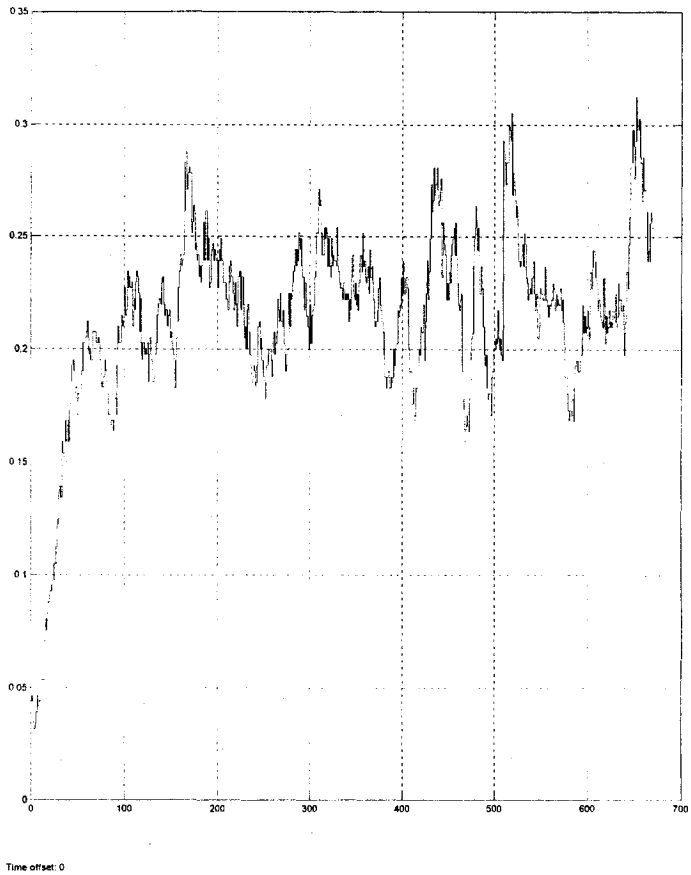

Figure 3.6.2 Noisy tachometer signal

The signal exhibits noise, which ideally is filtered out by the FDAtool, within MATLAB. This block is shown in figure 3.6.3, and is extremely useful when

designing digital filters. The FDAtool allows quick design of FIR or IIR filters (finite impulse response or infinite impulse response).

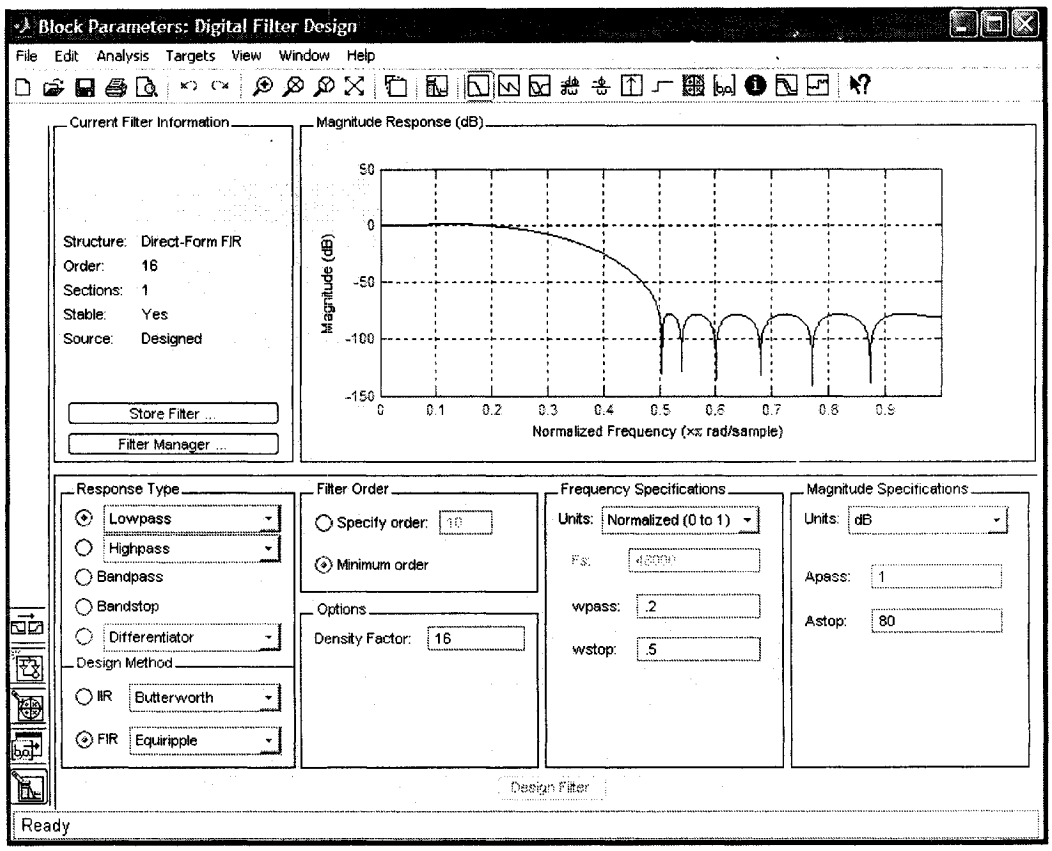

Figure 3.6.3 MATLAB Simulink FDATool

The chosen filter for this application, the Butterworth filter, is an IIR type filter. To design this simple filter, three variables must be known:

1. Order of filter (n) – The order of filter determines the drop off rate, the slope after the cutoff frequency is equal to the order of filter (n) times - 6dB per octave.

2. Sampling Frequency (F_s) – The sampling frequency must be higher than that of the cutoff frequency.

3. Cutoff Frequency (F_c) –The cutoff frequency is the point to which all values that are higher will be attenuated.

For the required filter of the DC generator, a lower order filter will suffice, for example in the order of 5 (-30 dB per octave) and the cutoff frequency of 50Hz, while the sampling frequency was chosen to be 1000Hz. The resultant plot of the magnitude response can be seen below in figure 3.6.4.

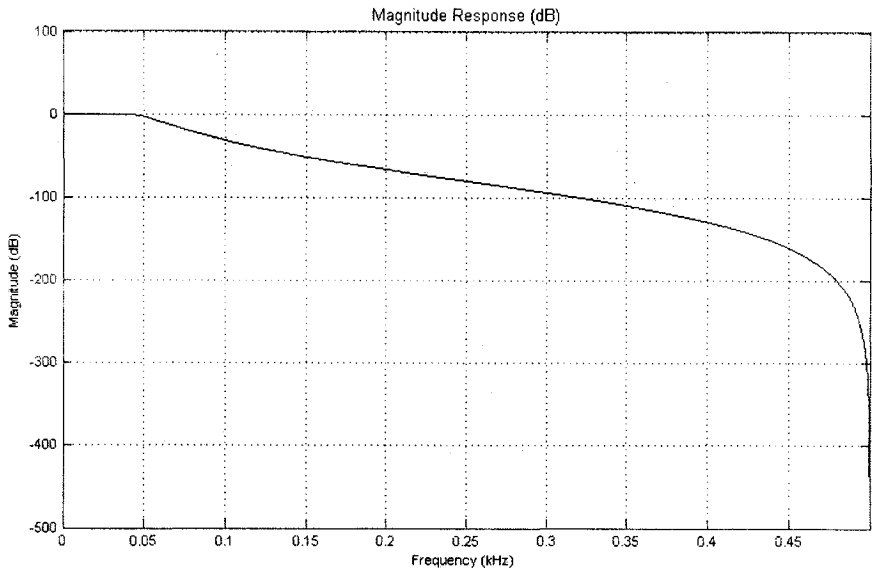

Figure 3.6.4 Magnitude response of Butterworth filter design

An example of the effect of this 5th order Butterworth filter can be seen below in figure 3.6.5.

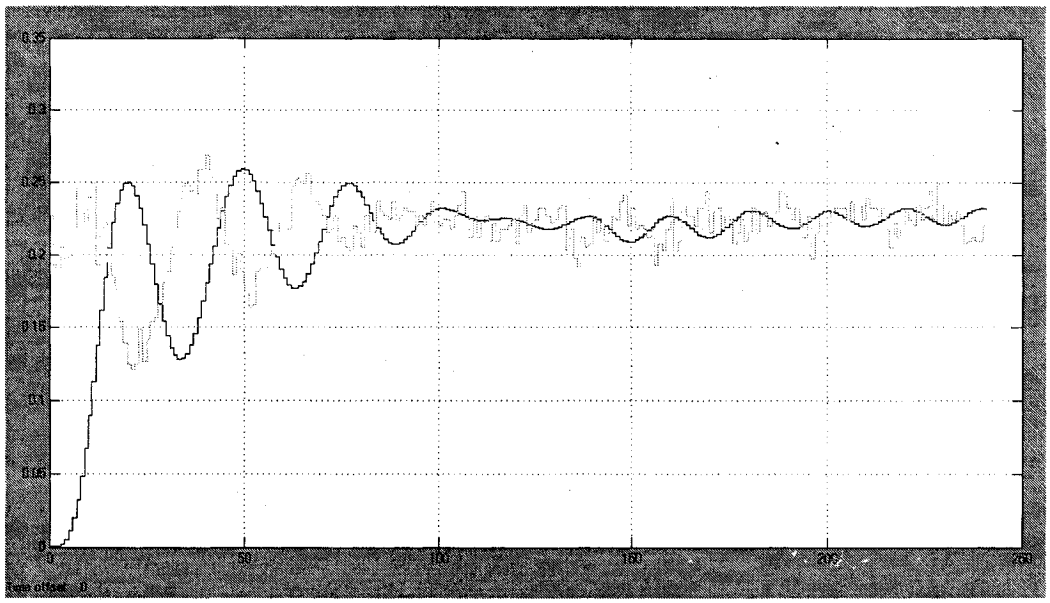

Figure 3.6.5 Plot of Butterworth filter performance

The output of the filtered signal in [v] is then sent through a simple conversion into [rpm] (where 20.8volts is equal to 1000 rpm or each volt = 48.07 rpm). After the conversion the signal is sent to be compared with the desired velocity.

3.7 Experimental Testing:

The first thing realized during running of the simulation was that the limit switch which were used due to there availability in the lab, were not sufficient in controlling the slack. The nature of the switches, on or off, meant that this tendon tensioning system was too susceptible to slack, often causing the system to ""jolt" the tendons tight, which could cause quivering in the positioning system. One simple alternative was to remove the micro switches and to use the frame as a tendon slack absorbing

system (TSAS). Through using a carefully chosen spring the system could be used to pull significant amounts of slack out of the system. The modified system is shown in figure 3.7.1, with the micro switches removed and the modified spring remounted to a higher location.

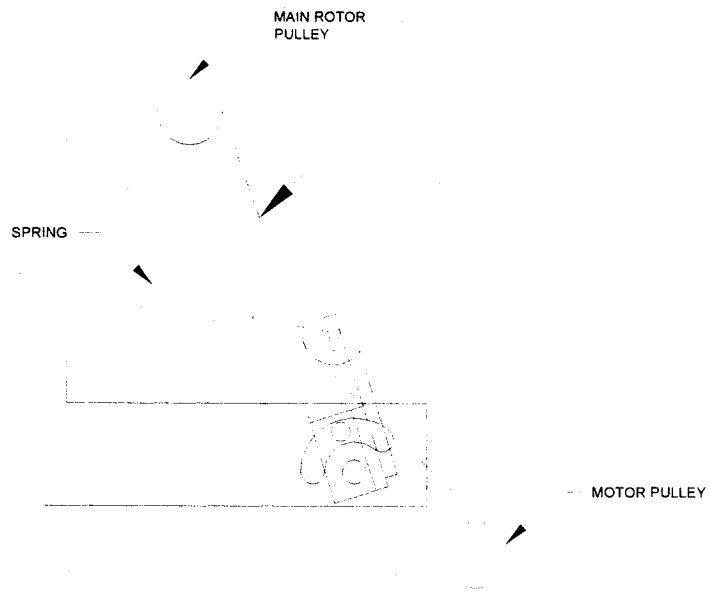

Figure 3.7.1 Modified tendon slack absorbing system (TSAS)

While this tendon tensioning setup was more than adequate for the trial 1-DOF system, a better solution would have been to use strain gauges. By measuring the tension with strain gauges (as is done with the UTAH/MIT Dexterous hand – chapter one) the shuddering experienced in the system would be avoided and the slack could be taken out proportionally.

The second thing observed was that a considerable amount of tendon slack could also be reduced by constraining each end of a tendon to a pulley (2 tendons – 4 pulleys),

instead of the conventional tendon system, where the tendon would go from one motor pulley up and over the main pulley and then to the other motor pulley.

After initial runs of the experiment, with the tensioning system was repaired, the system seemed stable enough to continue fine tuning of the controllers. The first system response plot to a variety of step inputs is shown below in Figure 3.7.2.

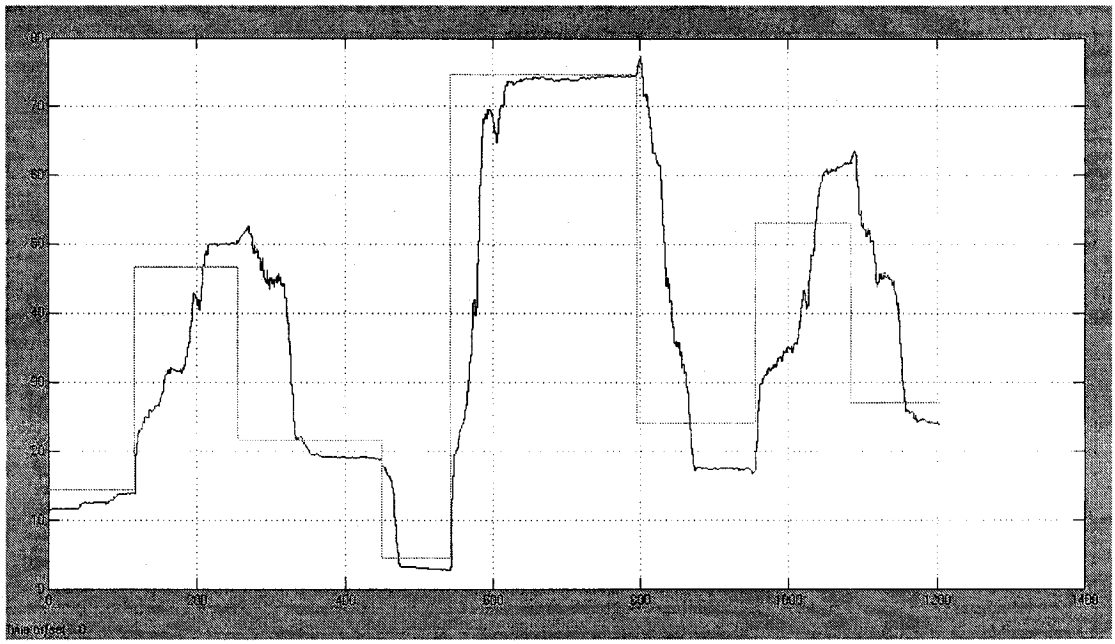

Figure 3.7.2 Initial system response to step inputs

Next values required for the PID controller of the closed loop system for angular position feedback were examined. The Ziegler-Nichols tuning rules were used to determine the values for the PID gains calculations [21].

In this method the T_i and T_d values are set to infinity and zero respectively and the PID controller is run initially as purely proportional gain. Setting K_p to zero and continually increasing until K_{cr} is reached, this occurs when the output of the system exhibits continuous sinusoidal oscillations. The period of these oscillations is then set

to P_{cr} and using this and K_{cr} will give suitable values for K_P, T_i and T_d, as shown in table 3.5.2. Through this method and some fine tuning of the parameters the values for the PID controller were found to be:

$$K_P = .02$$
$$T_i = .032$$
$$T_d = .008$$

With this PID controller, the system was able to give a system response shown in figure 3.7.3.

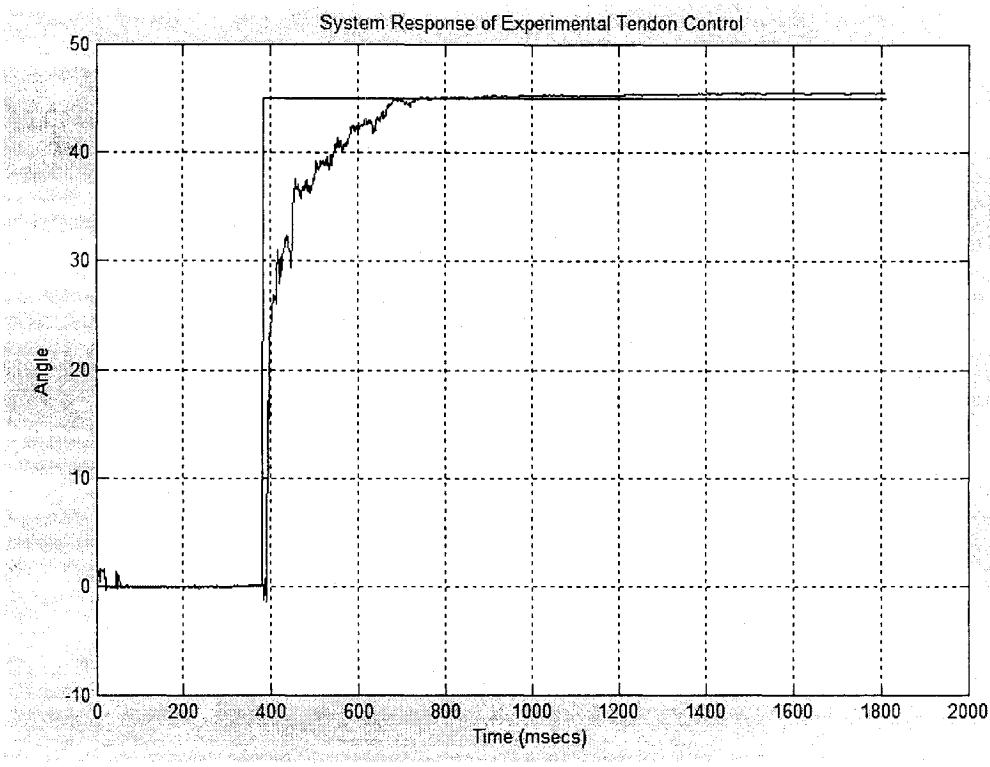

Figure 3.7.3 System response of experimental tendon control

This proved that the experimental setup could give good results, and the next step was to go onto the observer for the 1 DOF system.

3.8 1 DOF Observer Development:

The observer and feedforward friction control system developed in Chapter two, was used to replace the PID control system. The system used is shown for the 1 DOF manipulator in Figure 3.8.1.

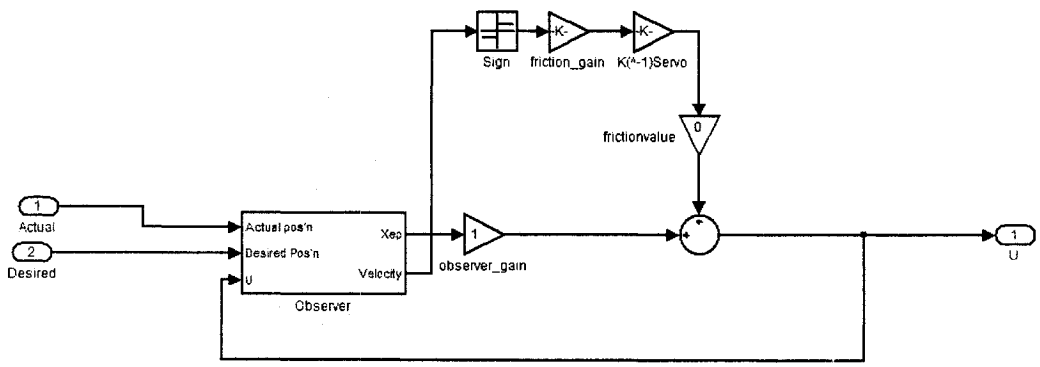

Figure 3.8.1 Observer and friction feedforward for 1 DOF manipulator.

Calculating new values for the variables in the observer equation yields:

$$\alpha = -103.74$$
$$\beta = 3772$$
$$K_1 = -34.58$$
$$K_2 = 184.67$$
$$g_1 = .31688$$
$$g2 = .3333$$

These values were used in the observer and a new value had to be found for the friction coefficient(s), in any system there can be any combination of up to the three different types of friction, defined as:

1. Static friction (μ_s) – occurs when two objects are not in motion, initial force required to get an object moving in relation to another, also referred to as stiction.
2. Kinetic friction (μ_k) – value of the limiting friction after movement has occurred
3. Rolling friction (μ_r) – limiting friction when two objects are rolling over one another.

Typical values of friction for a variety of materials are as listed below in table 3.8.1. [22, 23]

Material	**(μ_s)**	**(μ_k)**	**(μ_r)**
Steel on Steel	0.74	0.57	-
Aluminum on Steel	0.61	0.47	-
Copper on Steel	0.53	0.36	-
Metal on Metal (lubricated)	0.15	0.06	-
Self-aligning ball bearings			
Cylindrical roller bearing	-	-	0.0010
Thrust ball bearings	-	-	0.0011
Single-row deep-groove ball bearings	-	-	0.0013
Tapered and spherical roller bearings	-	-	0.0015
Needle bearings	-	-	0.0018
	-	-	0.0045

Table 3.8.1 Typical coefficients of friction

The ECP Model 505, Inverted Pendulum at all joints uses single-row deep groove ball bearings giving a μ_r= 0.0015, which was rounded to .002 as the bearings were not new. With the observer defined and modeled in the Simulink control system for the 1

DOF manipulator, the 45° step input was once again used to test the system. The 1 DOF manipulator's system response to this input is shown in figure 3.8.2.

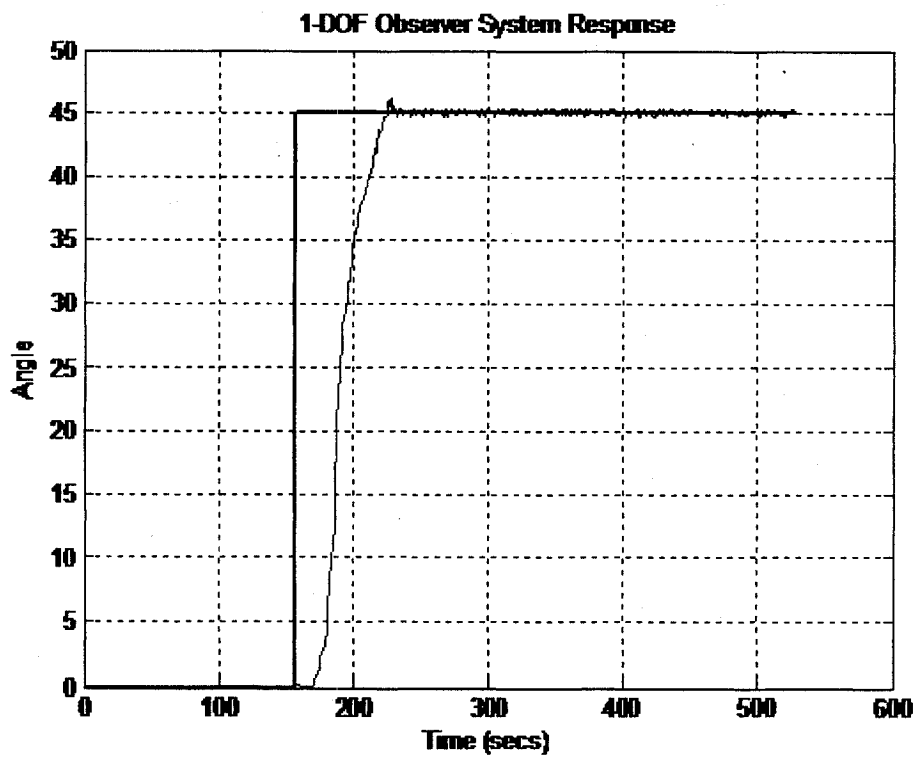

Figure 3.8.2 1 DOF systems response to 45° step input

The response to the step input is good, with no overshoot and the system behaves linearly right up until reaching the desired angle. Comparing this with the previous PID system, as in figure 3.8.3, as expected the observer has given better results.

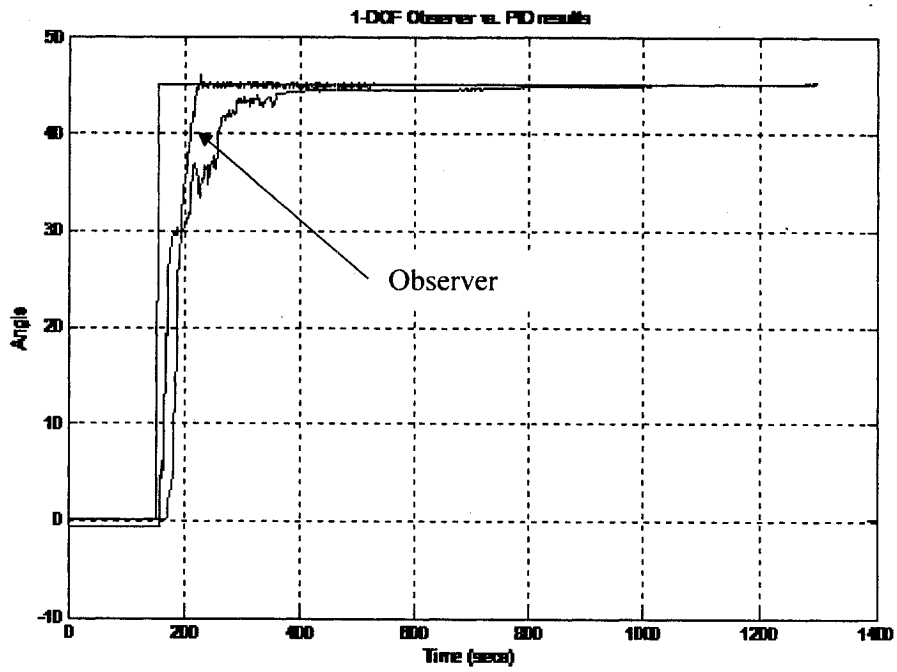

Figure 3.8.3 PID vs. observer for 1 DOF manipulator

Figure 3.8.3, shows the observer controller getting to the desired angle much faster and with almost zero settling time, but there is however a small amount of overshoot as can be seen, considered acceptable performance for this experiment.

These results proved that the 1DOF system responds well to the control system, and the next step was the simulation of this 1DOF experiment.

CHAPTER 4
SIMMECHANICS ASSISTED SIMULATION

4.1 Introduction:

The results of the 1 DOF experiment can be used to validate results obtained when simulating the same experiment. This was done using MathWorks SimMechanics, to confirm that the same results could be obtained in both experiment and simulation, with an error of no more than 5%. Once it was confirmed that the simulation and experimental results were similar, a 3 DOF device could be designed using the simulated system.

4.2 Introduction to SimMechanics:

SimMechanics is an add-on for MATLAB that has tools for modeling and simulating a variety of mechanical systems. The toolbox has a wide variety of blocks that can be configured to replicate any mechanical structure. Through entering parameters including masses, moments of inertia, inertia tensor matrix among others, the assembly will give results similar to those expected from the real-time hardware. The first step in building the SimMechanics model was to determine all of the parameters required, which include:

1. Geometry – SimMechanics requires extensive knowledge of the simulation geometry to be able to give accurate results. All distances, radii, and angles must be specifically defined, so that the system can be constrained correctly.
2. Moments of Inertia – All bodies must have an inertia tensor matrix defined.

3. Volumes/Masses – All bodies as well must have closely defined volumes and masses.

When all the geometry, moments of inertias and Volumes/masses have been defined it is possible to start to build the simulation geometry. SimMechanics uses specialized blocks to allow developing of rigid body machines and their motions, using standard Newtonian dynamics of forces and torques [20].

Instead of just the normal Simulink input/output ports the SimMechanics blocks have two different types of specialized connection ports.

1. Body Coordinate System (CS) Ports – appear on the body and ground blocks and are able to connect body and ground blocks to each other as can be seen in Figure 4.2.1. These blocks use a coordinate system whose origin specifies the location of the associated connection. .

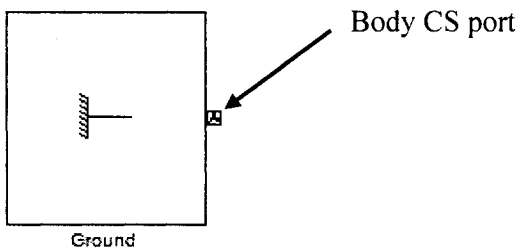

Figure 4.2.1 Body coordinate system port

2. General-purpose connection Ports – appear on joints, constraints, drivers, sensors and actuator blocks. These connection ports allow connection of joints to bodies and connect sensors and actuators to joints, constraints and

drivers. An example of a general-purpose connector port appears in figure 4.2.2.

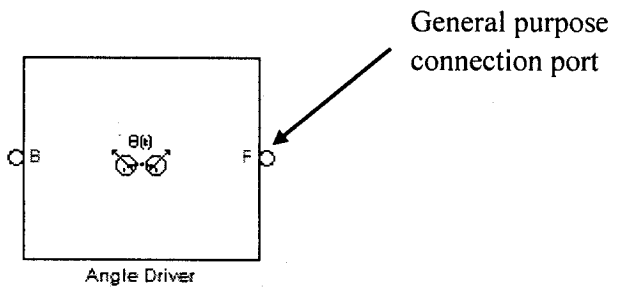

Figure 4.2.2 General purpose connector block in SimMechanics

Within the SimMechanics toolboxes are all the libraries required to build a realistic simulation, which include: [20]

1. Bodies – this library contains blocks that represent rigid bodies and ground points
2. Joints – representing all DOF's (over 15 types) and custom blocks that allow the user to build massless connections.
3. Constraints & Drivers – Specialty blocks that allow or restrict external drive methods between pairs of bodies DOF's.
4. Sensors & Actuators – Blocks to motivate or sense bodies and their motions, that includes blocks for detailing the bodies initial conditions.
5. Force Elements – Include blocks to create forces/torques between bodies for example between springs, dampers, etc.

6. Utilities – miscellaneous blocks for interaction between Simulink Files and/or Virtual Reality scenes.

4.3 Building a Simple SimMechanics Model:

SimMechanics was designed to be user friendly and to be easy to implement. To aid understanding of how SimMechanics works a simple completed SimMechanics model will be demonstrated. This is the first step in modeling the single DOF system, the pulley driven by the DC motor. Figure 4.3.1 depicts the pulley as it is attached to the DC motor.

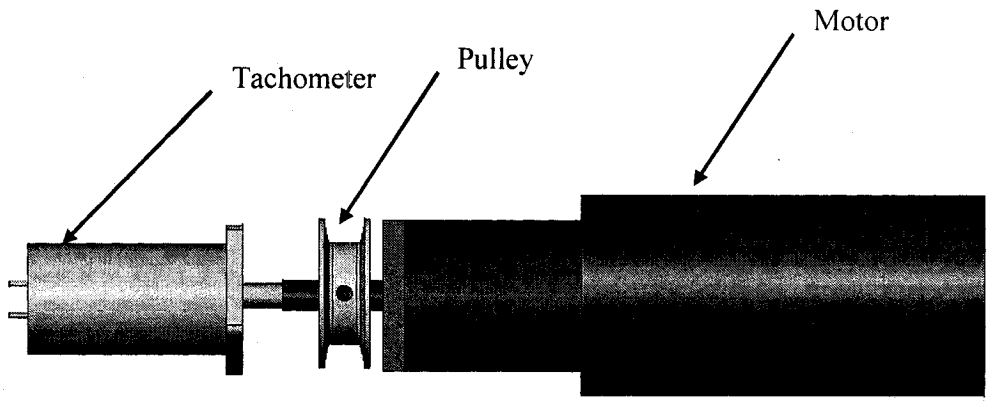

Figure 4.3.1 DC Motor with installed pPulley

The DC motors used, PITTMAN No: GM14602D261 (Appendix III) were also required to be modeled as their performance directly affects the simulation results.

First step was to model the DC motors, by doing this the motor's influence on the simulation would be better understood, and it could be identified how each parameter of a DC motor can affect the outcome. From Chapter 3, it was found that the equations for a DC motor were:

$$U = Ri + L\frac{di}{dt} + E_m$$

$$\mathrm{E}_m = K_e\omega$$

$$T = K_t i$$

$$T = J\frac{d\omega}{dt} + b\omega$$

by eliminating E_m and T, the model is reduced to two differential equations with four variables: [15]

$$U = Ri + L\frac{di}{dt} + K_e\omega$$

$$K_t i = J\frac{d\omega}{dt} + b\omega + \mathrm{T}$$

Most DC motors have very negligible armature-winding inductance (L), so in this equation L is assumed to be zero and eliminated. Solving for the cut variables on the mechanical side (T, ω) and (U, i) on the electrical side gives:

$$\omega = \left(\frac{1}{K_e}\right)U - \left(\frac{K_e}{R}\right)\omega$$

$$T = -\left(\frac{J}{K_e}\right)\frac{dU}{dt} - \left(\frac{b}{K_e}\right)U + \left(\frac{JR}{K_e}\right)\frac{di}{dt} + \left(K + \frac{bR}{K_e}\right)i$$

To model this in Simulink, it is rewritten it in the form below, sometimes referred to as the data flow form [15].

$$i = \left(\frac{1}{R}\right)U - \left(\frac{K_e}{R}\right)\omega$$
$$\frac{d\omega}{dt} = \left(\frac{K}{J}\right)i - \left(\frac{b}{J}\right)\omega - \left(\frac{1}{J}\right)T$$

The Simulink model is shown by figure 4.3.2.

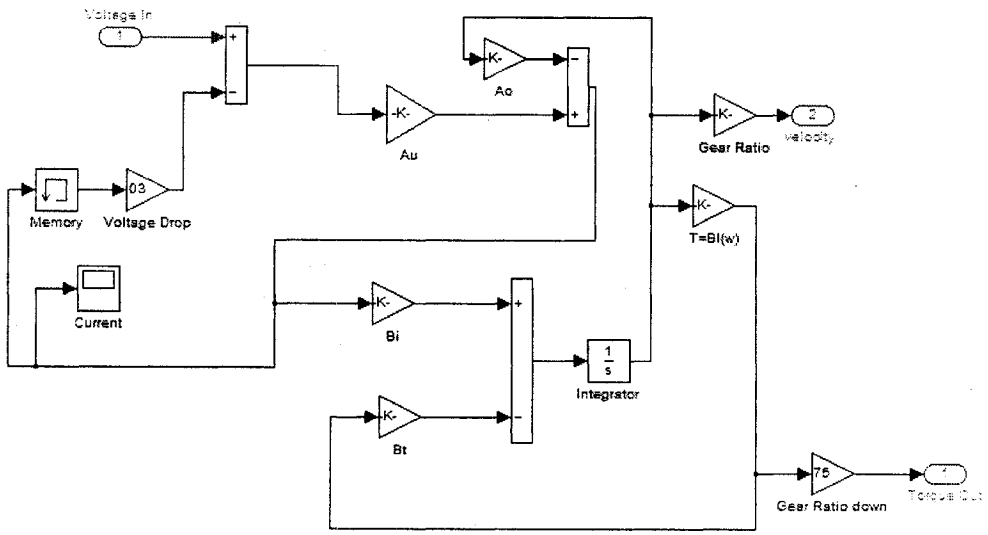

Figure 4.3.2 Simulink model of DC motor

Following conventional notation, the diagram in figure 4.3.2 uses the following nomenclature, for ease of labeling. [15]

$$A_u = \frac{1}{R} \quad A_0 = \frac{K_e}{R}$$
$$B_i = \frac{K}{J} \quad B_o = \frac{b}{J}$$
$$B_t = \frac{1}{J}$$

The values used for this model are the same as that in table 3.5.1. To build the SimMechanics portion of the model, the first step is to create a body joint, and then enter all the parameters required. figure 4.3.3 depicts the bodies parameter dialog box.

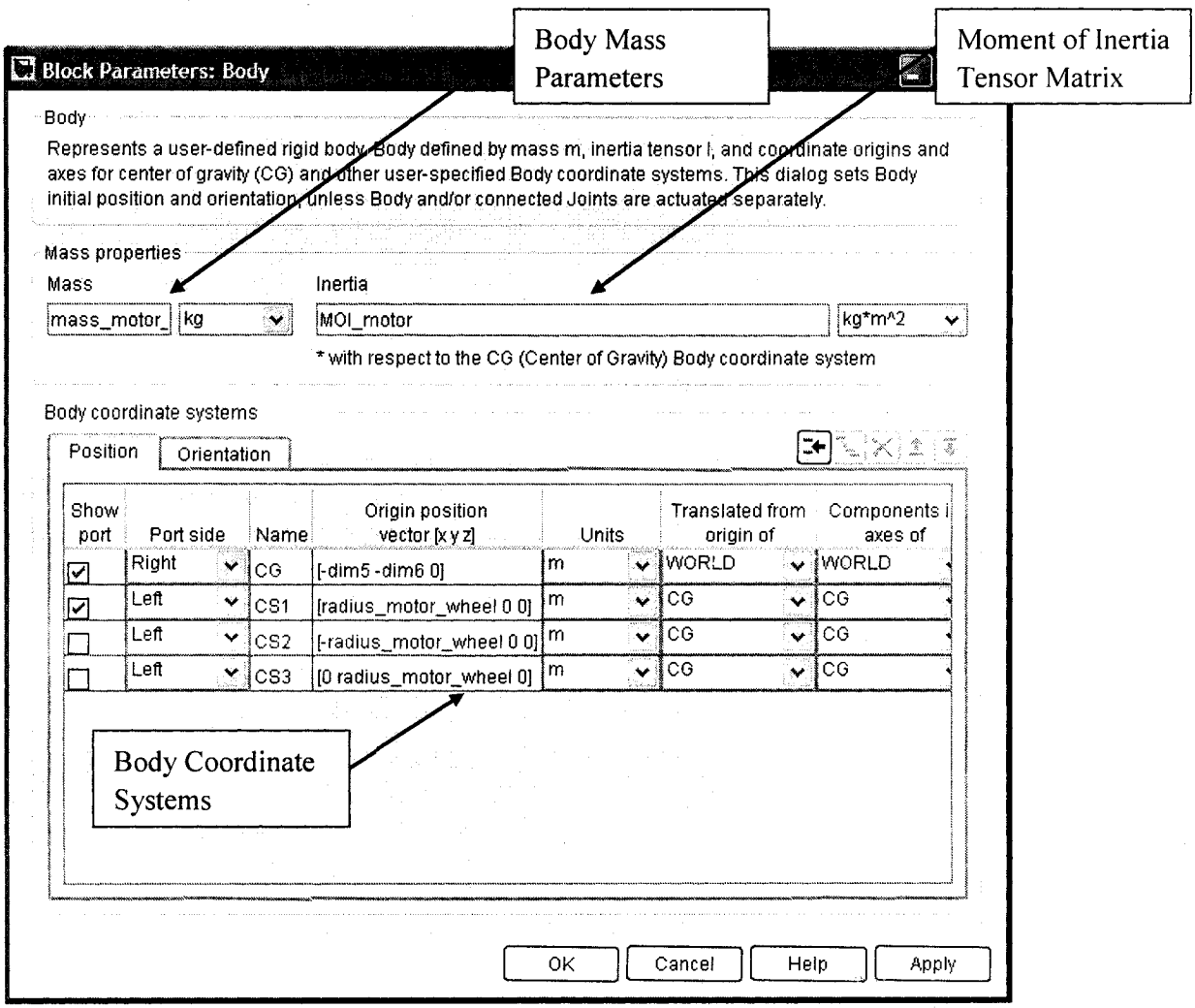

Figure 4.3.3 Block parameter dialog box for SimMechanics rigid body

As can be seen in Figure 4.3.3, there are basically three sets of data for any rigid body, the mass, the moment of inertia tensor matrix and the body's coordinate system.

To determine the mass and moment of inertia tensor matrix, there are basically two methods, one is through the classical analytical determination, and the other is to use a Computer Aided Engineering (CAE) program to determine the parameters. Since the system had already been drawn, and modeled in SolidWorks to have it manufactured (as shown in Chapter three), it was simpler to give each body a density parameter (steel – 7850kg/m^3) and then record the values obtained.

The mass determined from SolidWorks for the pulley was 61.23 * 10^{-3} kg. Next was to determine the inertia tensor matrix, which must be in the following format:

$$\begin{bmatrix} I_{XX} & -I_{XY} & -I_{YZ} \\ -I_{XY} & I_{YY} & -I_{XZ} \\ -I_{YZ} & -I_{XZ} & I_{ZZ} \end{bmatrix}$$

For the motor pulley it was found to be:

$$\begin{bmatrix} 417*10^{-6} & 0 & 0 \\ 0 & 417*10^{-6} & 0 \\ 0 & 0 & 417*10^{-6} \end{bmatrix} \frac{kg}{m^2}$$

The body coordinate system is required to define all the "ports" of the body, as shown in Figure 4.3.3, for this motor simulation there is one default port which is the centre of gravity (CG) port, and the simplest method is to define all ports in relation to the CG port. First, the CG port must be defined and its relation to the world coordinate system (WCS). Figure 4.3.4 explains the pulleys CG dimensions in relation to the WCS.

For the Tendon system, the WCS are at the centre of the main rotor shaft and all CG's are defined accordingly. The special port's coordinate systems (CS_n – where n denotes number of port 1,2,3.....n) is then specified in relation to the bodies CG. Through this method, the dimensions that are used to define locations are kept to a minimum and hence so are rounding errors and tolerances.

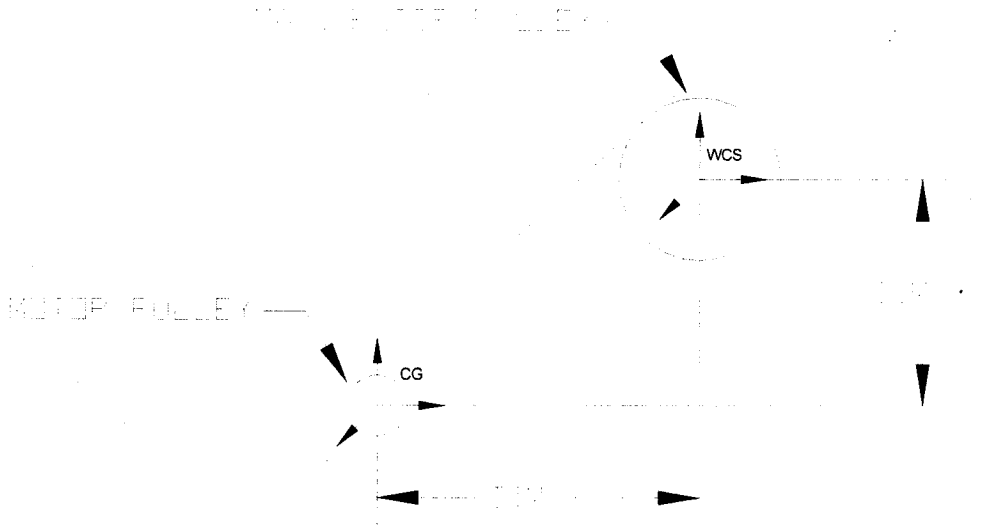

Figure 4.3.4 WCS and CG for SimMechanics

With the body block fully defined, the next step was to add an actuator and a ground block. The ground block also has its own coordinate system; for this setup the CG is also the ground position, and hence uses the same coordinates for defining the CG for the body block. The actuator of the motor assembly is clearly the revolute joint (which represents the pulley), and its only specifications are the axis of rotation (Z-

axis in this simulation) and the number of ports required for sensors; the movement is generated through entering the angular position, angular velocity and angular acceleration. The final requirement for this simulation is the addition of two sensor blocks, which measure the velocity and torque respectively. The complete simulation diagram is shown in figure 4.3.5.

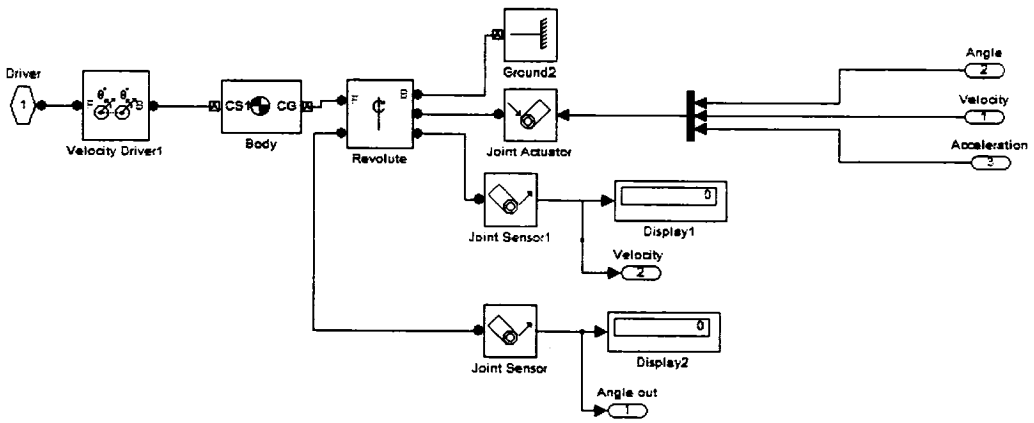

Figure 4.3.5 DC motor pulley SimMechanics block diagram

All components in figure 4.3.5 are then contained in a subsystem block, which can be viewed in the overall assembly in SimMechanics figure 4.3.6. Figure 4.3.5 also shows a velocity driver block; this is used to drive the tendons that connect to this motor pulley in the simulation. A velocity driver works on the principal of a linear combination of the translational and angular velocities of the two bodies involved. [20] The basic concept of the velocity driver in this simulation is to take the rotation of the DC motor's pulley, convert it into terms of circumferential movement and translate this to the tendons. The SimMechanics subsystem is then twinned to the DC

motor and PID control (similar to that of the actual experiment, detailed in Chapter three), shown below in figure 4.3.6.

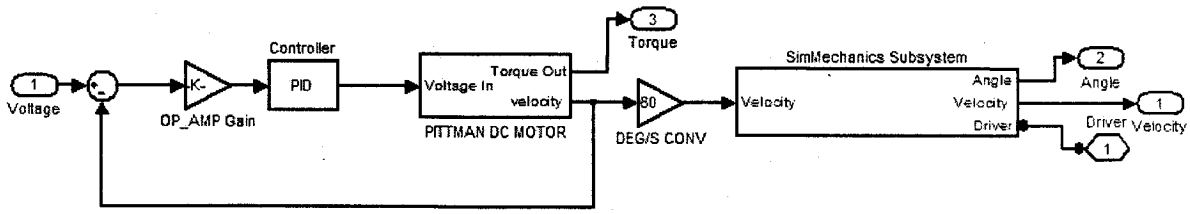

Figure 4.3.6 Complete motor assembly in SimMechanics

The complete motor assembly, as shown in figure 4.3.6, can then run independently to give a realistic simulation of the DC motor.

4.4 Development of 1 DOF System Simulation:

With the motor and tachometer simulated and running accurately, the next step was to elaborate the remainder of the 1 DOF simulation around the basic concept derived above.

The first phase was to determine all geometry of the apparatus, which was extracted from the SolidWorks file. This SimMechanics model is made up almost entirely of subsystems. The main system which can be considered as the user panel is shown below in Figure 4.4.1.

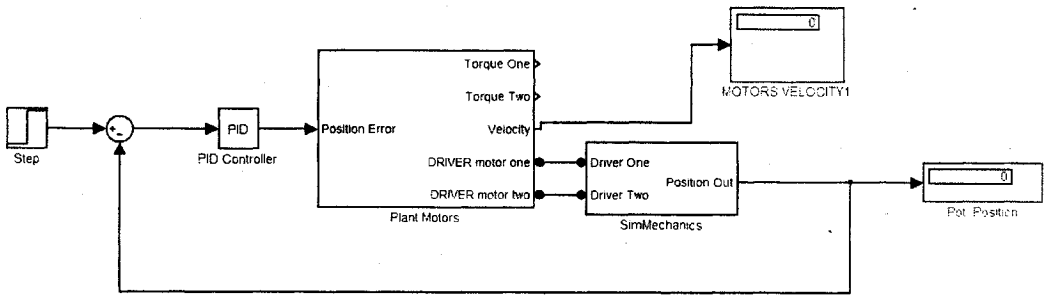

Figure 4.4.1 Simulink 1 DOF model

The plant motors subsystem holds all the parameters for the two DC motors and pulleys. The position error (θ_e) which is determined by desired angular position (θ_d) – actual angular position (θ_a) is then put into the two DC motors, as shown in figure 4.4.2.

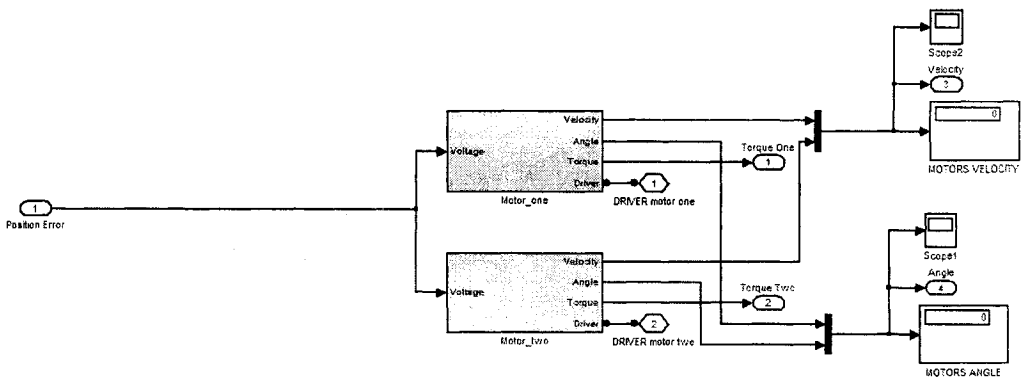

Figure 4.4.2 Motor subsystem block

Within this subsystem are the two DC motors subsystems, containing the DC Motor simulation and the SimMechanics Simulation of the DC Motor pulley, and is identical to that of figure 4.3.6.

The outputs from this subsystem are the velocity drivers block, used to power the tendons, and also data on the angular position and the angular velocity of the two DC motors. One important issue for the tendon driven systems is that the motors need to be synchronized and therefore there operation is closely monitored.

The main user panel (figure 4.4.1) together with the DC motor subsystem are the core SimMechanics equations. This is where the tendon information and main rotor pulley is contained. Figure 4.4.3 shows this subsystem.

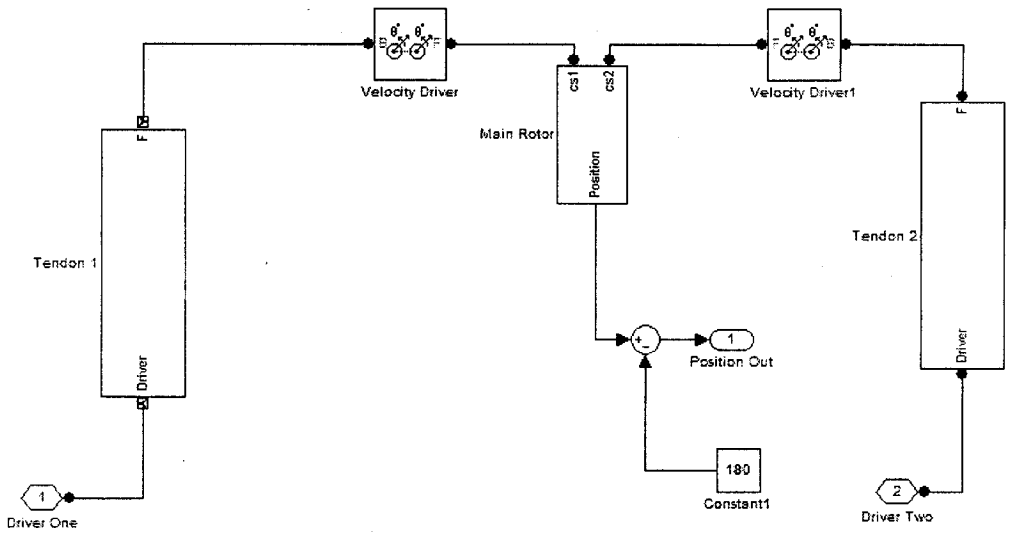

Figure 4.4.3 Tendon and rotor subsystem

The principle of this drive system is that the velocity driver from the motor pulleys controls the tendons, and the tendon velocity driver then controls the main rotor, as shown in figure 4.4.3. The tendons subsystem block contains the body and joint information for both tendons. The tendons are constrained with a prismatic joint to only move in the two directions of travel, and their movement is traced and observed and passed onto the main rotor pulleys.

The two tendons drive information is coupled to the main rotor body, and continuously compared for discrepancies in tendon movement. Figure 4.4.4, shows

the main rotor body, revolute joint, sensor, ground, and most importantly, the friction model.

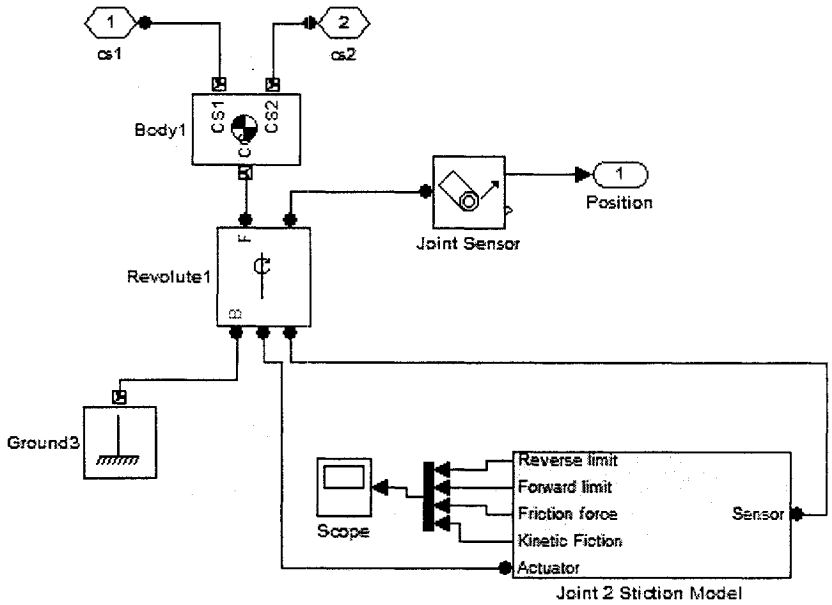

Figure 4.4.4 Main rotor SimMechanics subsystem

Up to the description of this block no friction or any other disturbance has been added to the SimMechanics model. Although the system uses low friction ball bearings and the tendons exhibit zero friction, there is still a small amount contained within the main rotor shaft, the potentiometers, the tachometers, etc.

Friction has to be added at the main rotor shaft of the SimMechanics simulation. In Chapter 3 the coefficient of friction was estimated to be $u_r = 0.002$, for rolling friction. There is no function in SimMechanics for rolling friction, and the output potentiometer that measures main rotor shaft angular position uses a wiper which

generates kinetic and static friction and it was decided to use the more conventional types of friction.

SimMechanics has a block that allows application of stiction friction to a prismatic or a revolute joint, and the friction is applied using MATLAB's 'friction model'.

The joint stiction actuator block, shown in figure 4.4.5, displays the five parameters required to build the friction model: external actuation, kinetic friction, stiction limit (forward and reverse) and static friction.

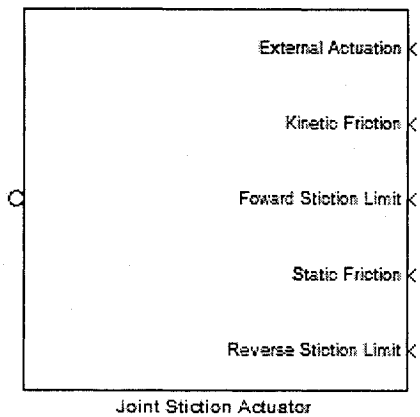

Figure 4.4.5 Joint stiction actuator block

Another subsystem with this joint stiction actuator block as the central part of the friction model was then designed. This block, which was modeled after a SimMechanics case study [20], is shown in figure 4.4.6.

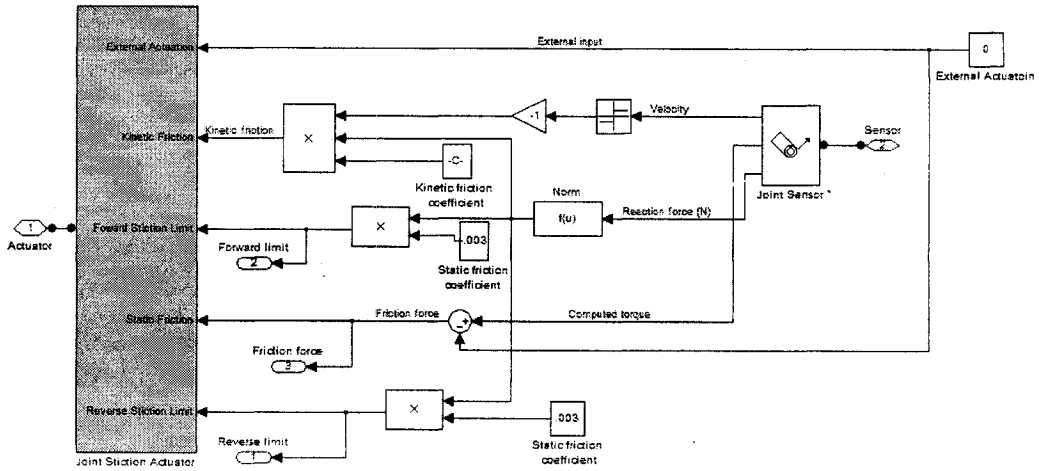

Figure 4.4.6 SimMechanics friction model

The basic principle is that the joint sensor measures the angular velocity, reaction force and the computed torque and uses this data and the force applied by the velocity driver to apply correct amounts of both kinetic and static friction.

4.5 Comparison of Results of Experiments and Simulations:

The results from the MATLAB SimMechanics simulation were close to experimental results but initially not close enough for the purpose of this thesis.

First the coefficients of friction, which were one of the few unknowns, had to be adjusted even if they could not be measured in the experimental system. The final values were found to be static friction 0.003 and kinetic friction .0023.

At this point, everything in the simulation were identical to that of the experimental setup, including values of the PID controller for angular position feedback, and the

fine tuning of the coefficients of friction. As a result the SimMechanics simulation gave good results when compared to the experimental results.

Figure 4.5.1 shows how close the comparison of the two systems were.

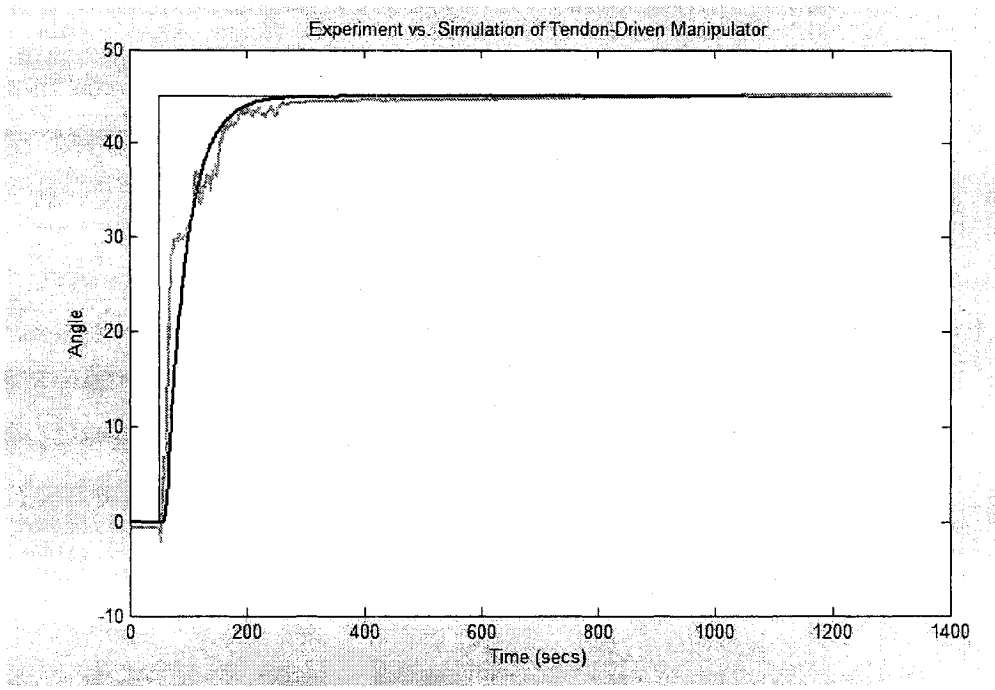

Figure 4.5.1 Experiment vs. simulation of tendon-driven manipulator

The two sets of data gathered, one from the experiment and the other from the simulation were compared to plot the average difference (degree vs. time). The average difference between the simulation and the experiment was calculated to be 1.0636°, which is reasonable for the simulation, as it is less than 2.3% error on a 45° step input. SimMechanics simulation was consequently verified by the experiment results and could be used to design and simulate a three DOF simulation.

CHAPTER 5
THREE DOF SIMULATION

5.1 Introduction

With the two different versions of the 1 DOF system compared and justified, the next step was to design what was considered a useable and realistic 3 DOF system simulation.

5.2 Design of a 3-DOF system:

A new design of the three DOF system was constructed, again using SolidWorks. The system had to be tendon driven and was required to have 3 rotational axis of freedom. The size was decided to match up to a typical laboratory grade robot (Puma, etc.) i.e. roughly the size of a human hand or the size of the UTAH/MIT Dexterous hand (see Chapter One). It was decided that the three axis of rotations would all cross at the same point (herein referred to as the $AXIS_{xyz}$ of the design), the reason being that the dynamics and kinematics of the manipulator would be kept simple and give the best response. After several iterations of the design, the best was chosen and the component drawings are contained within Appendix II. The overall design can be seen below in Figure 5.2.1.

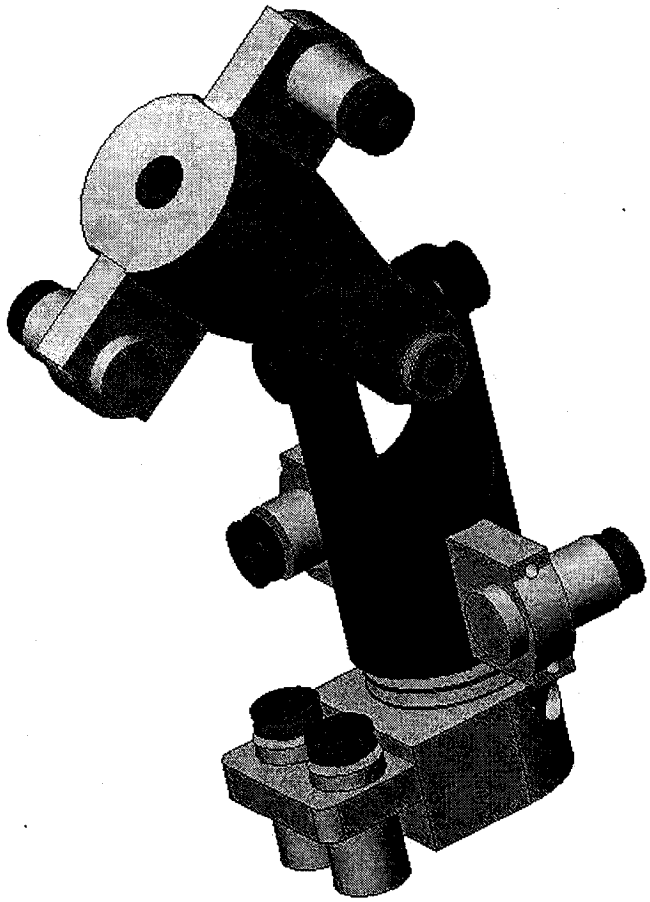

Figure 5.2.1 3 DOF final design

5.3 DC Motor Transfer Function and Simulink Model

For the 3 DOF system, new motors were selected to suit the estimates of size, torque and velocity requirements of the new system. Again PITTMAN DC Motors offered the solution in their micro sized motors – the LO-COG line. LO-COG motors are 22mm diameter (O.D.) brush commutated DC motors, the motor chosen No. 6X12 is also valuable for its wide variety of gear heads available (from 4:1 – 107:1) and the possibility of adding optical encoders in the future. To model the motors performance

and develop the control system once again, the transfer function is required. The transfer function (derived in Chapter three) is once again used:

$$\frac{S\cdot\omega(s)}{U(s)}=\frac{\frac{K_t}{Rb}}{\tau_m\tau_a S^2+(\tau_a+\tau_m)S+\left[\frac{K_eK_t}{Rb}+1\right]}$$

The parameters of the selected motor (appendix IV) required to solve for the transfer function are seen below in table 5.3.1.

Parameter	Nomenclature	Value
Torque Constant	K_t	0.013 N-m/A
Electrical Constant	K_e	0.013 Vs/Rad
Moment of Inertia	J	$5.15*10^{-7}$kg/m^2
Armature-Winding Resistance	R	7.75Ω
Armature-Winding Inductance (negligible)	L	$4.05*10^{-3}$
Viscous Friction Coefficient of Motor (negligible)	b	$4.85*10^{-7}$ N-m/(Rad/s)
Viscous Friction of Load (negligible)	B_t	0.0001

Table 5.3.1 DOF system DC motor parameters

Giving the transfer function the following end value:

$$U(s)=\frac{435.69}{6.9*10^{-4}S^2+1.3382S+57.641}$$

Next step, the Routh array is found by setting the characteristic equation for the closed-loop system to:

$$6.9*10^{-4}S^2+1.3382S+57.641+K_p=0$$

Using the Routh-Hurwitz stability criterion, the Routh array becomes:

$$\begin{array}{ll} s^2 & 6.9*10^{-5} \quad 57.641 \\ s^1 & 1.3382 \quad K_p \\ s^0 & \dfrac{1.3382(57.641)-6.9*10^{-5}K_p}{1.3382} \end{array}$$

Now setting the equation to zero and solving for K_p will give the critical gain.

$$0 = 57.641 - 5.23*10^{-4}K_p$$
$$K_p \approx .67.64$$

A critical gain K_{CR}= 57.64, was chosen and the characteristic equation becomes:

$$6.9*10^{-4}S^2 + 1.3382S + 115.28 = 0$$

To find the frequency of oscillation after substituting s = jω, the characteristic equation gives:

$$6.9*10^{-4}(j\omega)^2 + 1.3382(j\omega) + 115.28 = 0$$
$$-6.9*10^{-4}\omega^2 + 1.3382j\omega + 115.28 = 0$$

The solutions are:

$$\omega = 2*10^3 or\ -4.03*10^{-5}$$

From these two values the frequency of the sustained oscillation can then be determined:

$$P_{cr} = \frac{2\pi}{\omega} = \frac{2\pi}{-4.03*10^{-5}} = -1.55*10^5$$
$$P_{cr} = \frac{2\pi}{2*10^3} = .0031$$

giving the following values for the gains:

$$K_p = 0.6K_{cr} = 34.58$$
$$T_i = 0.5P_{cr} = .00165$$
$$Td = 0.125P_{cr} = 3.875 * 10^{-4}$$

For these gain values MATLAB based simulations were performed. The system response was found to be excellent, so the gains calculated will be the gains used in the simulation. The Simulink model of this motor, the velocity control system and the pulley geometry was built in SimMechanics, using the same method but with the new geometry as the 1-DOF system.

5.4 Simulation of a 3-DOF system:

With this 3 DOF design, the SimMechanics model was the next step. The orientation of the manipulator (in simulation the home position is with all angular positions set to zero) is shown in figure 5.4.1.

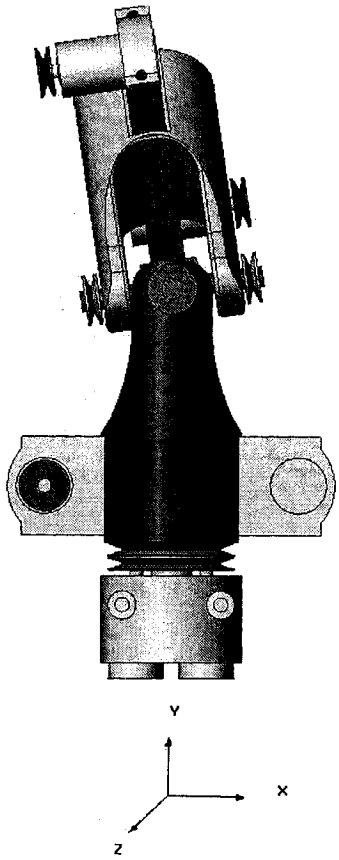

Figure 5.4.1 Orientation of 3 DOF manipulator

For the simulation all geometry is required as are all the moment of inertias for all components, these were again determined using SolidWorks CAD software and were entered into SimMechanics. The simulation can be broken down into similar sub-blocks. All six motors (3 sets of 2 pairs of tendons for each rotation) are all identical and differ only in the direction of rotation. Also the pulleys, and tendons are identical (X/Z direction) and top and bottom u-joints.

The simplified block diagram for the system was conceived for simulating the system and is shown in figure 5.3.2.

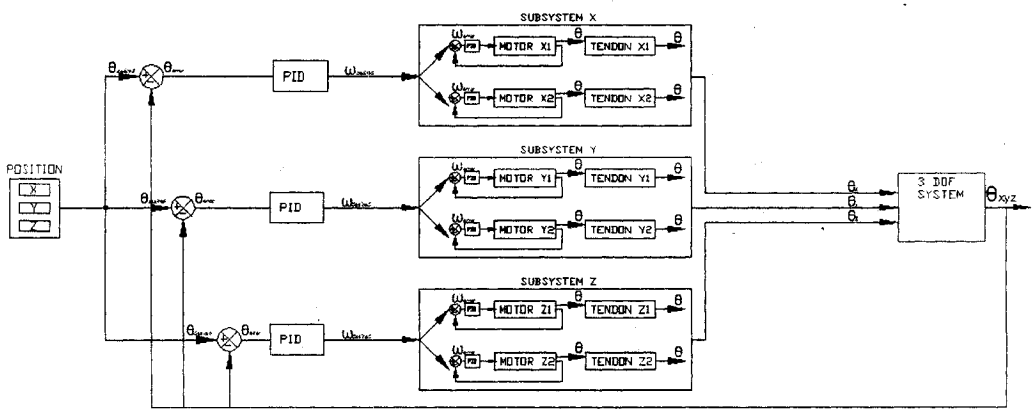

Figure 5.4.2 3-DOF simulation block diagram

The user defined angular position ($\theta_{desired}$) is entered where it is compared to the 3 DOF system position (θ_{actual}) giving the positional error (θ_{error}), this is then put through the controller. The PID controller as shown in figure 5.3.2 was used only to prove that the system worked, and later would be changed to use the observer type system as discussed in chapter two. Individual motors then receive their comments for the angular velocity which is controlled by individual PID controllers, the motors then drive the tendons which in turn drive the 3 DOF system.

Figure 5.3.3 shows the Simulink file, with the three XYZ inputs.

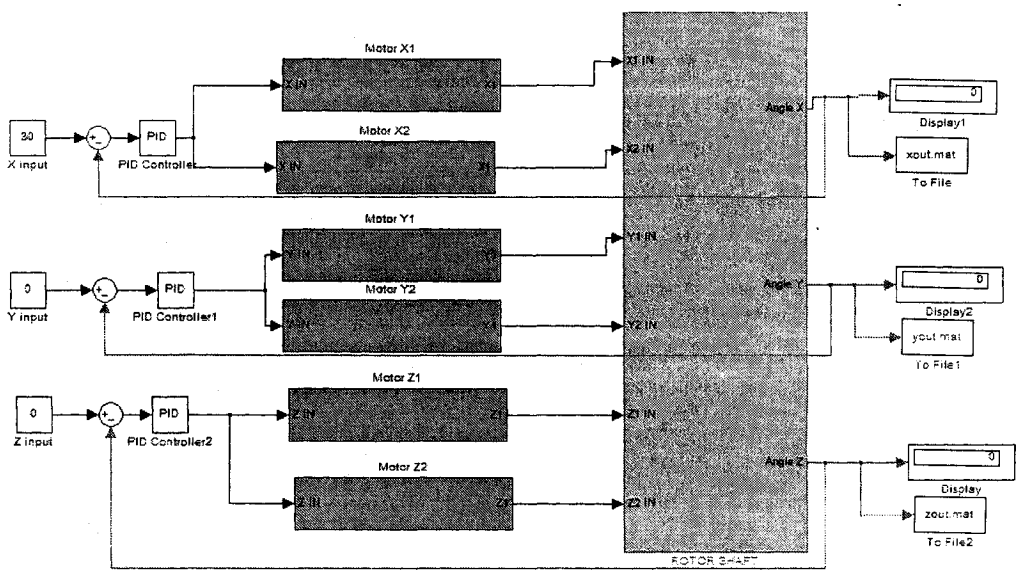

Figure 5.4.3 3 DOF Simulink file

Within each Motor block are identical PITTMAN LO-COG DC Motors models as derived above, and the individual pulley that each motor drives. Connected to this are the tendons, which are then inserted into the main rotor shaft block and can be seen in figure 5.3.3. The Main rotor shaft contains all data required for the main rotor 3 DOF joint.

5.5 Special Considerations of a 3-DOF system:

When Mutually perpendicular axis intersect (point of $AXIS_{xyz)}$, cross coupling (sometimes referred to as crosstalk) must be avoided, cross coupling, a phenomenon whereby the rotation of joint *n* has a direct effect on the rotation of joint *n-1*. Cross coupling can be expressed in terms of degrees/degrees (degrees of cross coupled rotation of joint *n* due to the degrees of rotation of joint *n-1*) or simply in terms of a percentage [24]. Cross coupling in any system is dependent on any number of factors

backlash for example is one of the main causes of high amounts of cross coupling, the moment of inertia also has an effect, figure 5.5.1 illustrates this inertia driven cross coupling problem.

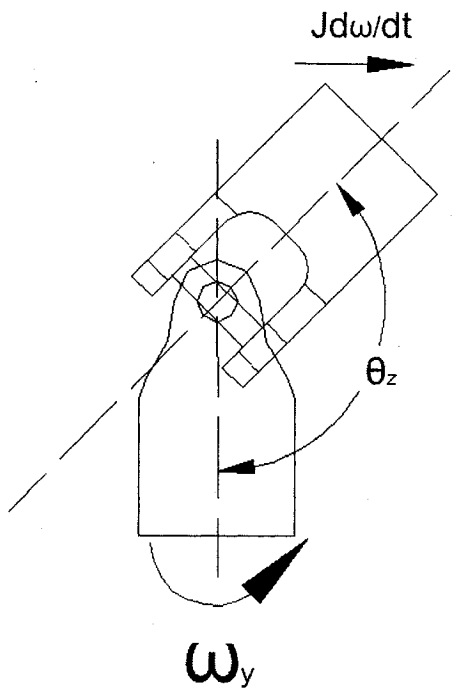

Figure 5.5.1 Inertia driven cross coupling

Due to low angular velocities (below 10rpm) and angular accelerations, this type of cross coupling is not a factor and was ignored. Cross coupling due to the effect from any slack in the tendon drive system, which can be considered directly as backlash, is a major concern in tendon based systems. In the experimental study of the 1 DOF tendon manipulator it was found that tendon slack could be considerably reduced by "anchoring" each end of a tendon to a pulley, and keeping the amount of tendon in the system to a minimum.

Tendon slack could not be generated by the SimMechanics equations, and therefore this data was taken from the 1-DOF experiment.

5.6 3-DOF System Response:

The first test of the 3 DOF tendon manipulator was to check the performance of the 3 different directions of motion. This was achieved by means of bypassing the PID controller and supplying the motors with a set voltage (in this case 10 volts, the normal maximum voltage output of most DAQ's) and plotting the systems response. This would ensure the system was modeled properly and also show how the motors would be affected by the three different varying loads and moment of inertias. Figure 5.6.1 shows the plot of results.

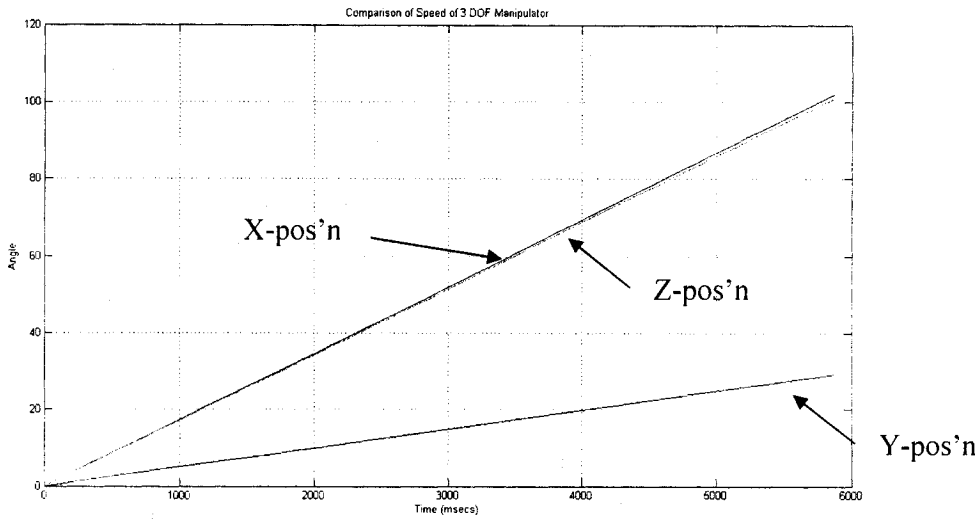

Figure 5.6.1 3 DOF manipulator response to common input

As expected the X and Z angular velocities (degree/sec) are very similar, Z angular motion is slightly different due to the added weight and inertia requirements of the

cross axis block (see appendix II), which results in the slightly slower response of Z angular velocity. The Y angular velocity lags much slower behind that of the two other DOF partly because of the much larger moment of inertia and also because of the slight variances in pulley size compared with that of the other two. Figure 5.6.2 shows the systems response to a 45 degree step input.

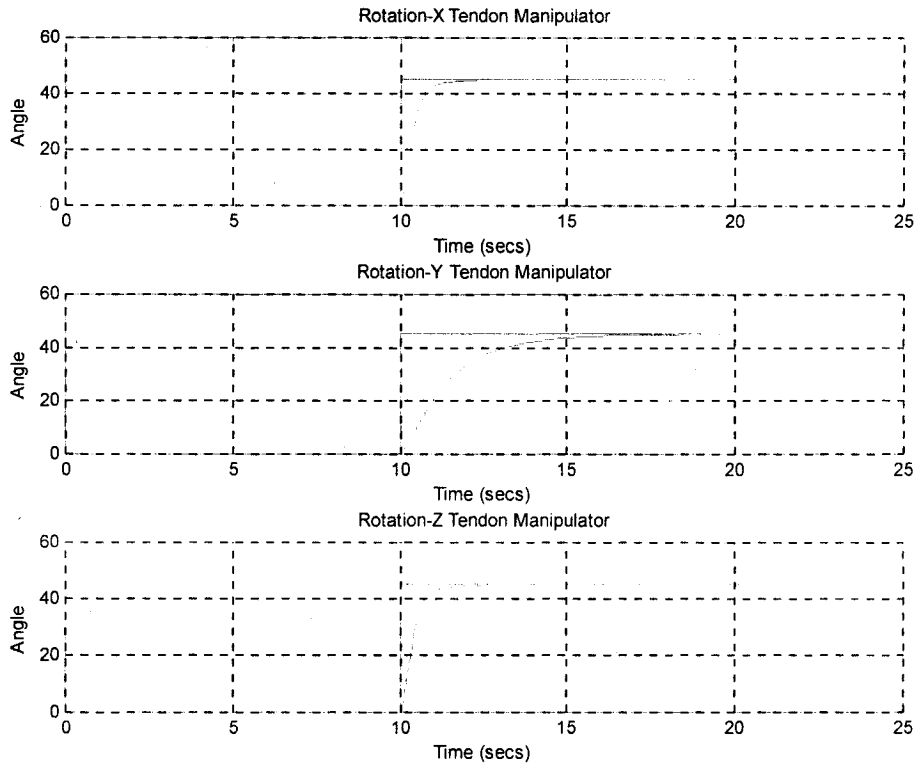

Figure 5.6.2 PID 3 DOF system response to a 45° step input

As can be seen the system response is acceptable for the X and Z directions, while in the direction Y might require improvement, an issue addressed later during the observer controller system design.

5.7 Observer for 3-DOF system:

As shown in chapter 2 and 3, the observer control system with the feedforward friction value can give better results than those expected from a normal PID control system. To develop an observer system for the 3 DOF system, each joint can be looked at independently. Figure 5.7.1 illustrates the simple joint (in this case the upper joint), and shows that in this portion of the manipulator it can be considered an inverted pendulum.

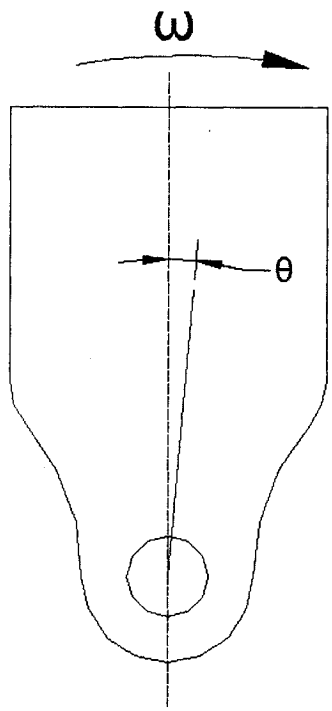

Figure 5.7.1 Simplified joint of the 3-DOF system

The joint can be simplified as that of Chapter 2, in that the observer is modeled for angular position control, and the estimate of velocity calculated by the observer is used for the friction value. As in Chapter 3, the variables used in the observer control simply need to be recalculated for the equipment and system considered in the design of a 3-DOF manipulator.

These values were used as:

$$\alpha = -42.34$$
$$\beta = 3257.1$$
$$K_1 = -28.22$$
$$K_2 = 199.2$$
$$g_1 = .0611$$
$$g2 = -.008$$

Each DOF receives its own observer control, same as for the PID control, and this allows independent joint motion and results in better performance for the system. In response to the same 45° step input response used as the benchmark for systems testing, the newly developed observer and the previous the PID controller response are shown in figure 5.7.2, on 1 DOF only (X axis).

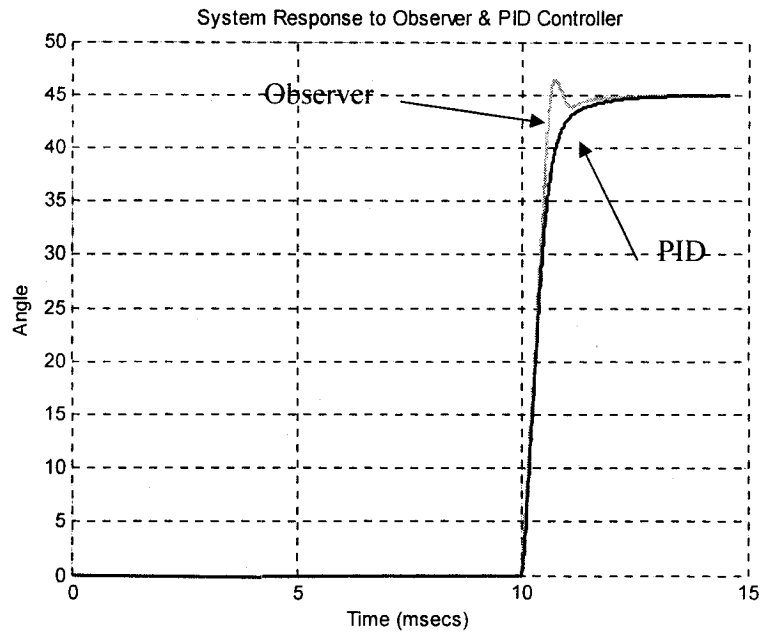

Figure 5.7.2 45 Step input system response for observer & PID control

As seen in the figure the observer control system does provide faster system response but at the expense of an overshoot; with some slight adjusting of the values for the observer, this response could be modified to give acceptable system response as seen in figure 5.7.3.

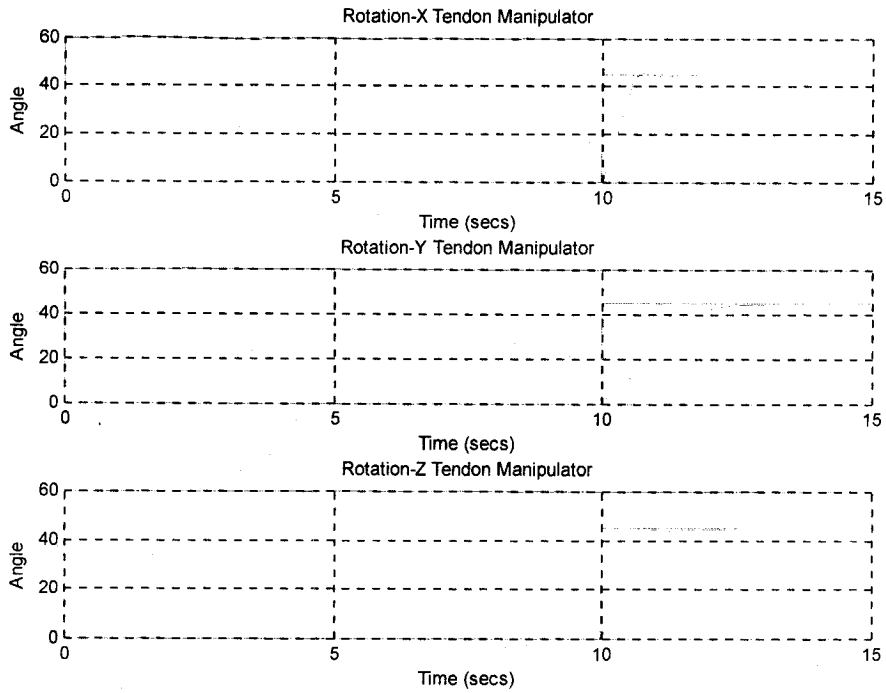

Figure 5.7.3 45° step input system response 3-DOF manipulator

The system response of the observer reaches the desired value just slightly quicker than the PID controller (approximately .35 seconds quicker).

Figure 5.7.4 shows the system response to a sinusoidal input of amplitude 90 (±90 is full lock for X and Z positions) and a magnitude of 1rad/sec (57.3°/sec).

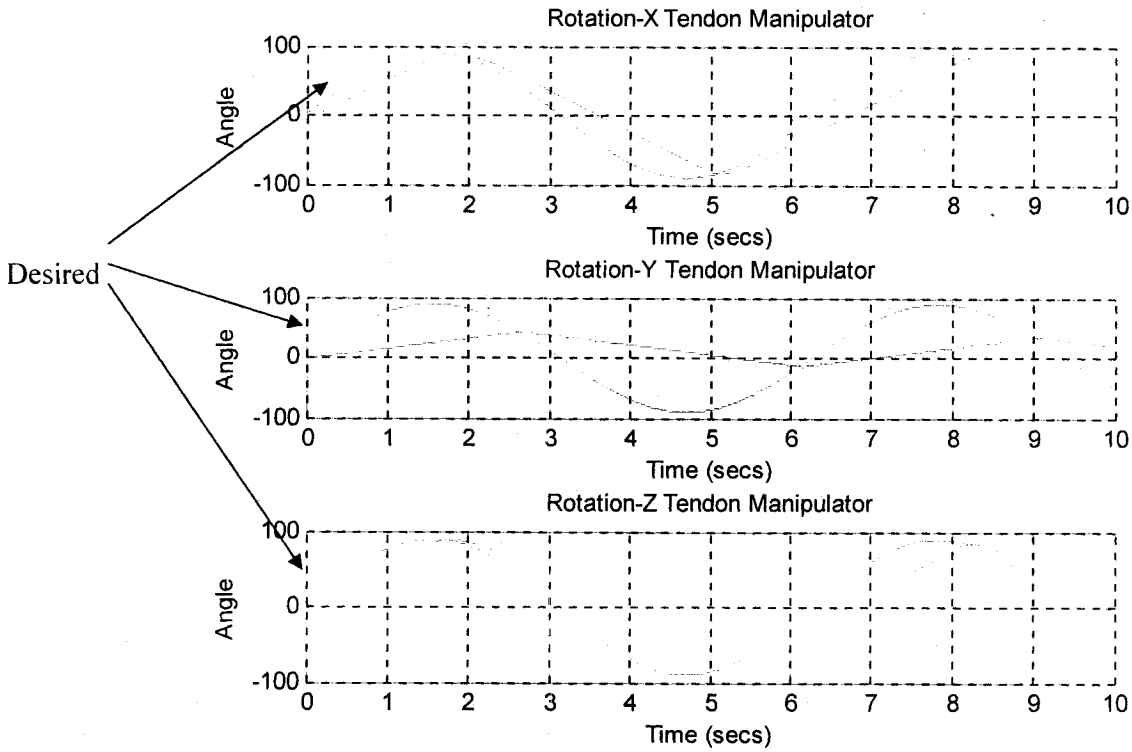

Figure 5.7.4 3 DOF system response to 1rad/sec 90° sinusoidal input

As seen in this figure, the rotation Y, lags slightly behind because of its limitation of geometry, the maximum angular velocities of the unloaded manipulator are approximately 58.5°/second in the X and Z rotations and approximately 16.8°/second for the Y direction. Therefore this system test is far exceeding the capabilities of the Y rotation and fast approaching that of the manipulator. It is therefore much easier to test the systems response on a smaller magnitude sinusoidal input, figure 5.7.5 shows the test approaching the maximum velocity of the manipulator as 90 amplitude and a magnitude of .261rad/sec (15°/sec)

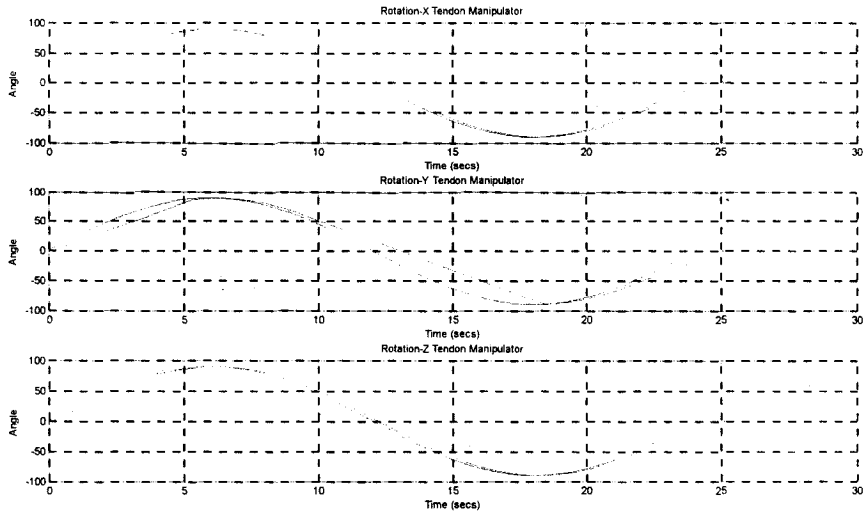

Figure 5.7.5 3 DOF system response to .261rad/sec 90° sinusoidal input

As seen in figure 5.7.5, the system response for the X and Z Rotations are very close to that of the desired sinusoidal input, the maximum difference is 4.5726°, which occurs directly at a time of t=.4234 milliseconds which is at the beginning of the simulation before the manipulator begins to move. The maximum difference for the rotation in direction Y however is much greater the largest error is 30.9458°, due to this test being so close to the maximum velocity of the manipulator. The error of the three DOF over the simulation is shown in figure 5.7.6.

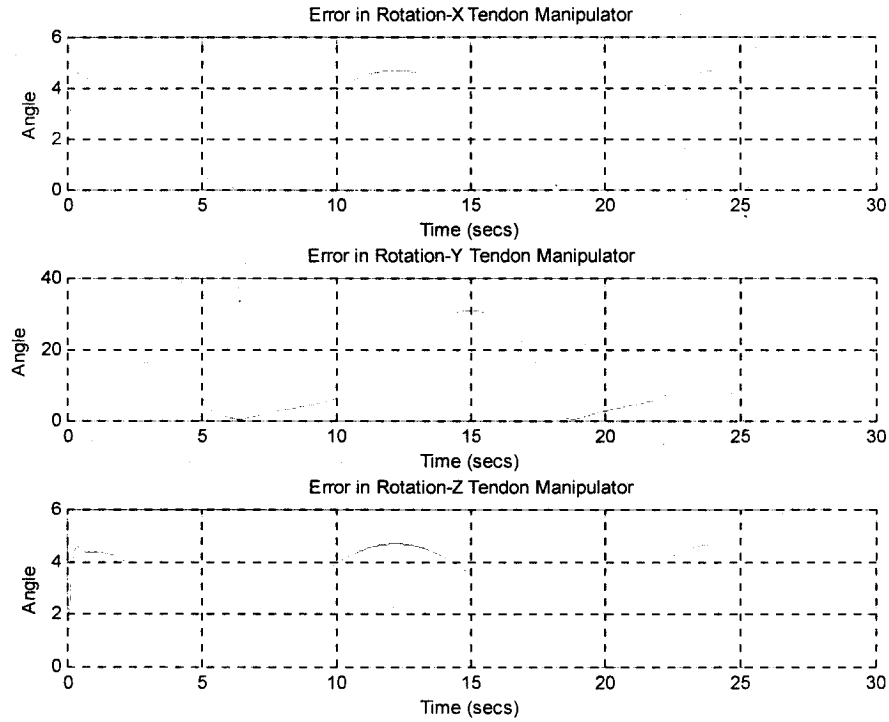

Figure 5.7.6 3 DOF manipulator error for sinusoidal input

The average difference over the 360° range is 2.8297 in rotation X, 3.0723 in rotation Z, and 11.4602 in rotation Y, this equates to .79%, .85% and 3.18% of error for the three DOF's.

CONCLUSIONS

General Remarks:

Over the course of this research project many lessons were learned - some very positive, and others negative. The steps taken along the way of any project are the unknowns, what is known is the hypothesis, which the outcome may or may not support. The basic requirement of this project was to design a new type of manipulator which would closely replicate that of the human wrist. It has been shown by the steps taken through this project that it is very possible. The ultimate goal of this project was to design a 3 DOF tendon manipulator system; the second was to build the best control system for it.

Discussion of Results:

The two experiments performed in this project, the observer experiment and the 1 DOF manipulator served their purpose very well. The purpose of the feedback instruments observer experiment was to implement an observer with feedforward friction compensation, which was shown to give very good results over the observer without the feedforward design. This step in the development of a 3 DOF manipulator was also very beneficial as it was also used to implement the control software, MathWorks MATLAB xPC Target.

The main experiment, building the 1 DOF tendon driven manipulator was one of the largest hurdles overcome in this project, but one of the most important lessons learned.

The results gathered in the course of its use were viable in all the other aspects of this project, especially the SimMechanics portion. Through proving that similar results could be gathered with SimMechanics gives great weight to the validity of the design and expected results of the 3-DOF manipulator. The actual retrofitting of the experiment, which included design and manufacturing of many components, gave valuable insight for the design of the 3 DOF manipulator, which was to come later in the project. Adjusting the observer control system to this experiment reinforced the development of the observer and also was the proving ground for whether or not this control system was best for the tendon driven application. While the use of the observer gives better results over traditional PID systems, the feedforward of friction may not be an absolute requirement on a system that is tendon based. Depending on the design of the system, friction compensation may not be required. If a system for example is not tendon based then friction compensation is a very valuable asset, however if the system is tendon based, with low friction to begin with (ball bearing design etc.) then friction compensation may not prove to be give much better results, due to other factors such as tendon slack.

Recommendations for Future Work:

The most obvious recommendation is to build the 3 DOF tendon driven manipulator, as it will prove to be the ultimate confirmation of this thesis' work. Besides that, a first recommendation is to continue improving and fine tuning the system that was built. The 1-DOF tendon manipulator's performance and reliability could very easily be improved as mentioned early. Through replacing all tachometers and potentiometers with optical encoders an important step forward would be experienced but at a large cost, the DAQ and xPC target software doesn't support so far optical encoders so then a microprocessor would have had to be used at a much larger cost. The second improvement to the 1-DOF system would have been to use strain gauges instead of the simple tendon slack absorbing system (TSAS) used to regulate slack, this however was not the purpose of the 1-DOF system, the purpose was to gather results and prove that tendon manipulated systems are easily designed and implemented.

REFERENCES

References

1. Jacobsen, S.C.; Ko, H.; Iversen, E.K.; Davis, C.C "Control strategies for tendon-driven manipulators" *Control Systems Magazine, IEEE* , Volume: 10 , Issue: 2 , Feb. 1990 Pages:23 – 28

2. D.E.T. Shepherd & A.J. Johnstone, "Design Considerations for a wrist implant" *Medical Engineering & Physics* Aug. 2002 pg. 641 – 650

3. Lorei, Matthew, et al. "Failed total Wrist Arthroplasty: Analysis of Failures and Results of Operative Management." *Clinical Orthopaedics and Related Research* Vol 1(342) Sept. 97 pg. 84-93

4. Guo, G.; Gruver, W.A.; Qian, X, "A robotic hand mechanism with rotating fingertips and motor-tendon actuation" *Systems, Man, and Cybernetics, 1991. 'Decision Aiding for Complex Systems, Conference Proceedings., 1991 IEEE International Conference on* , 13-16 Oct. 1991 Pages:1023 - 1028 vol.

5. Kurtz, R.; Hayward, V. "Dexterity measure for tendon actuated parallel mechanisms" Advanced Robotics, 1991. *'Robots in Unstructured Environments', 91 ICAR., Fifth International Conference on* , 19-22 June 1991 Pages:1141 - 1146 vol.2

6. Kaneko, M.; Wada, M.; Maekawa, H.; Tanie, K., "A new consideration on tendon-tension control system of robot hand" *Robotics and Automation, 1991. Proceedings., 1991 IEEE International Conference on* , 9-11 April 1991 Pages:1028 - 1033 vol.2

7. Kaneko, M.; Yamashita, T.; Tanie, K, "Basic considerations on transmission characteristics for tendon drive robots"Advanced Robotics, 1991. *'Robots in Unstructured Environments', 91 ICAR., Fifth International Conference on* , 19-22 June 1991 Pages:827 - 832 vol.1

8. Jacobsen, S.; Iversen, E.; Knutti, D.; Johnson, R.; Biggers, K, "Design of the Utah/M.I.T. Dextrous Hand" *Proceedings. 1986 IEEE International Conference on Robotics and Automation.*Page(s): 1520- 1532

9. Benjamin C. Kuo, "*Automatic Control Systems 7th Ed.*", Prentice Hall, New Jersey 1995.

10. Hristu, D.; Babb, J.; Singh, H.; Gottschlich, S, "Position and force control of a multifingered hand: a comparison of fuzzy logic to traditional PID control"

Intelligent Robots and Systems '94. 'Advanced Robotic Systems and the Real World', IROS '94. Proceedings of the IEEE/RSJ/GI International Conference on , Volume: 2 , 12-16 Sept. 1994
Pages:1391 - 1398 vol.2

11. Zadeh, L.A, "Fuzzy logic: issues, contentions and perspectives", *Acoustics, Speech, and Signal Processing, 1994. ICASSP-94., 1994 IEEE International Conference on* , Volume: vi , 19-22 April 1994
Pages:VI/183 vol.6

12. Bernard Friedland, "*Control System Design: An Introduction to State-Space Methods"* McGraw Hill Book Company New York 1986.

13. http://www.fbk.com/ Feedback Instruments Ltd. Website. Visited Sept 2003 – Oct 2004

14. http://www.ni.com/ National Instruments Website. Visited Sept 2003 – Oct 2004

15. Dan Necsulescu, "*Mechatronics*", Prentice Hall, Upper Saddle River, NJ, USA, 2002

16. Gorran Basic, *"Hardware in the Loop Simulation of Mechanical Loads for Mechatronics System Design"* University of Ottawa Master of Applied Science 2003.

17. http://www.ecpsystems.com ECP Systems Website Visited Sept 2003 – Oct 2004

18. Hermann Henrichfreise "Observer-based nonlinear compensation of Friction in a positioning system" *German-Polish Seminar, Cologne*, Oct. 1997 pg. 1-10

19. Mayer-Baese, U., "*Digital Signal Processing with Field Programmable Gate Arrays*", Springer, 2001.

20. Mathworks, "MATLAB Help: On-line (www.Mathworks.com, development tools for MATLAB V14.0)

21. Ogata, Katsuhiko. "*Modern Control Engineering 2nd Ed.*" Prentice Hall, New Jersey 1990.

22. . Giancoli, Douglas C. "*Physics for Scientists and Engineers with Modern Physics 3rd Ed.*" Prentice Hall New Jersey 1999.

23. Palmgren, A., "*Ball and Roller Bearings, 3rd ed*"., Philadelphia: SKF Industries, Inc., 1959.

24. Syh-Shiuh Yeh; Pau-Lo Hsu , "Design of precise multi-axis motion control systems" *Advanced Motion Control, 2000. Proceedings. 6th International Workshop on* , 30 March-1 A pril 2000, pg. 234-239

25. Jackson, Leland B. "*Digital Filters and Signal Processing*" Kluwer Academic Publishers, Boston, 1986

APPENDIX I
Drawings for 1 DOF Experiment Setup

NOTES:
1. ALREADY EXISTING PART ONLY NEEDS TO BE MODIFIED AS PER DRAWING
2. DIMENSIONS ARE IN INCHES UNLESS OTHERWISE NOTED
3. DRAWING CANNOT BE SCALED

REVISIONS				
ZONE	REV.	DESCRIPTION	DATE	APPROVED

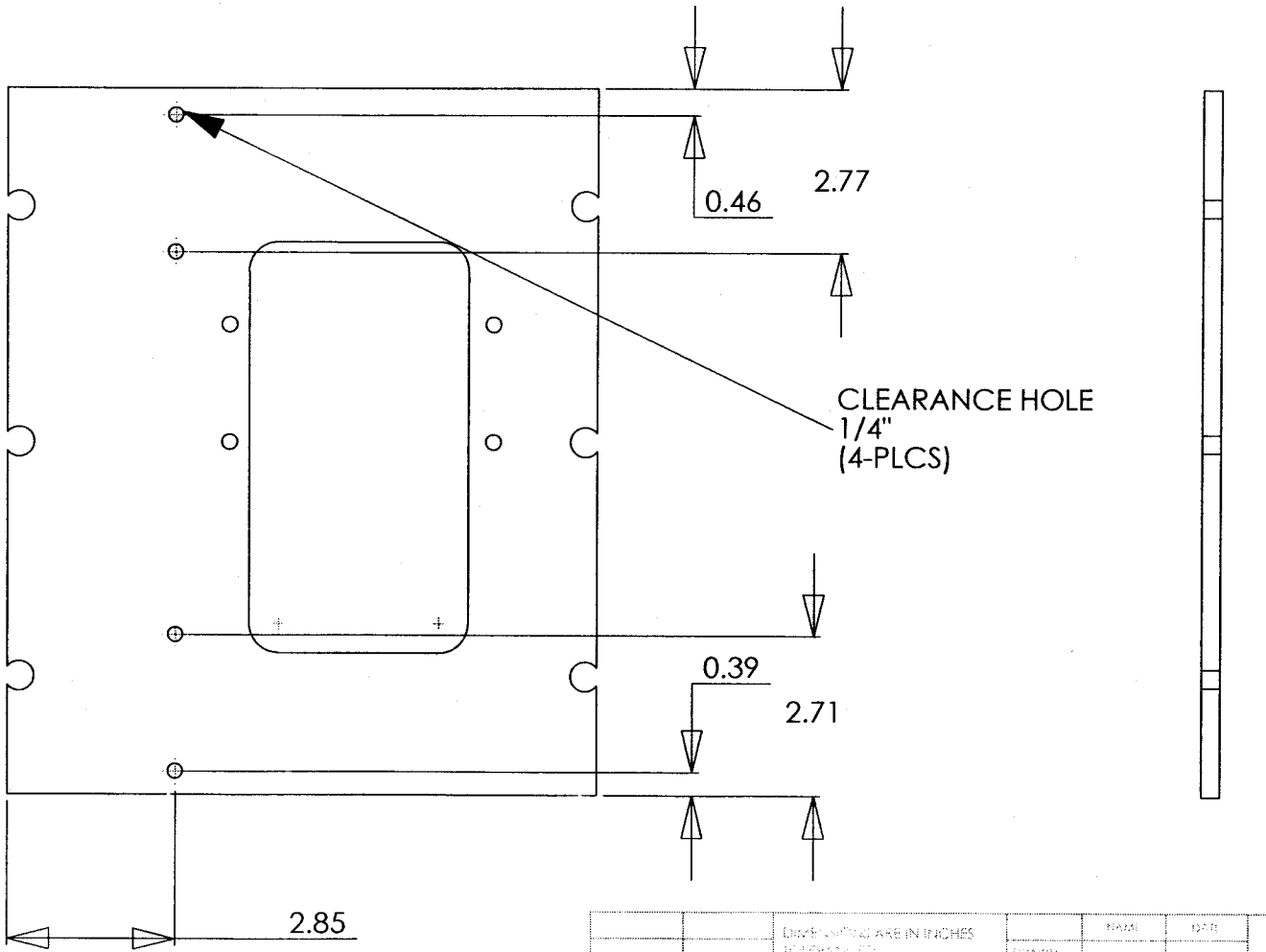

SolidWorks Educational License
Instructional Use Only

PROPRIETARY AND CONFIDENTIAL

	NAME	DATE
DRAWN		
CHECKED		
ENG APPR.		
MFG APPR.		
Q.A.		

UNIV. OF OTTAWA

BASE PLATE

MATERIAL: STEEL

SIZE: A

KEVIN GILBANK

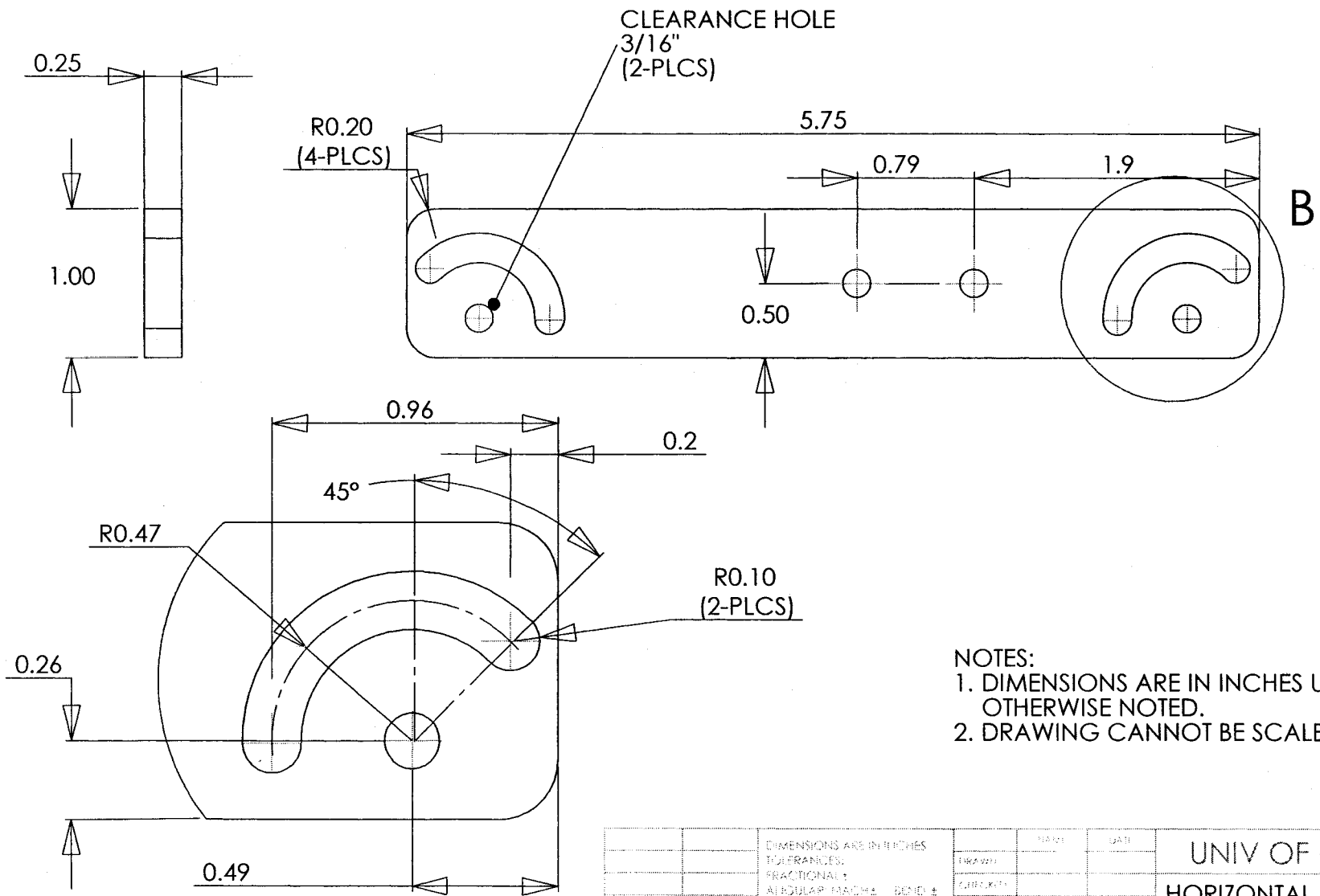

B (2 : 1)

NOTES:
1. DIMENSIONS ARE IN INCHES UNLESS OTHERWISE NOTED.
2. DRAWING CANNOT BE SCALED

UNIV OF OTTAWA

HORIZONTAL STRAIN BAR

STEEL

KEVIN GILBANK

A

PROPRIETARY AND CONFIDENTIAL

SolidWorks Educational License
Instructional Use Only

2-REQUIRED

ZONE	REV.	DESCRIPTION	DATE	APPROVED

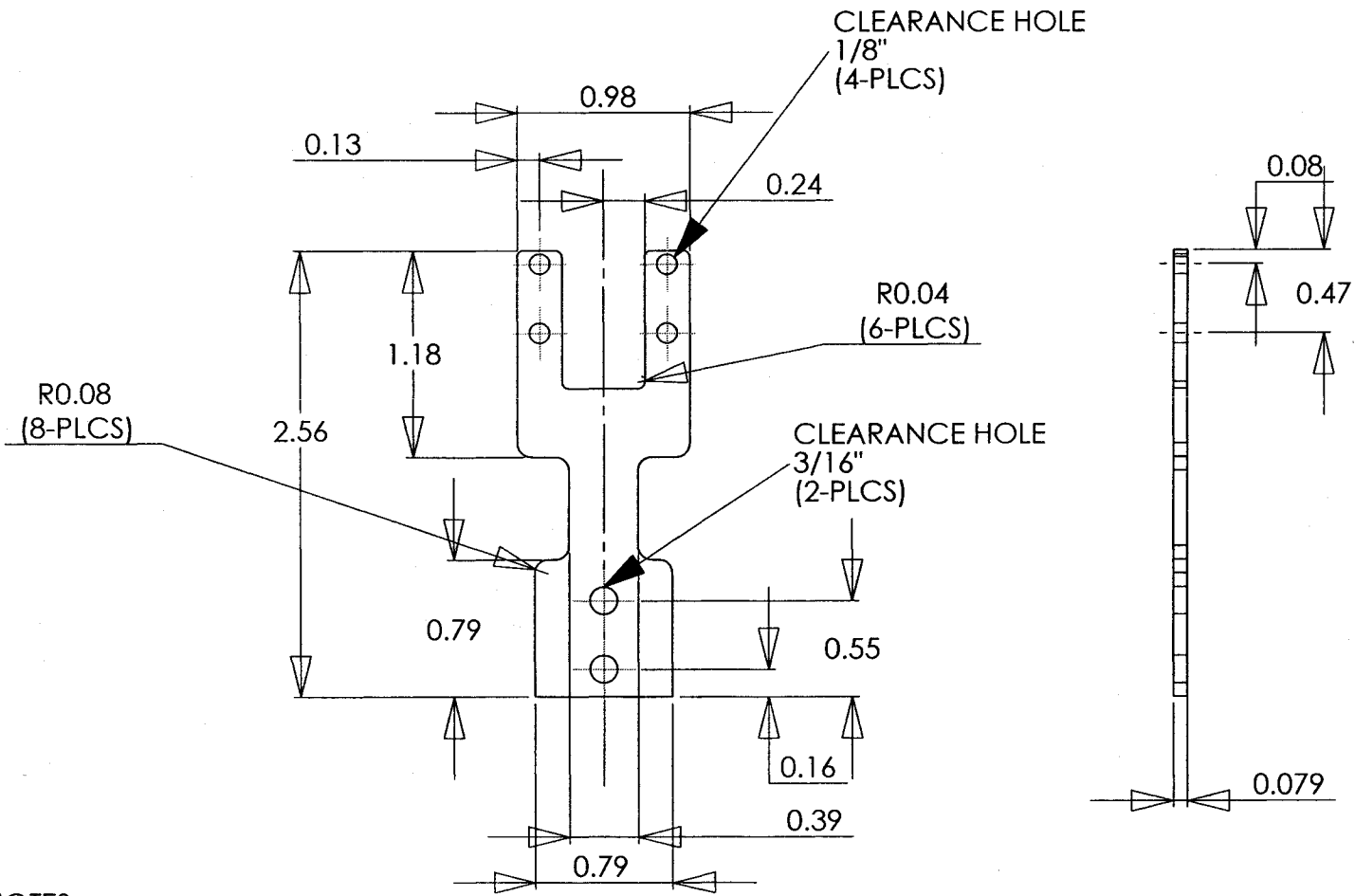

NOTES:
1. DIMENSIONS ARE IN INCHES UNLESS OTHERWISE NOTED.
2. DRAWING CANNOT BE SCALED

		DIMENSIONS ARE IN INCHES TOLERANCES: FRACTIONAL ± ANGULAR: MACH ± BEND ± TWO PLACE DECIMAL ± THREE PLACE DECIMAL ±		NAME	DATE
			DRAWN		
			CHECKED		
			ENG APPR.		
			MFG APPR.		
			Q.A.		
		MATERIAL —	COMMENTS:	STEEL	
		FINISH —			
NEXT ASSY	USED ON				
APPLICATION		DO NOT SCALE DRAWING			

UNIV. OF OTTAWA

STRAIN GAUGE PLATE

SIZE A | DWG. NO. KEVIN GILBANK | REV

PROPRIETARY AND CONFIDENTIAL
THE INFORMATION CONTAINED IN THIS DRAWING IS THE SOLE PROPERTY OF <INSERT YOUR COMPANY NAME HERE>. ANY REPRODUCTION IN PART OR AS A WHOLE WITHOUT THE WRITTEN PERMISSION OF <INSERT YOUR COMPANY NAME HERE> IS PROHIBITED.

SolidWorks Educational License
Instructional Use Only

2-REQUIRED

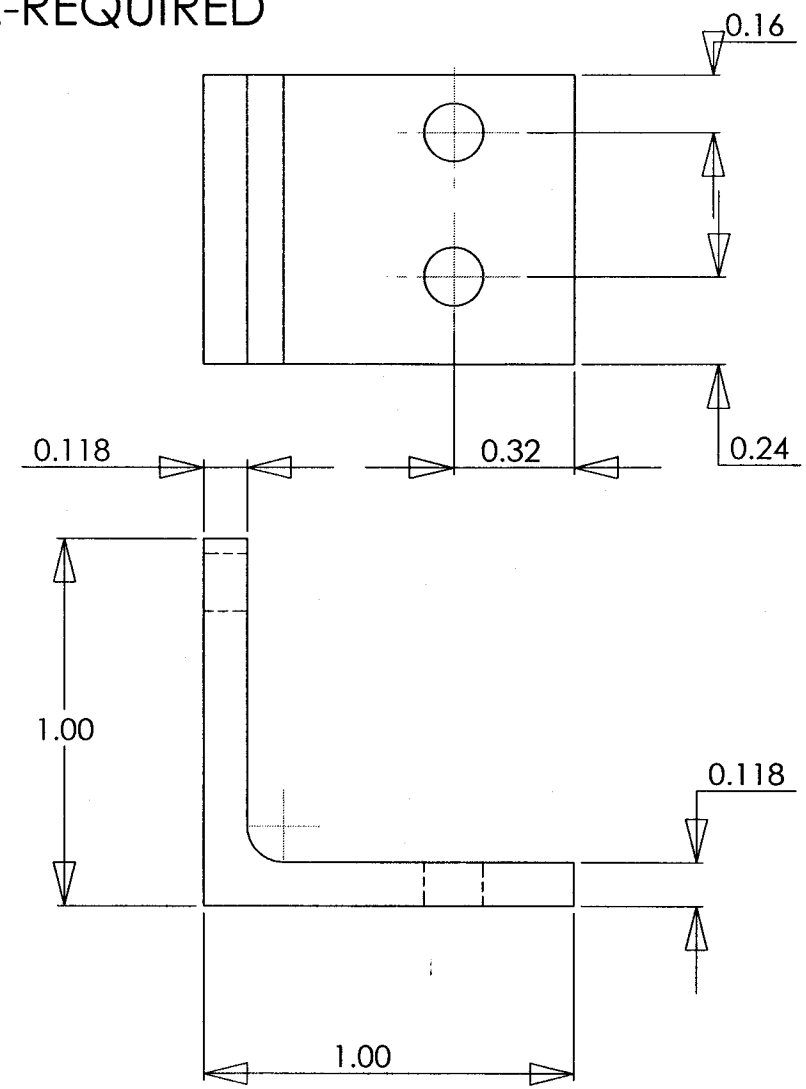

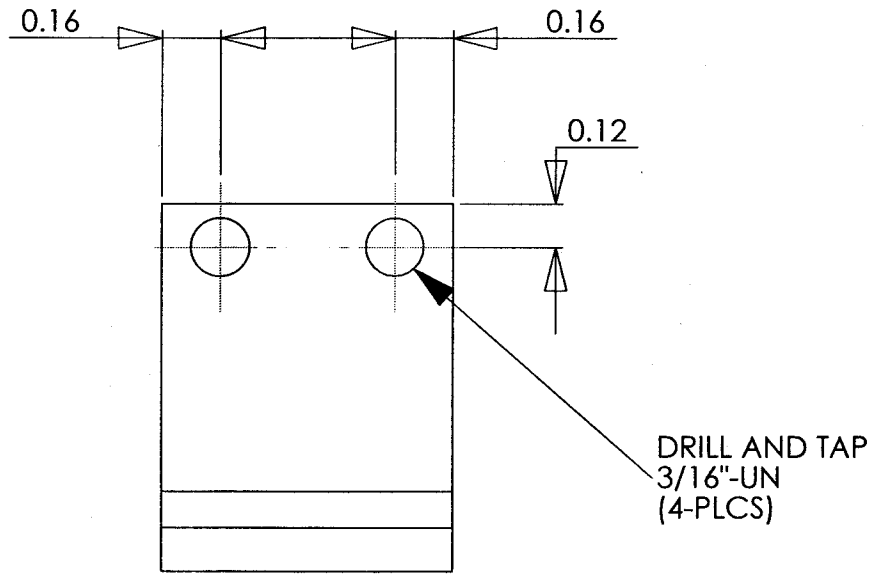

NOTES:
1. DIMENSIONS ARE IN INCHES UNLESS OTHERWISE NOTED.
2. DRAWING CANNOT BE SCALED

SolidWorks Educational License
Instructional Use Only

PROPRIETARY AND CONFIDENTIAL

DIMENSIONS ARE IN MM
TOLERANCES:
FRACTIONAL ±
ANGULAR: MACH ± BEND ±
TWO PLACE DECIMAL ±
THREE PLACE DECIMAL ±

	NAME	DATE
DRAWN		
CHECKED		
ENG APPR.		
MFG APPR.		

MATERIAL: STEEL

UNIV. OF OTTAWA

STRAIN GAUGE ANGLE BAR

SIZE A

KEVIN GILBANK

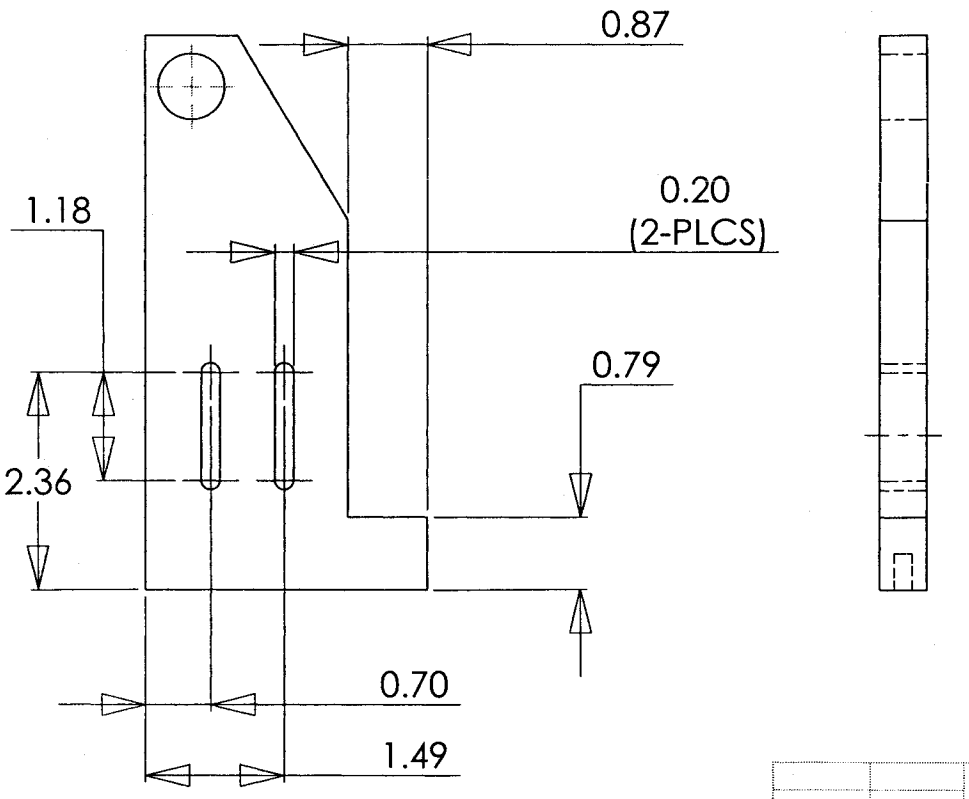

NOTES:
1. ALREADY EXISTING PART ONLY NEEDS TO BE MODIFIED AS PER DRAWING
2. DIMENSIONS ARE IN INCHES UNLESS OTHERWISE NOTED
3. DRAWING CANNOT BE SCALED

SolidWorks Educational License
Instructional Use Only

PROPRIETARY AND CONFIDENTIAL

UNIV. OTTAWA

PULLEY SUPPORT

A

KEVIN GILBANK

4-REQUIRED

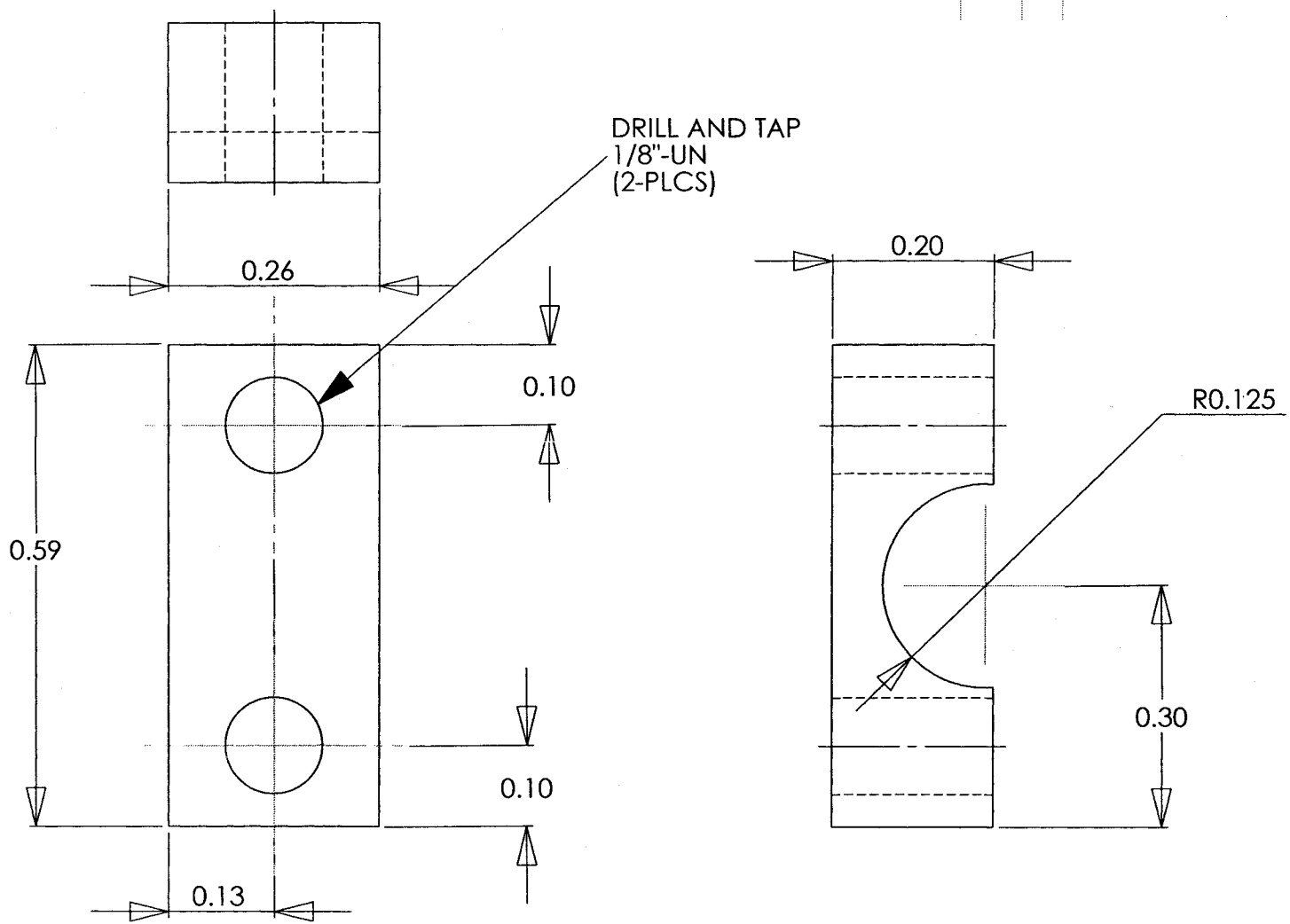

NOTES:
1. DIMENSIONS ARE IN INCHES UNLESS OTHERWISE NOTED.
2. DRAWING CANNOT BE SCALED

SolidWorks Educational License
Instructional Use Only

PROPRIETARY AND CONFIDENTIAL

DIMENSIONS ARE IN INCHES
TOLERANCES:
FRACTIONAL ±
ANGULAR: MACH ± BEND ±
TWO PLACE DECIMAL ±
THREE PLACE DECIMAL ±

STEEL

UNIV. OF OTTAWA

STRAIN GAUGE
PLATE SUPPORT

SIZE A

KEVIN GILBANK

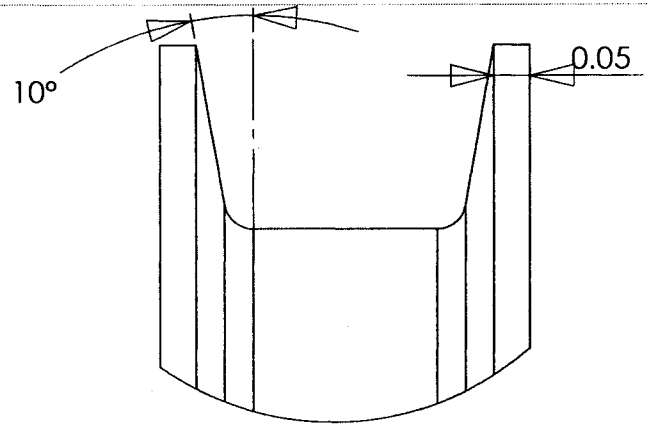

B (4 : 1)

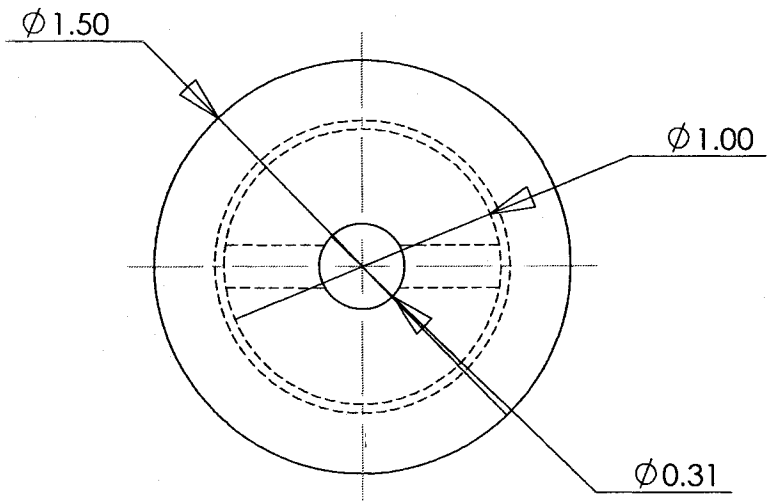

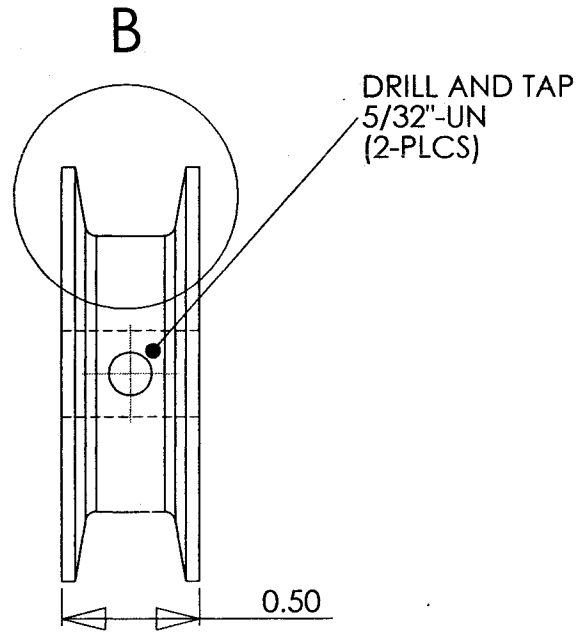

NOTES:
1. ALL DIMENSIONS ARE IN INCHES
   UNLESS OTHERWISE NOTED.
2. DRAWING CANNOT BE SCALED

SolidWorks Educational License
Instructional Use Only

PROPRIETARY AND CONFIDENTIAL

DIMENSIONS ARE IN INCHES
TOLERANCES:
FRACTIONAL ±
ANGULAR: MACH ± BEND ±
TWO PLACE DECIMAL ±
THREE PLACE DECIMAL ±

MATERIAL —

FINISH —

STEEL

UNIV. OF OTTAWA

MOTOR
WHEEL

SIZE A

KEVIN GILBANK

2-REQUIRED

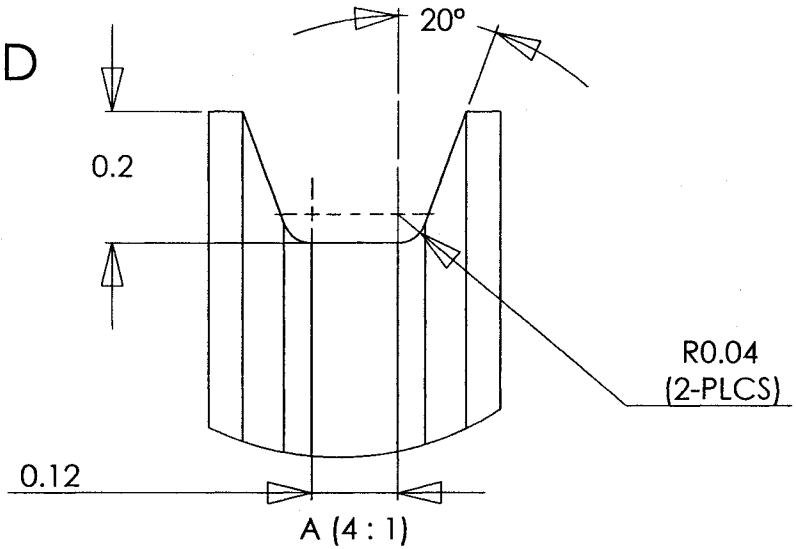

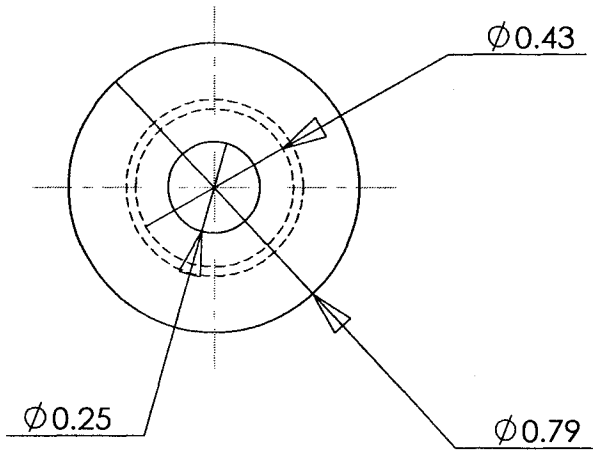

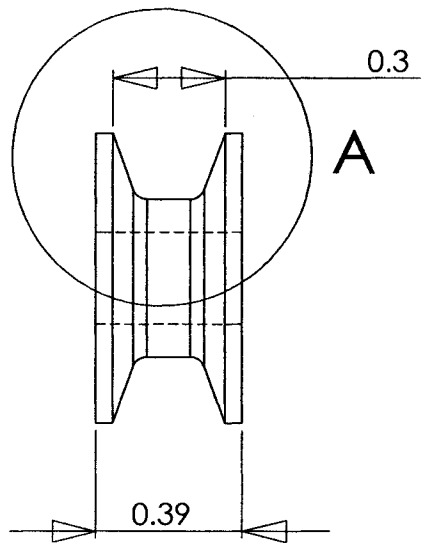

NOTES:
1. DIMENSIONS ARE IN INCHES UNLESS OTHERWISE NOTED.
2. DRAWING CANNOT BE SCALED

SolidWorks Educational License
Instructional Use Only

PROPRIETARY AND CONFIDENTIAL

UNIV. OF OTTAWA	
STRAIN GAUGE WHEEL	
STEEL	
KEVIN GILBANK	

2-REQUIRED

ZONE	REV	REVISIONS DESCRIPTION	DATE	APPROVED

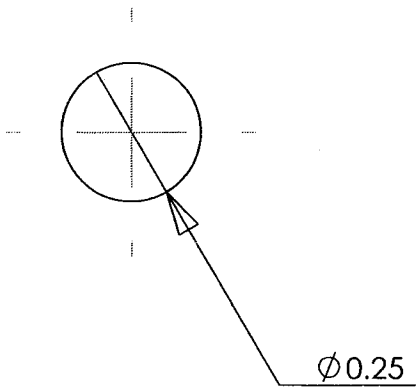

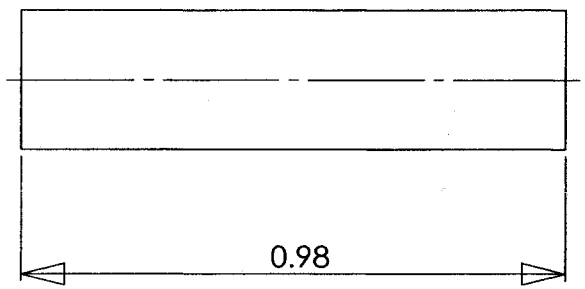

NOTES:
1. DIMENSIONS ARE IN INCHES UNLESS OTHERWISE NOTED.
2. DRAWING CANNOT BE SCALED

SolidWorks Educational License
Instructional Use Only

PROPRIETARY AND CONFIDENTIAL
THE INFORMATION CONTAINED IN THIS DRAWING IS THE SOLE PROPERTY OF <USED COMPANY NAME HERE>. ANY REPRODUCTION IN PART OR AS A WHOLE WITHOUT THE WRITTEN PERMISSION OF <INSERT COMPANY NAME HERE> IS PROHIBITED.

DIMENSIONS ARE IN INCHES
TOLERANCES:
FRACTIONAL ±
ANGULAR: MACH ± BEND ±
TWO PLACE DECIMAL ±
THREE PLACE DECIMAL ±

MATERIAL —
FINISH —
NEXT ASSY | USED ON
APPLICATION | DO NOT SCALE DRAWING

	NAME	DATE
DRAWN		
CHECKED		
ENG APPR.		
MFG APPR.		
Q.A.		
COMMENTS:		

STEEL

UNIV. OF OTTAWA

STRAIN GAUGE WHEEL SHAFT

SIZE A

KEVIN GILBANK

APPENDIX II
Drawings for 3 DOF Manipulator

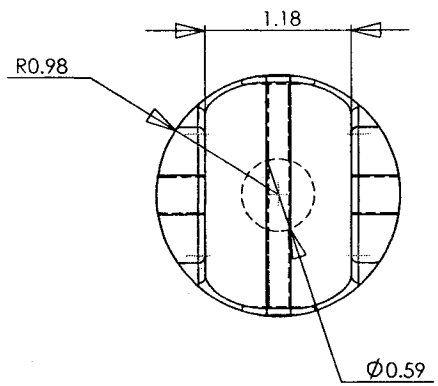

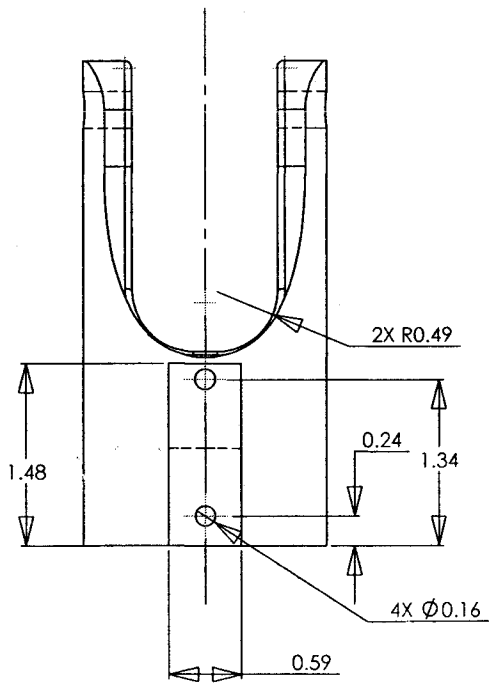

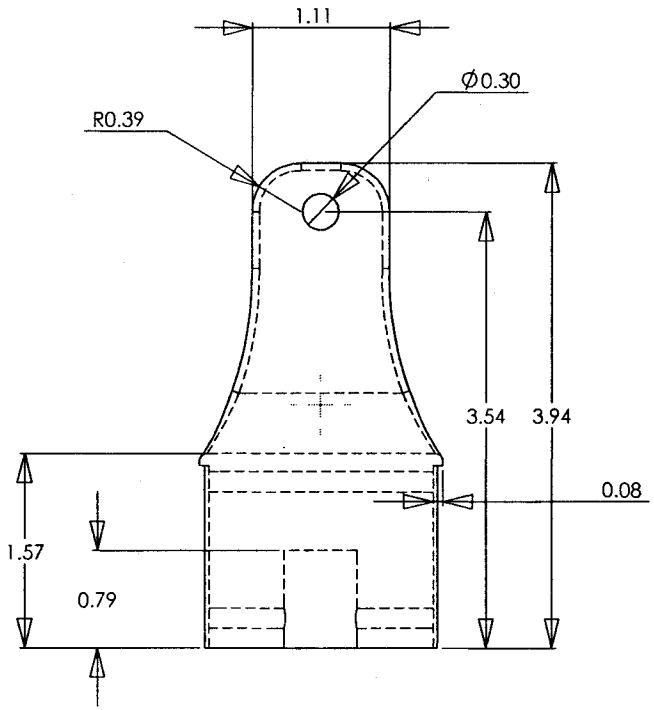

NOTES:
1. UNLESS OTHERWISE SPECIFIED ALL RADII AND FILLETS ARE TO BE 0.05

SolidWorks Educational License
Instructional Use Only

UNLESS OTHERWISE SPECIFIED: DIMENSIONS ARE IN INCHES
SURFACE FINISH:
TOLERANCES:
LINEAR:
ANGULAR:

FINISH

DEBUR AND BREAK SHARP EDGES

DO NOT SCALE DRAWING

REVISION

	NAME	SIGNATURE	DATE
DRAWN	KG		
CHK'D			
APPV'D	KG		
MFG			
Q.A			

TITLE:

MANIPULATOR JOINT

MATERIAL:
ALUMINIUM

DWG NO
000001

A3

WEIGHT:

SCALE 1:1

SHEET 1 OF 1

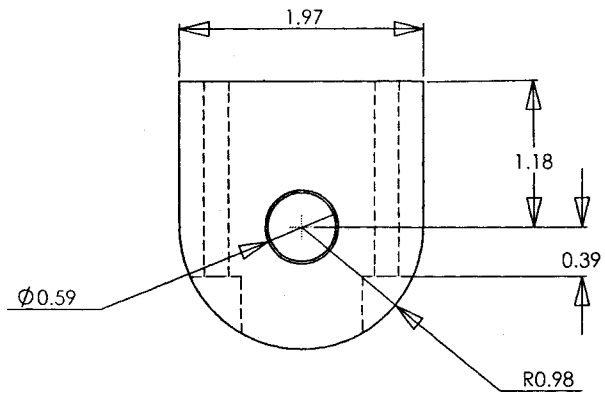

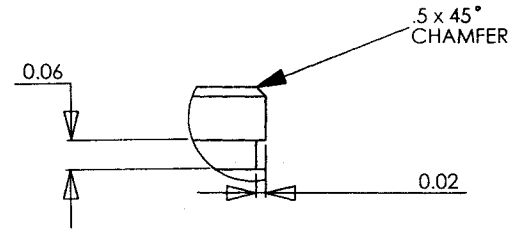

DETAIL C
SCALE 4 : 1

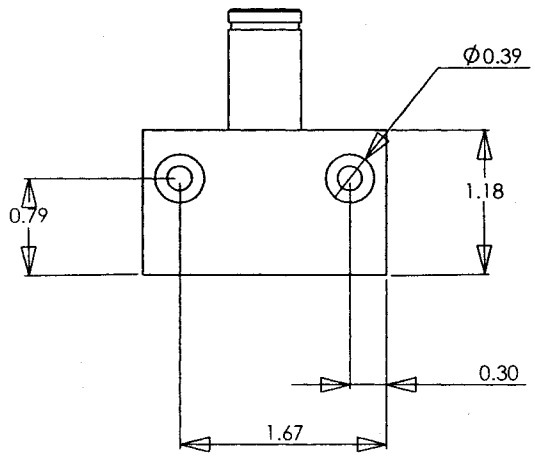

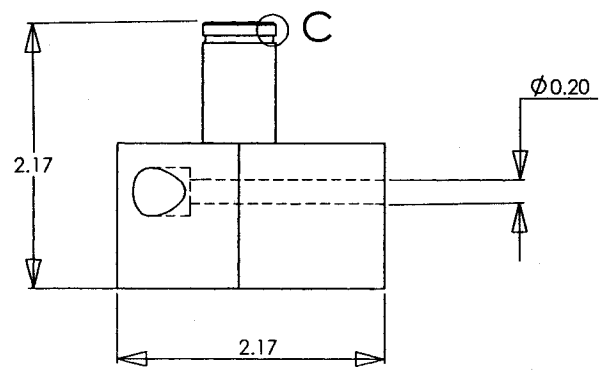

UNLESS OTHERWISE SPECIFIED:
DIMENSIONS ARE IN INCHES
SURFACE FINISH:
TOLERANCES:
LINEAR:
ANGULAR:

FINISH:

DEBUR AND BREAK SHARP EDGES

DO NOT SCALE DRAWING

REVISION

	NAME	SIGNATURE	DATE
DRAWN	KG		
CHK'D			
APP'D	KG		
MFG			
Q.A			

TITLE:

ROTATIONAL BASE JOINT

MATERIAL
ALUMINUM

DWG NO.
000002

A3

WEIGHT:

SCALE: 1:1

SHEET 1 OF 1

SolidWorks Educational License
Instructional Use Only

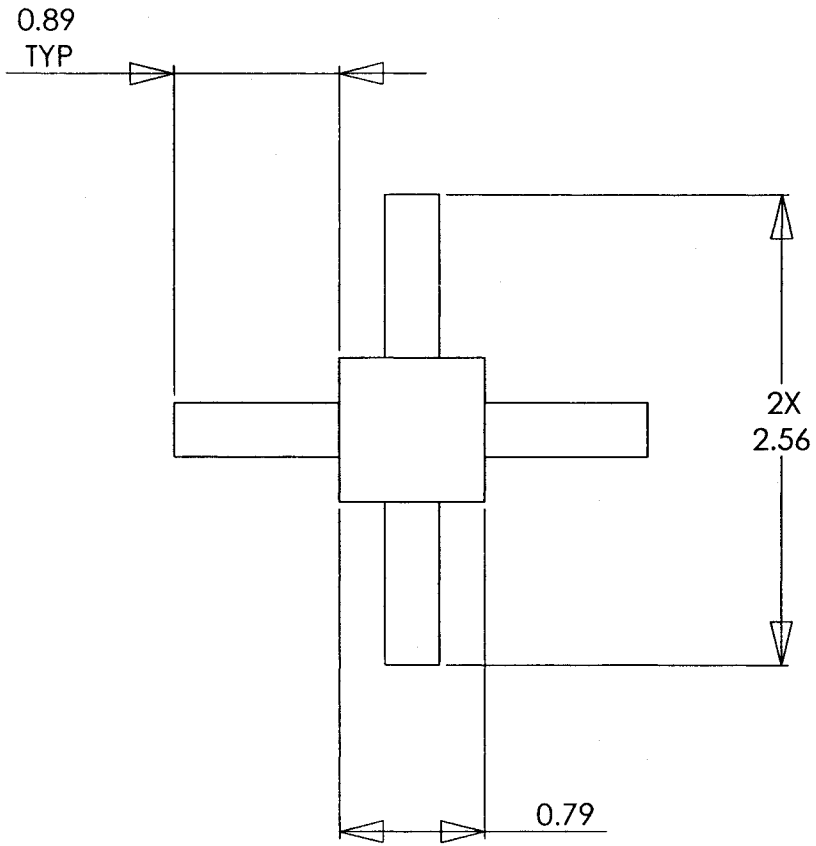

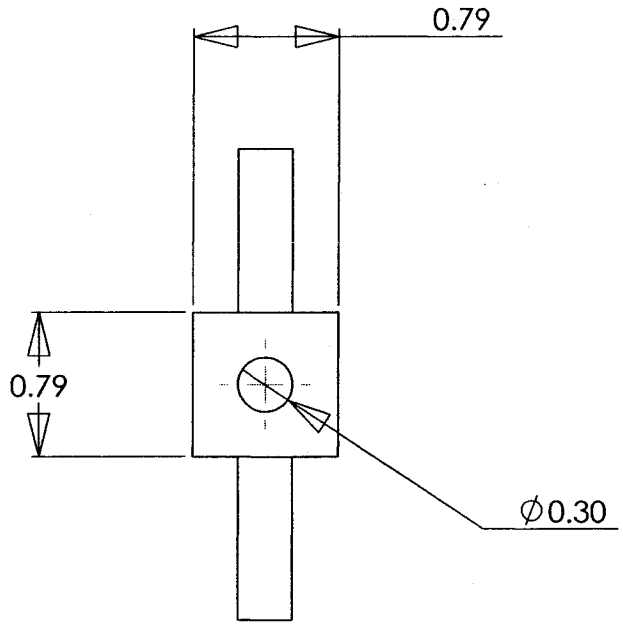

		DIMENSIONS ARE IN INCHES TOLERANCES: FRACTIONAL ± ANGULAR: MACH ± BEND ± TWO PLACE DECIMAL ± THREE PLACE DECIMAL ±		
		MATERIAL —		
NEXT ASSY	USED ON	FINISH —		
APPLICATION		DO NOT SCALE DRAWING		

	NAME	DATE
DRAWN		
CHECKED		
ENG APPR.		
MFG APPR.		
Q.A.		
COMMENTS:		

STEEL

UNIV. OF OTTAWA

3 DOF MANIPULATOR
AXIS SHAFT

PART NO. 000003

SIZE	DRAWN BY	REV
A	KEVIN GILBANK	
	WEIGHT	

PROPRIETARY AND CONFIDENTIAL
THE INFORMATION CONTAINED IN THIS DRAWING IS THE SOLE PROPERTY OF <INSERT YOUR COMPANY NAME HERE>. ANY REPRODUCTION IN PART OR AS A WHOLE WITHOUT THE WRITTEN PERMISSION OF <INSERT YOUR COMPANY NAME HERE> IS PROHIBITED.

SolidWorks Educational License
Instructional Use Only

REVISIONS				
ZONE	REV.	DESCRIPTION	DATE	APPROVED

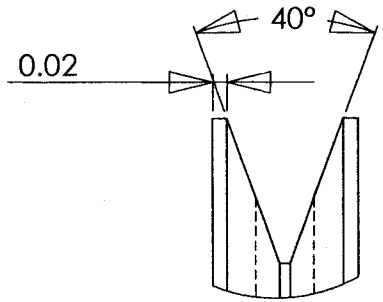

DETAIL C
SCALE 4 : 1

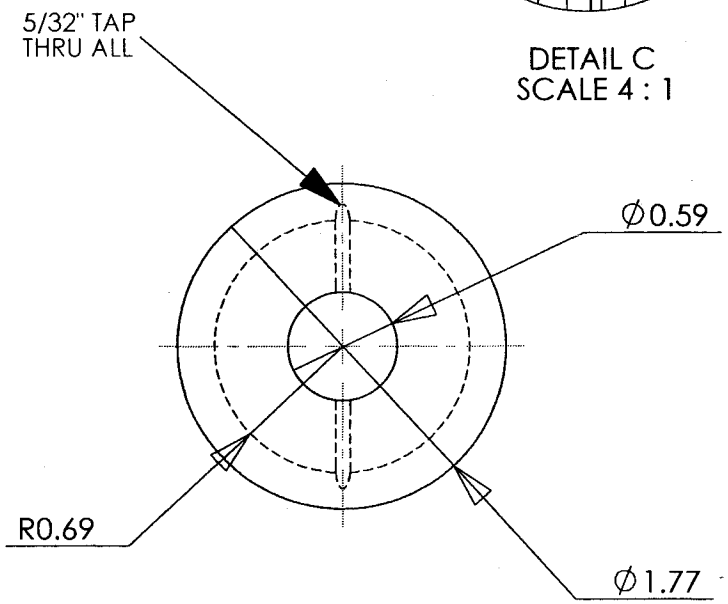

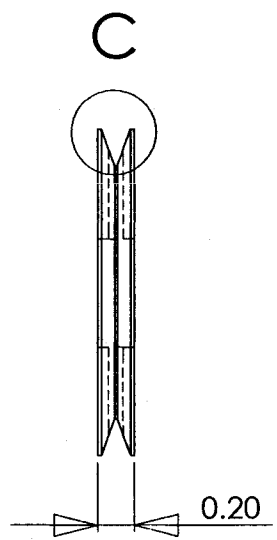

SolidWorks Educational License
Instructional Use Only

PROPRIETARY AND CONFIDENTIAL
THE INFORMATION CONTAINED IN THIS DRAWING IS THE SOLE PROPRIETARY OF <INSERT COMPANY NAME HERE> ANY REPRODUCTION IN PART OR AS A WHOLE WITHOUT THE WRITTEN PERMISSION OF <INSERT COMPANY NAME HERE> IS PROHIBITED.

DIMENSIONS ARE IN INCHES
TOLERANCES:
FRACTIONAL ±
ANGULAR: MACH ± BEND ±
TWO PLACE DECIMAL ±
THREE PLACE DECIMAL ±

MATERIAL —
FINISH —

NEXT ASSY | USED ON

APPLICATION | DO NOT SCALE DRAWING

	NAME	DATE
DRAWN		
CHECKED		
ENG APPR.		
MFG APPR.		
Q.A.		
COMMENTS:		

ALUMINUM

UNIV. OF OTTAWA

3 DOF MANIPULATOR
BOTTOM PULLEY

PART NO. 000004

SIZE A | DRAWN KEVIN GILBANK | REV.

SCALE: | WEIGHT: | SHEET

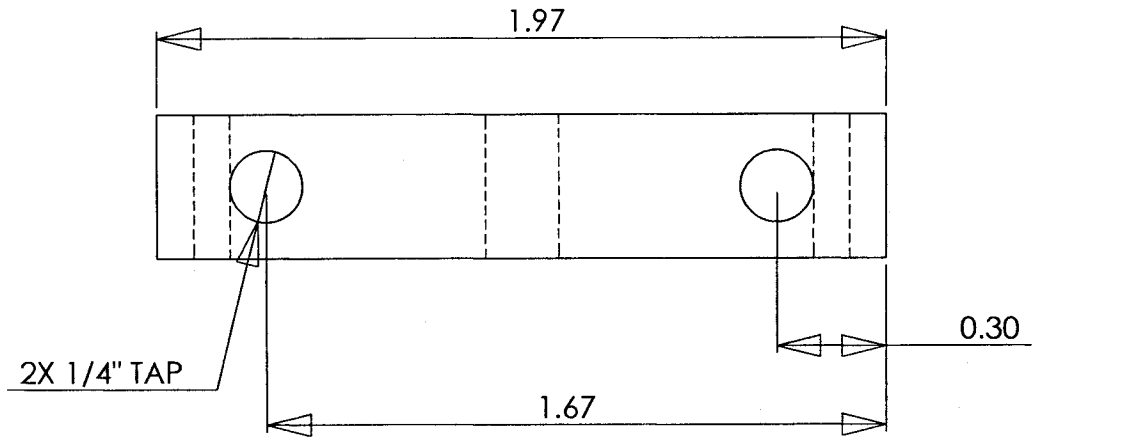

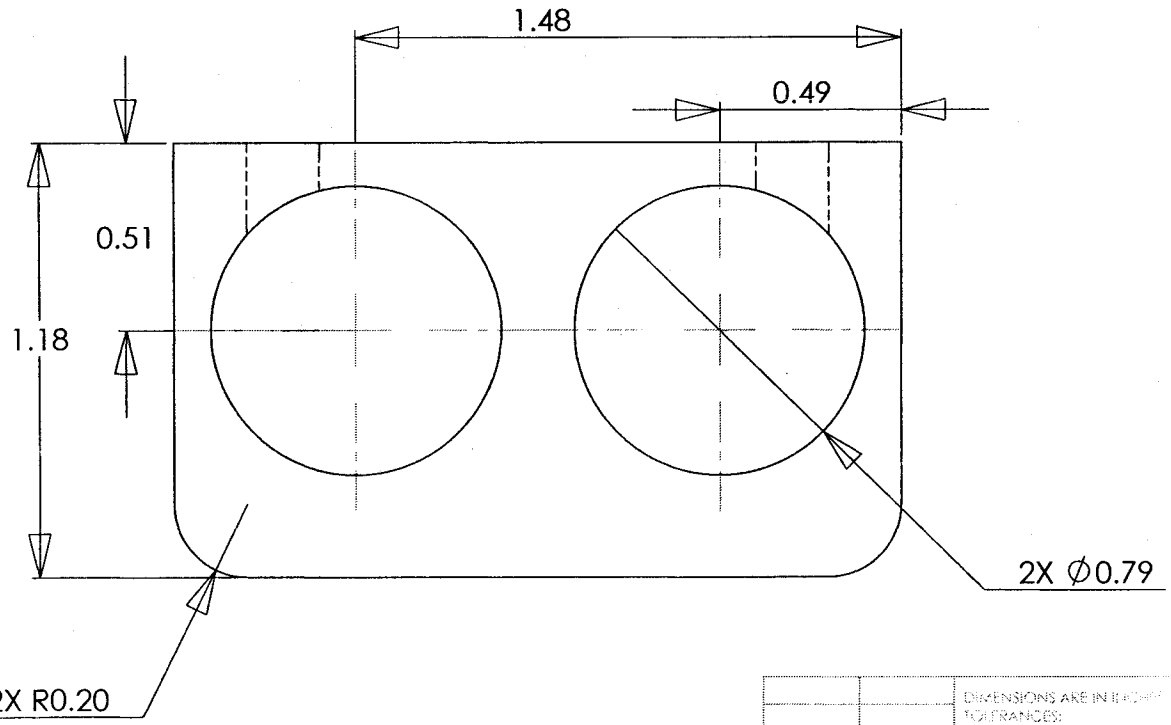

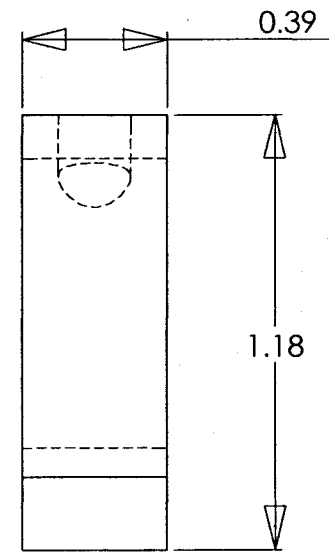

REVISIONS				
ZONE	REV.	DESCRIPTION	DATE	APPROVED

SolidWorks Educational License
Instructional Use Only

PROPRIETARY AND CONFIDENTIAL
THE INFORMATION CONTAINED IN THIS DRAWING IS THE SOLE PROPERTY OF <USER'S COMPANY NAME>. ANY REPRODUCTION IN PART OR AS A WHOLE WITHOUT THE WRITTEN PERMISSION OF <USER'S COMPANY NAME> IS PROHIBITED.

DIMENSIONS ARE IN INCHES
TOLERANCES:
FRACTIONAL ±
ANGULAR: MACH ± BEND ±
TWO PLACE DECIMAL ±
THREE PLACE DECIMAL ±

	NAME	DATE
DRAWN	KG	
CHECKED		
ENG APPR.		
MFG APPR.		
Q.A.		
COMMENTS:		

MATERIAL: ---
FINISH: ---
NEXT ASSY | USED ON
APPLICATION | DO NOT SCALE DRAWING

ALUMINUM

UNIV. OF OTTAWA

DUAL
MOTOR MOUNT

PART NO. 000005

SIZE	DRAWING NO.	REV
A	KEVIN GILBANK	

SCALE: | WEIGHT: | SHEET 1 OF 1

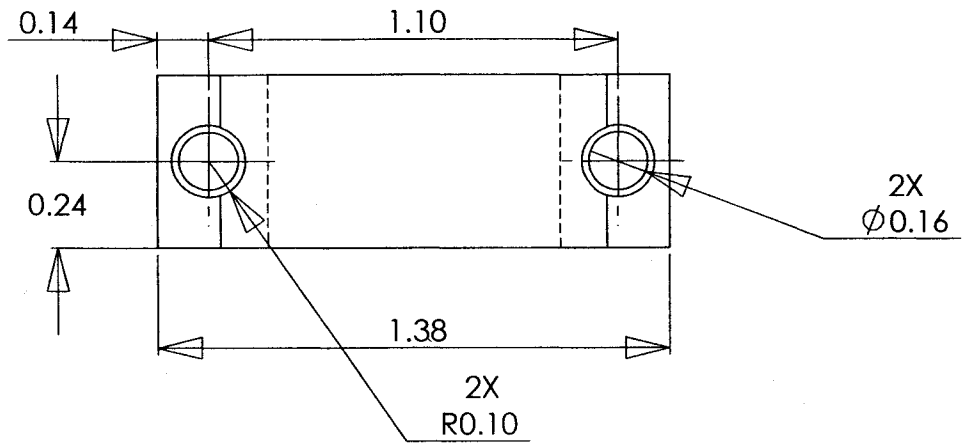

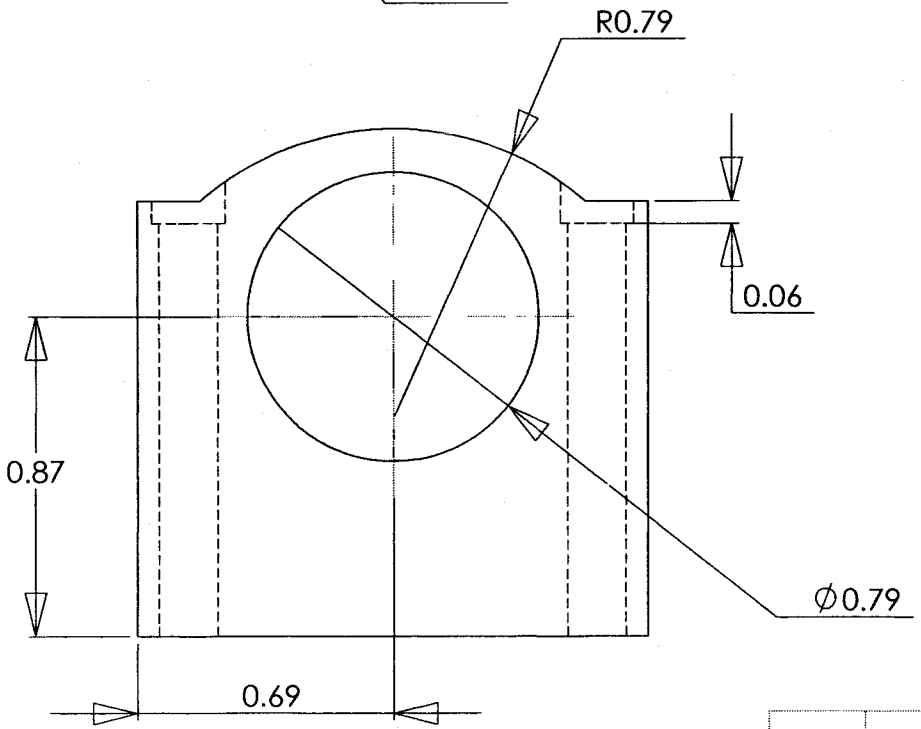

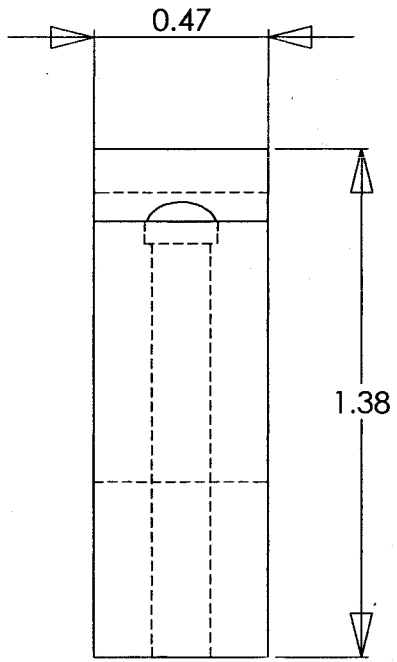

SolidWorks Educational License
Instructional Use Only

PROPRIETARY AND CONFIDENTIAL

DIMENSIONS ARE IN INCHES
TOLERANCES:
FRACTIONAL ±
ANGULAR: MACH ± BEND ±
TWO PLACE DECIMAL ±
THREE PLACE DECIMAL ±

NAME
DATE

ALUMINUM

UNIV. OF OTTAWA

3 DOF MANIPULATOR
MOTOR MOUNT

PART NO. 000006

A

KEVIN GILBANK

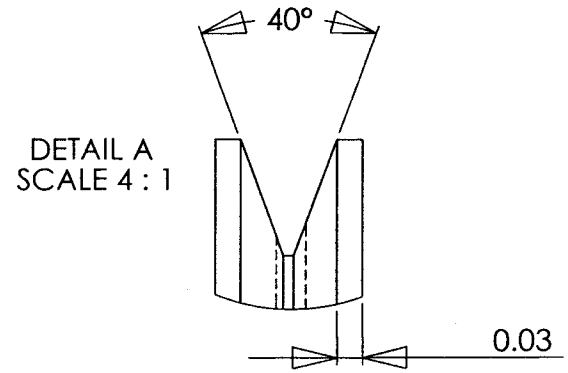

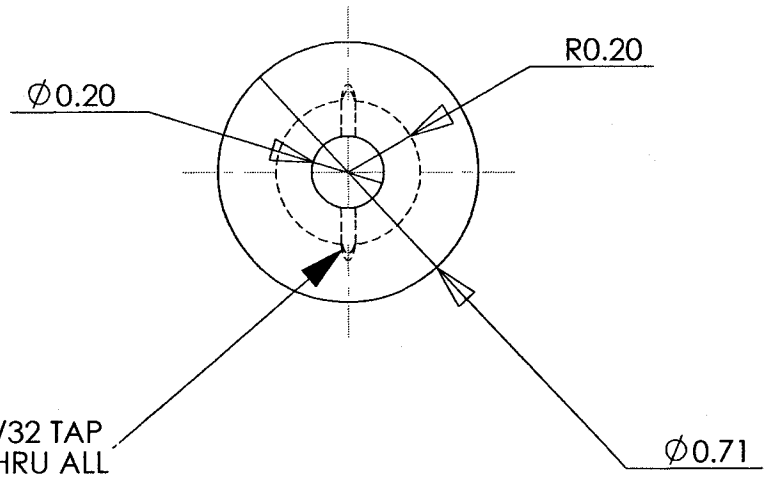

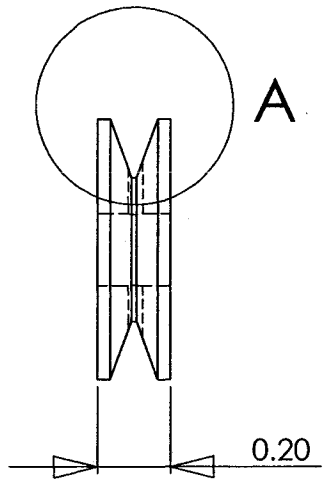

REVISIONS			
ZONE	REV.	DESCRIPTION	DATE	APPROVED

SolidWorks Educational License
Instructional Use Only

PROPRIETARY AND CONFIDENTIAL
THE INFORMATION CONTAINED IN THIS DRAWING IS THE SOLE PROPERTY OF [illegible]. ANY REPRODUCTION IN PART OR AS A WHOLE WITHOUT THE WRITTEN PERMISSION OF [illegible] IS PROHIBITED.

DIMENSIONS ARE IN INCHES
TOLERANCES:
FRACTIONAL ±
ANGULAR: MACH ± BEND ±
TWO PLACE DECIMAL ±
THREE PLACE DECIMAL ±

MATERIAL —
FINISH —

NEXT ASSY | USED ON

APPLICATION | DO NOT SCALE DRAWING

	NAME	DATE
DRAWN		
CHECKED		
ENG APPR.		
MFG APPR.		
Q.A.		
COMMENTS:		

ALUMINUM

UNIV. OF OTTAWA

3 DOF MANIPULATOR
MOTOR PULLEY

PART NO. 000007

SIZE	DWG. NO.	REV
A	KEVIN GILBANK	
SCALE	SHEET	

APPENDIX III
Pittman GM14602D261 DC MOTOR

GM14602D261
OBSOLETE

150-140
Rev C

AUG-19-04 10:54 FROM-Pittman 215 256 1338 T-411 P.003/003

REVISIONS				
LTR	DESCRIPTION	DRFT/ENGR	DATE	APPR
B	REDRAWN & UPDATED IN AUTOCAD	DCS/DCS	8/10/95	JVM
C	.187 TYP WAS DIMENSIONED WRONG	KUH/KUH	1-5-96	JVM

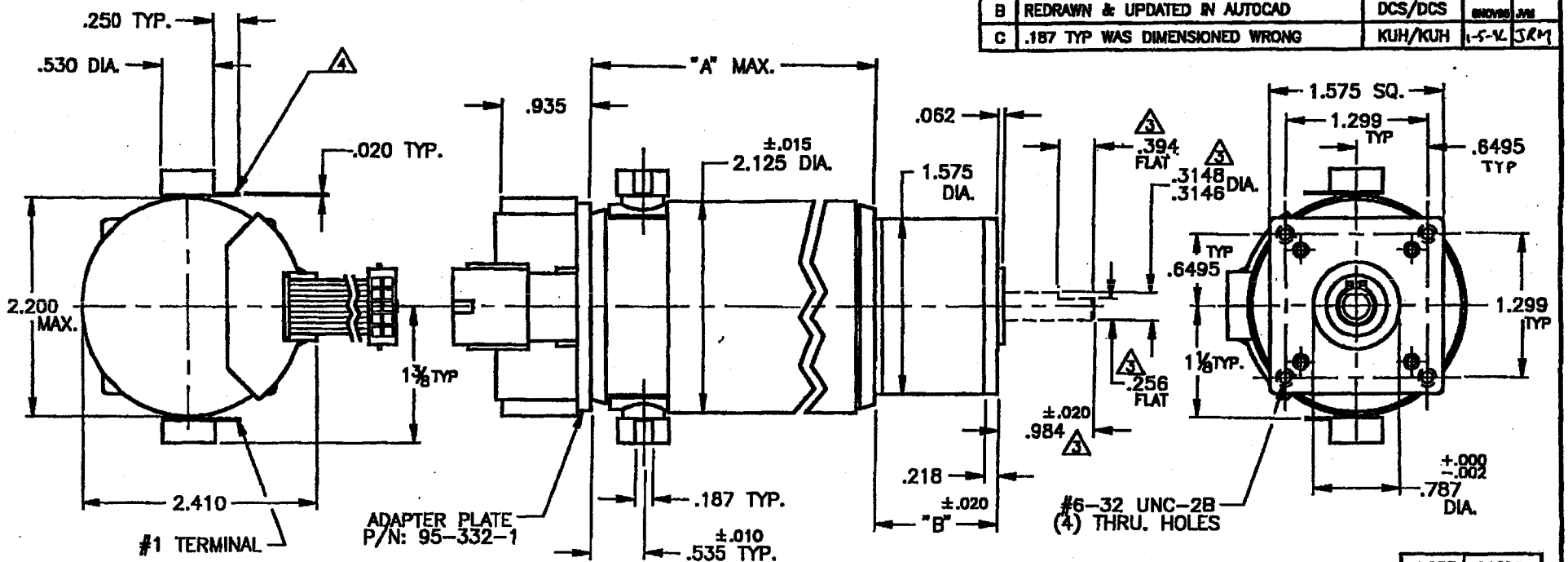

GEAR RATIO	"B"	"A"	MOTOR
5184/1410.37:1	2.600	4.953	14606
864/325.47:1	2.300	4.453	14605
144/75.11:1	2.000	4.078	14604
24/7.33:1	1.700	3.703	14603
4.1:1	1.400	3.203	14602
		2.953	14601

NOTES:

1. SHAFT ROTATION IS CW, WHILE VIEWING THE MOUNTING END, WITH POSITIVE VOLTAGE (+) APPLIED TO #1 TERMINAL.
2. STANDARD MOTOR SHAFT IS (13-770-00□). FOR ALL OTHER SHAFT CONFIGURATIONS, REFER TO DATA SHEET FOR PART NUMBERS.
3. PLANETARY OUTPUT SHAFT DIMENSIONS NOTED ARE STANDARD (11-699-1). FOR ALL OTHER PLANETARY OUTPUT SHAFT CONFIGURATIONS, REFER TO DATA SHEET FOR PART NUMBERS.
4. TERMINALS WILL MATE WITH '187' SERIES AMP INC. OR EQUIV. PUSH-ON RECEPTACLES.
5. BALL BEARINGS ARE PRELOADED PER P-107.
6. OUTPUT SHAFT ENDPLAY: .020 MAX. FOR SLEEVE BEARINGS. BALL BEARING PRELOAD: 8 LBS. AND WILL YIELD .002-.010 MOVEMENT.
7. MAX TORQUE RATING: 2000 oz.-in.
8. MOTOR TO BE PREPARED FOR ENCODER APPLICATION PER 150-139 DWG.

UNLESS OTHERWISE SPECIFIED DIMENSION ARE IN INCHES TOLERANCES ARE: FRACTION ±1/64 DECIMAL .X ±.015 .XX ±.010 .XXX±.005 ANGLES ±1°

MATERIAL:

FINISH:

FILE: 150\140

		DATE
DRAFTED BY	DCS	11/8/95
ENGINEERED BY	DCS	11/8/95
APPROVED BY	JVM	11/8/95
NEXT ASSY:		
USED ON:		

PITTMAN
HARLEYSVILLE, PA 19438-0903 USA
A DIVISION OF PENN ENGINEERING & MANUFACTURING CORP.

TITLE: OUTLINE & MOUNTING DIMENSIONS 1460X WITH HEDS-6010

DWG. NO. B- 150-140 REV. C

SCALE: DNS SHEET 1 of 1

1000 CPR

UNCONTROLLED

Gearmotor Data

Line No.	Parameter	Symbol	Units	Reduction Ratios 5.9:1	19.7:1	65.5:1*
MECHANICAL SPECIFICATIONS (Standard and High-Torque Gears)						
1	Max. Load Standard Gears[1]	T_L	oz-in (N-m)	175 (1.24)	175 (1.24)	175 (1.24)
2	Max. Load High-Torque Gears[1]	T_L	oz-in (N-m)	N/A N/A	300 (2.12)	300 (2.12)
3	Gearbox Shaft Rotation[2]	—	—	CW	CCW	CW
4	Gearbox Efficiency	—	%	81	73	66
5	Gearbox Weight (Mass)	W_G	oz (g)	5.90 (167.3)	6.26 (177.5)	6.62 (187.7)
6	Gearbox Length	L_2	in max (mm max)	1.373 (34.87)	1.373 (34.87)	1.373 (34.87)
7	Length, GM14901	L_3	in max (mm max)	4.322 (109.78)	4.322 (109.78)	4.322 (109.78)
8	Length, GM14902	L_3	in max (mm max)	4.572 (116.13)	4.572 (116.13)	4.572 (116.13)
MECHANICAL SPECIFICATIONS (High-Torque, Wide-Face Gears)						
9	Max. Load[1]	T_L	oz-in (N-m)	N/A N/A	500 (3.53)	500 (3.53)
10	Gearbox Shaft Rotation	—	—	CW	CCW	CW
11	Gearbox Efficiency	—	%	81	73	66
12	Gearbox Weight (Mass)	W_G	oz (g)	N/A N/A	6.52 (184.8)	6.88 (195.0)
13	Gearbox Length	L_2	in max (mm max)	N/A N/A	1.373 (34.87)	1.373 (34.87)
14	Length, GM14901	L_3	in max (mm max)	N/A N/A	4.322 (109.78)	4.322 (109.78)
15	Length, GM14902	L_3	in max (mm max)	N/A N/A	4.572 (116.13)	4.572 (116.13)
NO-LOAD SPEED (All Gears)						
16	GM14901	S_{NL}	rpm (rad/s)	713 (75)	214 (22)	64.2 (7)
17	GM14902	S_{NL}	rpm (rad/s)	690 (72)	207 (22)	62.1 (6)

[1]Represents gearbox capability only. Continuous load torque capability will vary with gear ratio, motor selection, and operating conditions.
[2]Shaft rotation is designated while looking at output shaft with motor operating in a clockwise direction. Gearmotor is polarity reversible.
*Contact factory for higher ratios.

PITTMAN®

Motor Data

Line No.	Parameter	Symbol	Units	14X01	14X02
18	Continuous Torque[3]	T_C	oz-in (N-m)	10.0 (70.6 X10^{-3})	14.0 (98.9 X 10^{-3})
19	Peak Torque (Stall)	T_{PK}	oz-in (N-m)	62.8 (.44)	107 (.76)
20	Motor Constant	K_M	oz-in/$\sqrt{W}$ (N-m/$\sqrt{W}$)	4.45 (31.4 X 10^{-3})	5.93 (41.9 X 10^{-3})
21	No-Load Speed	S_0	rpm (rad/s)	4230 (443)	4087 (428)
22	Friction Torque	T_F	oz-in (N-m)	1.20 (8.5 X 10^{-3})	1.20 (8.5 X 10^{-3})
23	Rotor Inertia	J_M	oz-in-s^2 (kg-m^2)	1.6 X 10^{-3} (1.13 X 10^{-5})	2.3 X 10^{-3} (1.62 X 10^{-5})
24	Electrical Time Constant	τ_E	ms	0.91	1.47
25	Mechanical Time Constant	τ_M	ms	11.4	9.26
26	Viscous Damping— Infinite Source Impedance	D	oz-in/krpm (N-m/(rad/s))	0.17 (1.15 X 10^{-5})	0.17 (1.15 X 10^{-5})
27	Viscous Damping— Zero Source Impedance	K_D	oz-in/krpm (N-m/(rad/s))	14.7 (9.91 X 10^{-4})	26.0 (1.75 X 10^{-3})
28	Maximum Winding Temperature	θ_{MAX}	°F (°C)	311 (155)	311 (155)
29	Thermal Impedance	R_{TH}	°F/watt °C/watt	49.8 (9.90)	48.2 (9.00)
30	Thermal Time Constant	τ_{TH}	min	22.0	24.0
31	Motor Weight (Mass)	W_M	oz (g)	20.8 (589.7)	26.0 (737.1)
32	Motor Length, 1410X, 1420X	L_1	in max (mm max)	2.953 (75.01)	3.203 (81.36)

[3]Continuous torque specified at 25°C ambient temperature and without additional heat sink.

Model GM14X01/GM14X02 Winding Data (Other windings available upon request)

Line No.	Parameter	Symbol	Units	GM14X01				GM14X02			
33	Reference Voltage	E	V	12.0	19.1	24.0	30.3	12.0	19.1	24.0	30.3
34	Torque Constant	K_T	oz-in/A (N-m/A)	3.72 (26.3 X 10^{-3})	5.89 (41.6 X 10^{-3})	7.44 (52.5 X 10^{-3})	9.46 (66.8 X 10^{-3})	3.90 (27.5 X 10^{-3})	6.16 (43.5 X 10^{-3})	7.80 (55.1 X 10^{-3})	9.85 (69.6 X 10^{-3})
35	Back-EMF Constant	K_E	V/krpm (V/rad/s)	2.75 (26.3 X 10^{-3})	4.36 (41.6 X 10^{-3})	5.50 (52.5 X 10^{-3})	6.99 (66.8 X 10^{-3})	2.88 (27.5 X 10^{-3})	4.55 (43.5 X 10^{-3})	5.77 (55.1 X 10^{-3})	7.29 (69.6 X 10^{-3})
36	Resistance	R_T	Ω	0.72	1.76	2.79	4.45	0.45	1.09	1.73	2.74
37	Inductance	L	mH	0.63	1.59	2.54	4.10	0.62	1.58	2.54	4.05
38	No-Load Current	I_{NL}	A	0.52	0.33	0.26	0.20	0.49	0.31	0.24	0.19
39	Peak Current (Stall)[4]	I_P	A	16.7	10.8	8.60	6.80	26.4	17.5	13.9	11.1

[4]Theoretical values supplied for reference only.

Model GM14X01

Motor Speed & Current vs. Torque
(24V Winding)

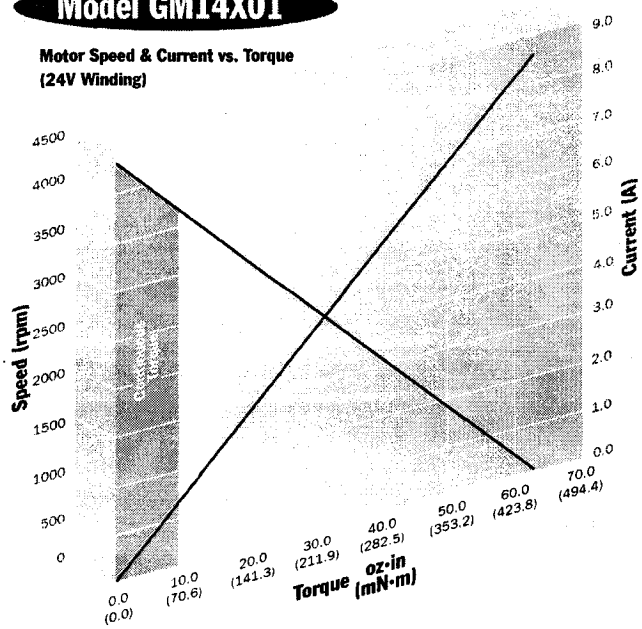

Model GM14X02

Motor Speed & Current vs. Torque
(24V Winding)

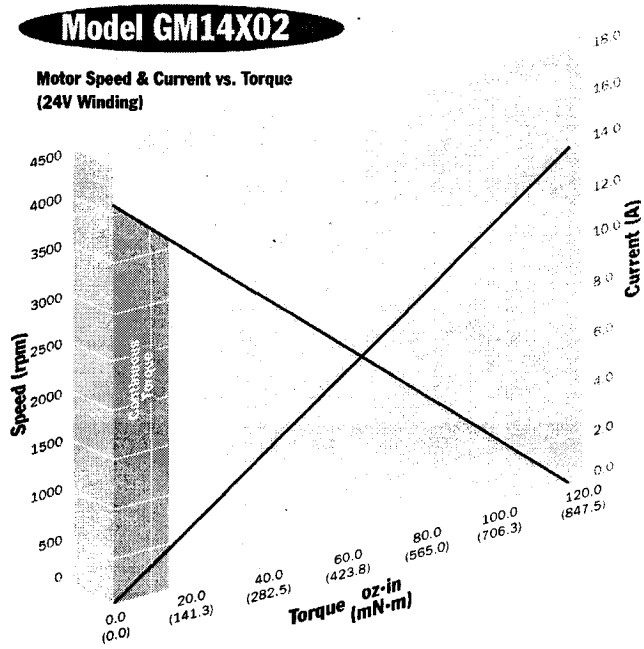

PITTMAN®

GM149XX Motor

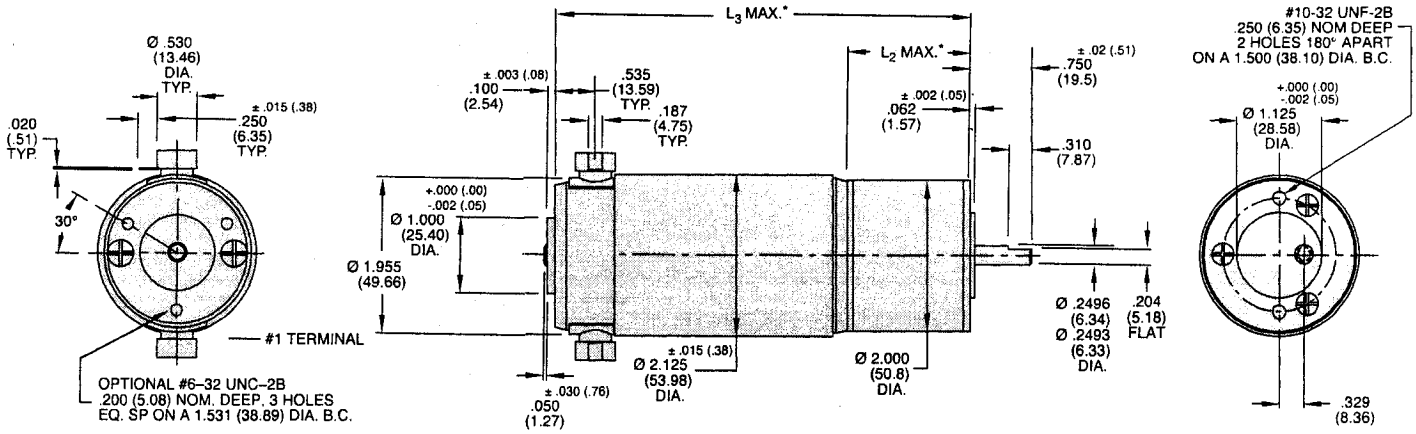

GM149XX Motor with 91X0 Encoder

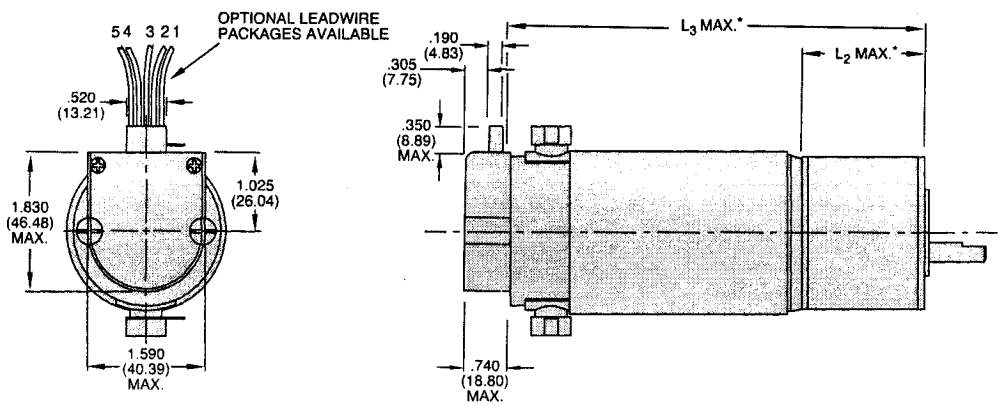

GM149XX Motor with 90X0 Encoder

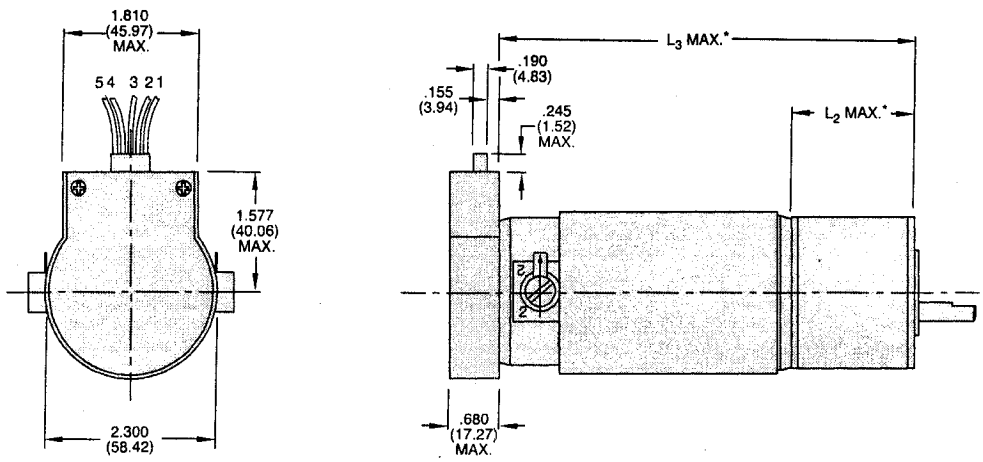

Encoder Connection Chart

Pin No.	Color	Connection
1	Black	Ground
2	Green	Index/NC
3	Yellow	Channel A
4	Red	Vcc
5	Blue	Channel B

Notes:
- Unless otherwise specified, all tolerances are to be ±.005 (.01)
- All measurements are in inches (mm)

*See line no. 6 through 8 and 13 through 15 in gearmotor data chart

PITTMAN®

APPENDIX IV
Pittman LO-COG DC No. 6X12 MOTOR

BULLETIN LC2

Series 6000

LO-COG® 22mm DC Motors

Pittman brand LO-COG® low cost, high performance 22 millimeter diameter brush-commutated DC motors are ideal for use in applications requiring the power of an "ironless core" or "coreless" motor, without the associated cost. This addition to our LO-COG® family is designed for use in image processing, semiconductor processing and mass data storage equipment, computer peripherals and office automation, as well as other applications for the medical and industrial markets. By using a skewed 5-slot armature design and bonded neodymium iron boron magnets, this motor provides more power than most other DC motors of similar size. Cost effective planetary gearheads are available to meet application specific speed and torque requirements. Our unique cartridge brush assembly reduces audible and electrical noise and significantly improves brush life by maintaining optimum brush force throughout the life of the motor. For precision motion control, optical encoders are available with several CPR ranges to meet your position, velocity and direction feedback needs.

Series 6000™

- **Available in 3 lengths**
- **Speeds up to 8550 RPM**
- **Peak Torques up to 10.2 oz-in**
- **Encoder resolutions from 16 to 256**

Construction

- **5 slot skewed armature**
- **2 pole permanent magnet stators are constructed of bonded neodymium iron boron magnets**
- **Diamond turned commutators ensure maximum brush life**
- **Standard copper graphite brushes**
- **Precision ground hardened stainless steel shafts**
- **Silicon-steel laminations**
- **Self-aligning sintered bronze bearings**

Options

- **Custom cables**
- **Shaft modifications**
- **Shaft-mounted pulleys and gears**
- **Ball bearings**
- **Multiple windings**
- **RFI suppression**
- **Dynamic armature balancing**
- **Customized versions available in production quantities**
- **Other brush materials available**
- **Optical encoders**

NEW!

Longer Length Added. Provides up to 40% More Continuous Torque!!

PITTMAN®
a PennEngineering® company
Power Your Ideas™

PittmanExpress℠

Get same day shipment of sample motors for models listed in the Pittman Express Catalog (Bulletin PE).

Every Pittman motor is subjected to automated performance testing prior to shipment.

Motor Data

Line No.	Parameter	Symbol	Units	6X12	6X13	6X14
1	Continuous Torque (Max.)[1]	T_C	oz·in (N·m)	0.80 (5.65×10^{-3})	1.32 (9.32×10^{-3})	2.00 (14.1×10^{-3})
2	Peak Torque (Stall)[2]	T_{PK}	oz·in (N·m)	2.70 (1.91×10^{-2})	5.56 (3.93×10^{-2})	10.20 (7.34×10^{-2})
3	Friction Torque	T_F	oz·in (N·m)	0.13 (9.18×10^{-4})	0.19 (1.34×10^{-3})	0.25 (1.76×10^{-3})
4	No Load Speed	S_{NL}	rpm (rad/s)	8260 (865)	7780 (815)	8550 (895)
5	Rotor Inertia	J_M	oz·in·s^2 (kg·m^2)	7.3×10^{-5} (5.15×10^{-7})	9.6×10^{-5} (6.78×10^{-7})	11.4×10^{-5} (7.98×10^{-7})
6	Electrical Time Constant	τ_E	ms	0.52	0.65	0.78
7	Mechanical Time Constant	τ_M	ms	23.4	14	11.5
8	Viscous Damping— Infinite Source Impedance	D	oz·in/krpm (N·m/(rad/s))	0.0072 (4.85×10^{-7})	0.0089 (6×10^{-7})	.0114 (7.68×10^{-7})
9	Damping Constant— Zero Source Impedance	K_D	oz·in/krpm (N·m/(rad/s))	.327 (2.2×10^{-5})	.714 (4.81×10^{-5})	1.193 (8.03×10^{-5})
10	Maximum Winding Temperature	θ_{MAX}	°F (°C)	266 (130)	266 (130)	266 (130)
11	Thermal Impedance	R_{TH}	°C/watt	37.80	29.00	22.3
12	Thermal Time Constant	τ_{TH}	min.	9.90	11.30	13.10
13	Motor Weight (Mass)	W_M	oz (g)	1.50 (42.52)	2.10 (59.53)	2.65 (75.12)
14	Motor Constant[2]	K_M	oz·in/√W (N·m/√W)	0.66 (4.66×10^{-3})	0.98 (6.92×10^{-3})	1.270 (8.97×10^{-3})
15	Motor Length	L_1	in max. (mm max.)	1.256 (31.90)	1.556 (39.52)	1.901 (48.28)

[1]Continuous torque specified at 25°C ambient temperature and without additional heat sink.
[2]Theoretical values supplied for reference only.

©1999 Pittman, a PennEngineering company. LO-COG, ELCOM, ELCOM SL, and ELCOM ST are brand names and trademarks for motors manufactured exclusively by Pittman.

PITTMAN®

Model 6X12

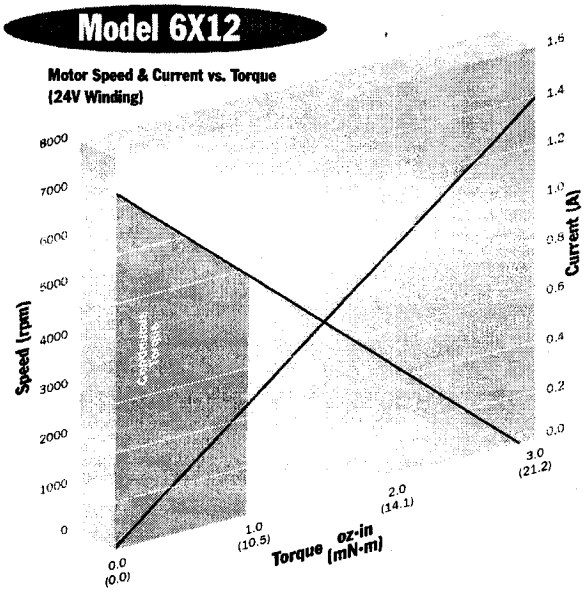

Model 6X13

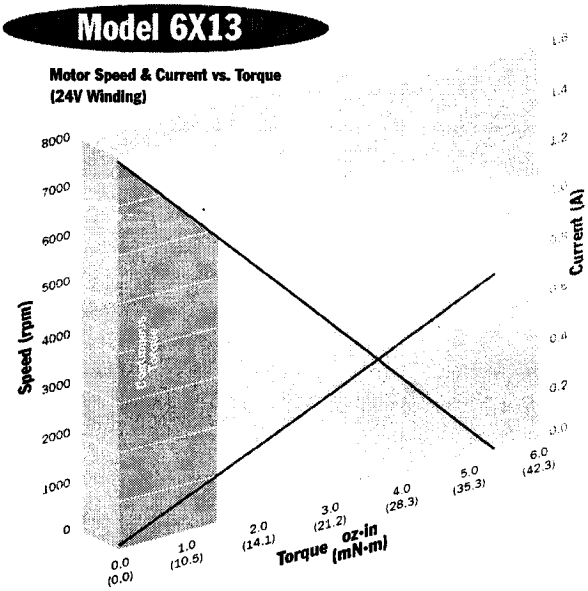

Model 6X14

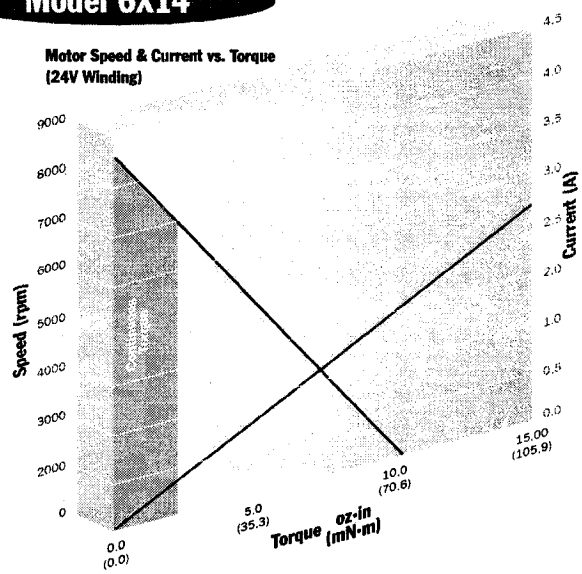

Motor 62XX (Wire Leads)

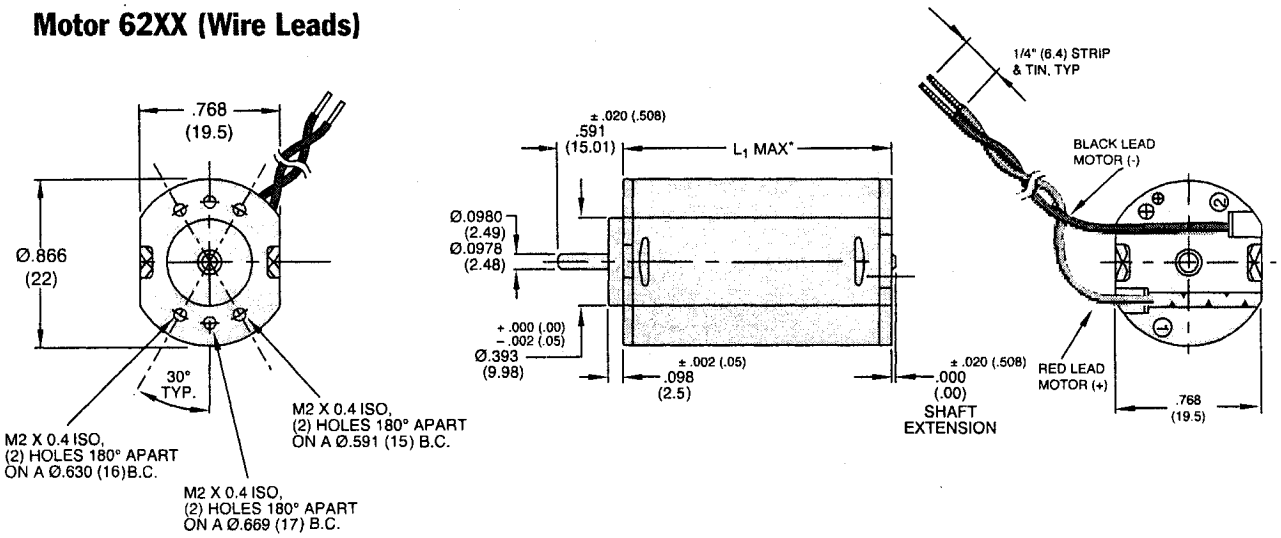

PITTMAN®

Motor 63XX (Terminals)

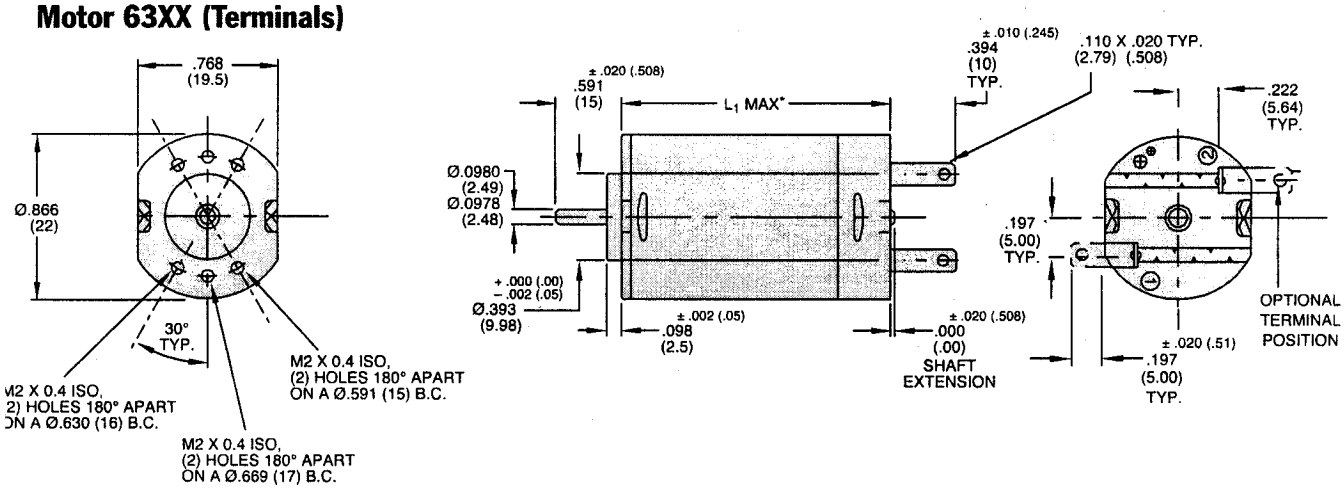

Gearmotor PG66XX with Planetary Gearbox (Wire Leads)

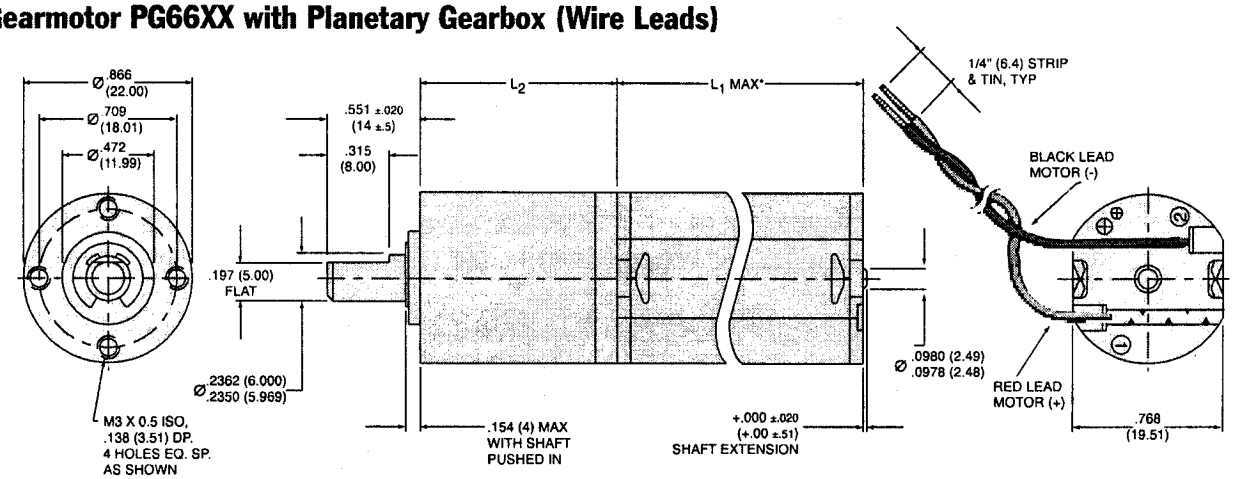

Gearmotor PG67XX with Planetary Gearbox (Terminals)

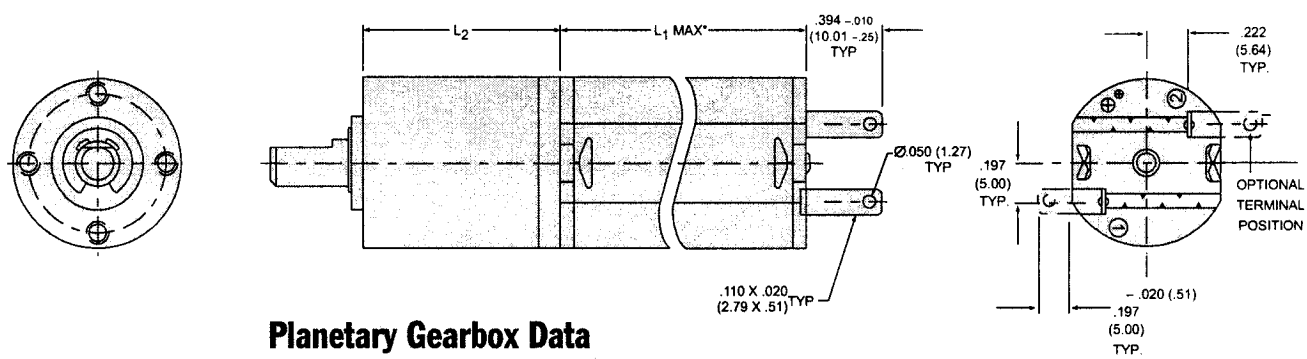

Planetary Gearbox Data

Max. Torque	L_2	No. Stages	Ratio
27.78 oz-in (.196 N-m)	1.161 (29.5)	3	107:1 64:1
13.89 oz-in (.098 N-m)	.965 (24.5)	2	23:1 16:1
6.94 oz-in (.049 N-m)	.768 (19.5)	1	4:1

Notes:
- All measurements are in inches (mm)
*See line number 15 in data chart

PITTMAN®

Motor 63XX with HEDR 8X00 Encoder 128/256 Line Count

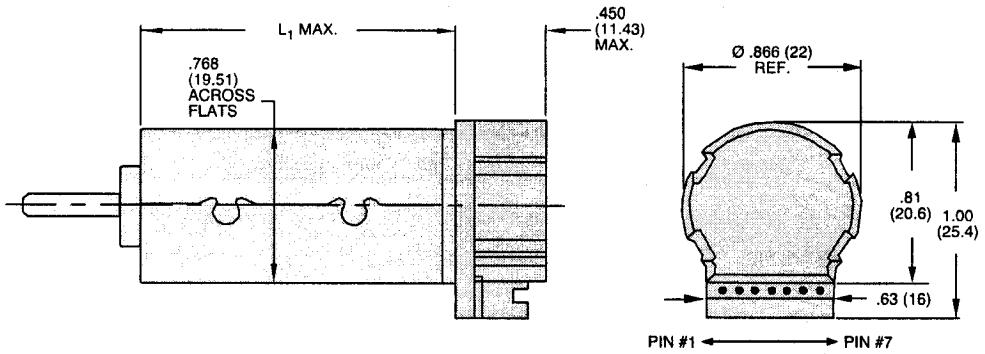

SEE CHART FOR FUNCTIONS

Receptacle will mate with Molex plug 87369-0700.

Pin No.	Function
1	Motor Ground
2	Motor (-) 2
3	Motor (+) 1
4	Encoder Ground
5	Vcc +5VDC
6	Channel A
7	Channel B

Motor 62XX with HRPG Encoder

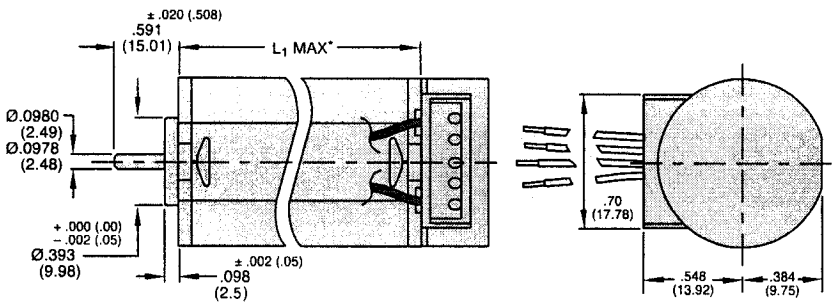

Encoder Connection Chart

Color	Connection
Gray	Ground
Violet	Channel B
White	Vcc (+5VDC)
Blue	Channel A

Notes:
- Unless otherwise specified, all tolerances are to be ±.005 (.01)
- All measurements are in inches (mm)

PITTMAN®

APPENDIX V

Feedback Instruments Modular MS150 System

APPENDIX VI
ECP Inverted Pendulum Apparatus

Model 505
ECP Inverted Pendulum

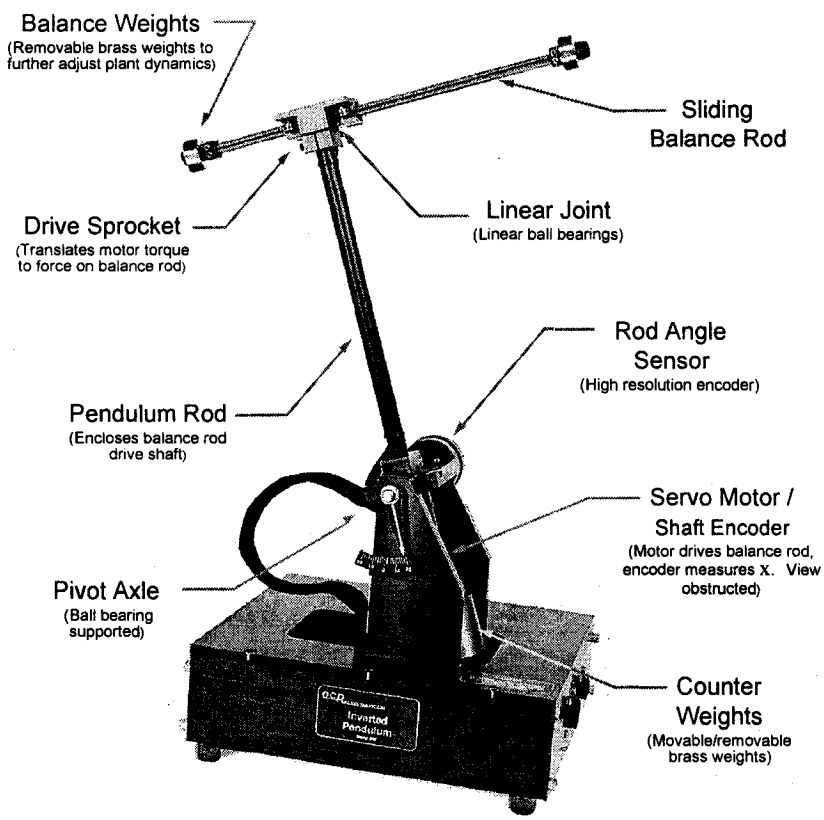

This unique ECP design vividly demonstrates the need for and effectiveness of closed loop control. It is *not* the conventional rod-on-cart inverted pendulum, but rather, it steers a horizontal balancing rod in the presence of gravity to control the vertical pendulum rod. As detailed in the manual, the plant has both right half plane poles and zeros as well as kinematic and gravitationally coupled nonlinearities. By adjusting mass properties, these roots may be varied to make the control problem range from being relatively simple to theoretically impossible! The system includes removable and adjustable moment arm counter-weights on the vertical and horizontal rods for quick adjustment of the plant dynamics. It features linear and rotary ball bearings at the joints for low friction and consistent dynamic properties.

Dynamics: 4th order, nonminimum phase, open loop unstable, kinematic & gravitationally coupled nonlinearities

Parameter Adjustment: Adjustable vertical and horizontal rod mass, inertia, and CG offset.

I/O: SISO, SIMO,

Poles: Adjustable 0.4-1.2 Hz

Feedback: High res. encoders (16,000 count/rev, θ, 44,000 count/m, x)

Actuator: High Torque density, rare earth magnet type

Bench-top size: 30x30x40 cm. (12x12x16 in.)

Safety Features: Travel limit microswitches (horizontal rod) , fail-safe shutdown, limit cushions (vertical rod), amplifier over-current protection. In firmware (complete system only): i^2t thermal protection

Plant Model	***Dynamic Equations***		***Characteristics***
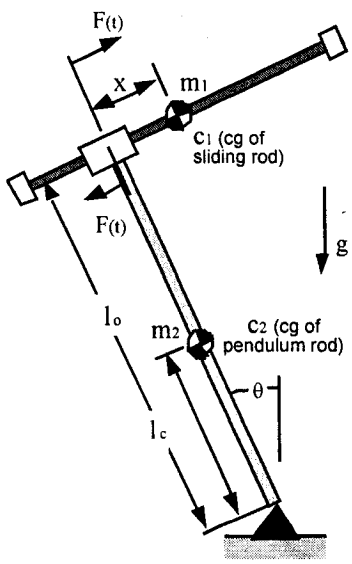	***"Exact"***	$m_1\ddot{x}(t)+m_1l_o\ddot{\theta}(t) - m_1x(t)\dot{\theta}(t)^2 - m_1g\sin\theta(t) = F(t)$ $m_1l_o\ddot{x}(t)+J_o(x)\ddot{\theta}(t)+2m_1x(t)\dot{x}(t)\dot{\theta}(t) - (m_1l_o+m_2l_c)g\sin\theta(t) - m_1gx(t)\cos\theta(t) = 0$ $J_o(x) = J_1+m_1(l_o^2+x^2)+J_1+m_2l_c^2$	• Nonlinearities in kinematic constraints and coordinate dependent mass properties.
	Linearized Time Domain	$m_1\ddot{x}(t)+m_1l_o\ddot{\theta}(t) - mg\,\theta(t) = F(t)$ $m_1l_o\ddot{x}(t)+J_o^*\ddot{\theta}(t) - (m_1l_c+m_2l_o)g\theta(t) - m_2gx(t) = 0$ $J_o^* = J_o\big\vert_{x=0}$	• Linearization about x = 0, θ = 0 shown to be valid for many control schemes.
	S-Domain	$\frac{\theta(s)}{F(t)} = \frac{-(l_os^2 - g)}{(J_o^* - m_1l_o^2)s^4 + (m_2l_o - m_1l_c)gs^2 - m_2g^2}$	• One RHP, 2 oscillatory poles. • Nonmin phase (RHP zero). • Attainable bandwidth bounded from above and below by RHP roots.

© 1995-2000 Educational Control Products, All Rights reserved

APPENDIX VII

SERVO-TEK DC tacho-generator Type SB 740B-1

SERVO-TEK®

SERVO-TEK PRODUCTS COMPANY, INC.

DC Tachometer Generators

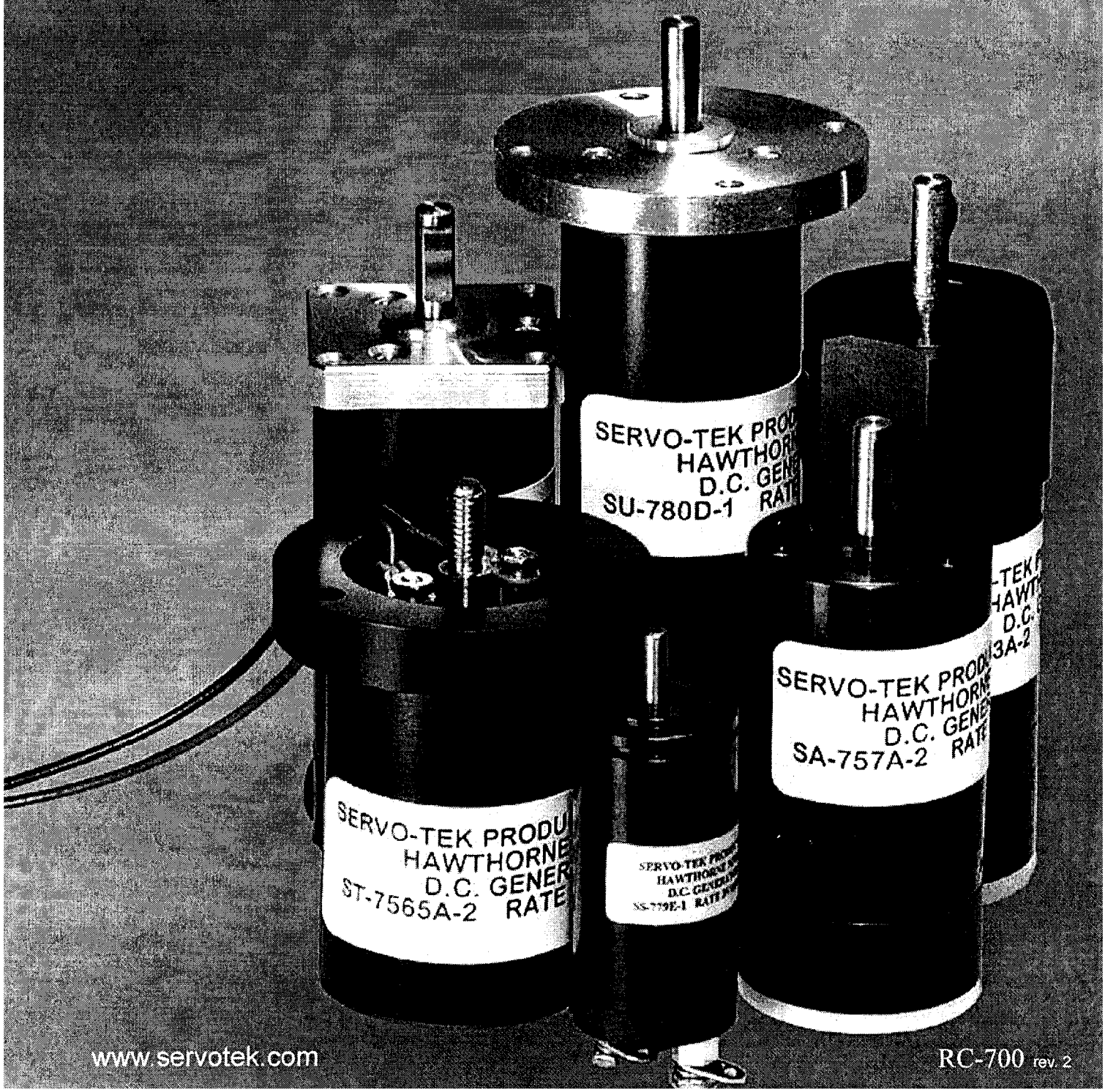

www.servotek.com

RC-700 rev. 2